2010-05-03

Delivering Stem Cells to the Heart

Michael Fakharzadeh
Worcester Polytechnic Institute

Department of Biomedical Engineering

Delivering Stem Cells to the Heart

A Thesis
Submitted to the Faculty of

WORCESTER POLYTECHNIC INSTITUTE
In partial fulfillment of the requirements for the
Degree of Master of Science

Submitted by:

_____
Michael Fakharzadeh

Approved by:

_____ _____
Glenn Gaudette, PhD George Pins, PhD

_____
Marsha Rolle, PhD

Acknowledgements

I would like to thank my advisors Marsha Rolle, George Pins, and Glenn Gaudette for their guidance throughout the course of my education.

I would also like to thank the following individuals for their vital assistance in completing this project:

Andrew James Kazanovicz
Alexander Thoms Madden
Evans John Burford
Jacques Paul Guyette
Jeremy Kenneth Skorinko
Xiaowen Zhen
Xiaolin Zhen
Melissa P. Kuhn
Kathryn Elisabeth Partridge
Bryan P. Choate
Nikole M. Connor
Sharon Shaw
Jennifer Lynn Makridakis
Jonathan Mark Grasman
Darshan Pravin Parekh
Jason Zicheng Hu
Tracy A. Gwyther
Lisa J. Wall
James A. Burrill
Matthew Aaron Whitman
Kayla Mae Rayworth
Victoria M. Huntress
Luis Vidali

Abstract

Myocardial infarction is a prominent medical problem in the world today. Current treatments are limited and do not strive to regenerate the myocardial tissue that is lost post-infarction. Human mesenchymal stem cells (hMSCs) have been shown to improve cardiac function when implanted post-infarction. The effectiveness of stem cell therapy largely depends on the delivery method. Current delivery methods are insufficient due to their low cell engraftment rate and inability to target the endocardium, where most myocardial infarctions occur. Biological microthreads are a promising new local cell delivery method that may improve upon these current limitations. We hypothesize that biological microthreads will increase efficiency of hMSC delivery to the beating rat heart compared to intramyocardial injection. To test our hypothesis we seeded biological microthreads *in vitro* with 100 μL of cell suspension (100,000 hMSCs). After one day, an average of 11,806 ± 3,932 hMSCs were counted on the biological microthreads. The biological microthreads were attached to suture needles to allow targeted delivery to the rat heart (in the left ventricular wall). Human mesenchymal stem cells were loaded with quantum dots prior to seeding the biological microthread bundles or delivery to the rat heart via injection. For intramyocardial injection, a cell suspension containing 10,000 hMSCs (35 μL) was injected into the myocardial wall using a 100 μL syringe. The delivery efficiency of each method was determined by sectioning the heart into 8 μm thick sections and analyzing three sections every sixty sections (24 μm every 480 μm) for quantum dot loaded hMSCs. These sections were stained with Hoechst dye and quantum dot loaded cells in the heart sections were manually counted. The delivery efficiency of each biological microthread implantation was calculated by dividing the number of counted quantum dot loaded hMSCs in the heart wall by the average number of hMSCs on the biological microthread bundles (normalized to the length that was implanted in the heart wall) after 24 hours. The delivery efficiency of intramyocardial injection was calculated by dividing the number of counted quantum dot loaded hMSCs in the heart wall by 10,000 (the number of cells injected). Biological microthread mediated hMSC delivery had a significantly higher delivery efficiency (66.6 ± 11.1%) compared to intramyocardial injection (11.8 ± 6.25%) after 1 hour ($p < 0.05$). Biological microthread implantation tracking illustrated that we were able to deliver hMSCs to the myocardium and endocardium of the left ventricular wall for hMSC delivery. This study illustrates that biological microthreads can serve as an efficient means of delivering hMSCs to the infarcted heart. Unlike the currently utilized delivery methods, biological microthreads can target the infarcted layer of the left ventricular wall and maximize hMSC engraftment to that layer.

Table of Contents

Acknowledgements 2

Abstract 3

Chapter 1: Introduction 8

Chapter 2: Background 10

2.1: Healthy Myocardial Function and the Infarcted Myocardium 10

2.1.1: The Rat Heart 11

2.2: Current Treatments for Myocardial Infarction 12

2.3: Myocardial Cellular Therapy 13

2.3.1: Current Drawbacks of Cellular Therapy 14

2.4: Cardiac Regeneration with Biomaterials 17

2.4.1: Collagen and Fibrin Microthreads 18

2.5: Cell Tracking with Quantum Dots 19

Chapter 3: Hypothesis and Specific Aims 20

Chapter 4: Materials and Methods 22

4.1: Collagen and Fibrin Microthread Production and Seeding 22

4.2: Quantifying Cells Seeded on Biological Microthreads 26

4.2.1: Qualitative analysis of cell seeding using Hoechst dye and Phalloidin stain 26

4.2.1: Quantification of cell seeding using a hemocytometer 28

4.3: Delivering hMSCs to the Rat Heart 29

4.3.1: Biological Microthread Implantation and Intramyocardial injection 29

4.4: Histological Analysis of the Rat Heart Post-Implantation or Injection 30

4.4.1: Heart sectioning and preparation 30

4.4.2: Heart section staining 31

4.4.3: Counting and calculating cells delivered to the heart 33

4.4.4: Tracking microthread implantation in the rat heart 37

4.5: Statistical Analysis 38

4.4.5: Confocal microscopy 40
Chapter 5: Results 43
5.1: Quantifying hMSC seeding on biological microthreads 43
5.2: Quantifying hMSC delivery to the ventricular wall 46
5.3: hMSC delivery distribution 52
5.3.1 Biological microthread implantation tracking 59
Chapter 6: Discussion 64
6.1 Biological Microthread Cell Seeding 64
6.2 hMSC Delivery to the Heart 66
6.2.1 hMSC delivery efficiency 66
6.2.2 hMSC delivery distribution 70
6.2.3 Microthread implantation tracking 72
6.3 Microscopy 74
Conclusion 76
References 77
Appendix A: Microthread Seeding Counts 82
Appendix B: hMSC Delivery Number Calculation 84
Appendix C: Microthread Implantation Tracking Measurements 88
Appendix D: Surgical Notes 91
Appendix E: Surgical Procedure 100

Table of Figures

Figure 1: Rat heart blood circulation pathway [26] 12
Figure 2: Fibrin microthread scanning electron micrograph (left) and extrusion diagram (right) [19] 22
Figure 3: Collagen microthread scanning electron micrograph [19] 23
Figure 4: Microthread bundling 24
Figure 5: Biological microthread seeding diagram 25
Figure 6: Microthreads placed in tube rotator 25
Figure 7: Whole 2 cm length of a biological microthread bundle after 1 day of seeding with hMSCs 27
Figure 8: Trypsinized whole biological microthread bundle 28
Figure 9: Bisecting and sectioning the rat heart 31
Figure 10: Masson's trichrome stained rat heart section 33
Figure 11: Quantum dot loaded hMSCs delivered to the rat heart 34
Figure 12: Counting hMSCs delivered to the rat heart 35
Figure 13: Determination of microthread implanted length and depth in the rat heart 37
Figure 14: Microthread implantation tracking 39
Figure 15: Confocal images before (left) and after (right) max projection 41
Figure 16: Confocal images before (left) and after (right) spectral analysis 41
Figure 17: Spectral absorbance and emission curves for Hoechst 33342 (top left), Alexa Fluor 488 (top right), and Qdot 655 ITK quantum dots (bottom) 42
Figure 18: Biological microthread seeding after 24 hours 43
Figure 19: hMSC engraftment rate (%): microthread implantation vs. intramyocardial injection 47
Figure 20: hMSC engraftment number comparison: microthread implantation vs. intramyocardial injection 48
Figure 21: hMSC delivery length comparison: microthread implantation vs. intramyocardial injection 51
Figure 22: Biological microthread bundle delivered to ventricular cavity 52
Figure 23: hMSC delivery distributions – microthread implantations 53
Figure 24: hMSC delivery distributions – intramyocardial injections 56
Figure 25: Microthread Implantation – Combined Delivery Distribution 58
Figure 26: Intramyocardial Injection – Combined Delivery Distribution 58
Figure 27: hMSC delivery localization to endocardium, myocardium, and epicardium 63
Figure 28: Microthread implantation tracking 59
Figure 29: Previously attempted microthread seeding methods: post method (left) and v-well method (right). 65
Figure 30: Biological microthread seeding after 24 hours – PDMS v-well method 66

Figure 31: hMSCs delivered in close proximity to biological microthread bundle 73

Table of Tables

Table 1: Scaffolds used for MSC delivery in rodent models and MSC seeding counts 16
Table 2a: Biological microthread hMSC seeding count (old counting protocol) 44
Table 3: Biological microthread adjusted hMSC seeding count 46
Table 4: Microthread implantation experiment cell delivery results 50
Table 5: Intramyocardial injection experiment cell delivery results 50
Table 6: Localization of delivered hMSCs 63

Chapter 1: Introduction

The heart provides the body with essential nutrients and allows for the exchange of oxygen and carbon dioxide. Without this pump, the organs and tissue that make up the body would not function. Since the heart is of such an utmost importance, any decrease in its function would alter the function of the entire body. Myocardial infarction is the death of heart muscle that is generally caused by the blockage of a blood vessel (coronary artery) that supplies a region of the heart with blood. Scar tissue forms post-infarction over the dead tissue where the cardiac myocytes perished. This scar tissue is a very hostile environment for cells due to its decreased blood flow and acidic pH. Scar tissue is also non-contractile, which reduces the overall cardiac output of the heart [1].

A majority of cardiac myocytes do not proliferate. At the age of 25 about 1% of myocytes proliferate annually, and 0.45% at the age of 75 [2]. It has been reported that this number increases to a maximum of 4% after a myocardial infarction [3]. However, clinically the heart is unable to regenerate itself [4]. The scar tissue that forms post-infarction has different mechanical properties than the healthy myocardial tissue. Over time, this weakened part of the heart can begin to swell and form a ventricular aneurysm [5]. The current treatment methods for ventricular aneurysms include direct linear closure and endocardial patch plasty. Both methods require the removal of the infarcted tissue, however direct linear closure sutures the heart closed while endocardial patch plasty uses a patch to replace the excised tissue [6]. Endocardial patch plasty as well as direct linear closure aim to transform the heart from the spherical shape it forms post-infarction back into the healthy elliptical shape it is naturally. Both of these methods focus on restoring the shape of the heart. However, they do not restore the tissue that was lost during the infarction, which contributed to the overall function of the heart before the infarction occurred.

Cardiac regeneration is possible with cellular therapy. Human mesenchymal stem cells (hMSCs) have been utilized to improve cardiac function by increasing vascularity as well as limiting scarring in the infarction zone [7],[8]. One of the major problems with cardiac cellular therapy is associated with the cell delivery method. Current delivery methods are inefficient, with cell engraftment rates ranging from 1-25% depending on the method [9],[10]. The efficiency of a delivery method is defined as the number of cells that engraft in the heart wall divided by the number of cells that were initially delivered. Another issue with the current delivery methods is the inability to deliver cells directly to the endocardium, the innermost layer of the ventricular wall where most infarctions occur. Biomaterials are being researched to improve localization and efficiency of cell delivery. These biomaterials, which include fibrin, gelatin, and collagen, are being formed into three-dimensional scaffolds as well as gels that can be implanted directly on or in the ventricular wall to allow for local delivery [10-12]. These biomaterial delivery methods do have a higher engraftment rate than other non-localized delivery methods, but also have limitations. Cell retention is the main problem in gels, while nutrient delivery to seeded cells is the main problem in three-

dimensional scaffolds [11],[13]. These problems need to be overcome in order to consistently deliver cells to the heart post-infarction. Our main objective is to overcome these limitations by developing a delivery method using a new scaffold that will allow efficient, targeted delivery of cells to the ventricular wall.

Fibrin microthreads, which were first developed by Cornwell et al., are a novel form of fibrin that are shaped like suture and have significantly higher tensile strength than other forms of fibrin including fibrin gels and glue [14]. Fibrin is found naturally at the site of wound healing where it serves as a matrix for the attachment and migration of cells. Fibrin gels have been used to deliver cells to the infarcted myocardium in several studies [11, 15]. Cornwell et al. utilized the fibrin microthreads as scaffolds for tissue regeneration. Specifically, the fibrin microthreads were shown to allow fibroblast attachment, proliferation, and alignment [14]. Fibrin microthreads have also been proven to support human mesenchymal cell (hMSC) growth and viability by Murphy et al. [16] Implantation of fibrin microthreads is possible since we are able to connect fibrin microthreads to suture needles. Several designs, which allowed the connection of the fibrin microthreads to suture needles, were developed to ensure consistent fibrin microthread delivery. With a proper design, we are able to implant the fibrin microthreads *in vivo*.

Self-assembled collagen microthreads were developed as scaffolds for tissue regeneration. Other forms of collagen have been used to deliver cells to the infarcted myocardium [17, 18]. Human mesenchymal stem cells attach at a higher rate to fibrin microthreads than self-assembled collagen microthreads. However, in terms of mechanical properties, self-assembled collagen microthreads have nearly double the tensile strength of fibrin microthreads (9.05 MPa vs. 4.78 MPa) [19]. A scaffold that has both the superior cell seeding properties of fibrin microthreads and the high mechanical strength of collagen microthreads would be ideal for *in vivo* implantation. “Hybrid” microthread bundles were developed based on the concept of combining fibrin microthreads with collagen microthreads to create a scaffold with sufficient mechanical properties and cell seeding ability.

Intramyocardial injection surgery involves the injection of a bolus of cells directly into the myocardium. Other than knowing how deep the syringe needle has gone, the most apparent shortcoming of this cell delivery method is low cell engraftment since the cells easily reach the blood circulation and engraft in other organs such as the lungs. A large percentage of the cells are also pushed out of the heart wall due to the outward pressure that the heart applies when it contracts [4].

We hypothesize that biological microthreads will increase the efficiency of hMSC delivery to the beating rat heart compared to intramyocardial injection. The biological microthreads can be implanted into the ventricular wall, in close proximity to the endocardium. The biological microthreads will improve upon efficiency because the surgeon can implant the biological microthread bundle into the heart wall, close to the infarction area and therefore increase the chances of the hMSCs seeded on the biological microthreads engrafting in the infarction area.

Chapter 2: Background

The main objective of this project is to improve upon the current myocardial cell delivery methods by developing a novel approach for stem cell delivery to the infarcted myocardium. Since a novel approach is being developed, the underlying aspects that support and define the method must be explored. Previous work has been done by this lab that proves that biological microthreads are capable of serving as a scaffold for human mesenchymal stem cell (hMSC) delivery [16]. This background section will illustrate the fundamentals of cardiac anatomy and myocardial infarction as well as explore the current methods of cardiac cell delivery.

2.1: Healthy Myocardial Function and the Infarcted Myocardium

The heart is the main pump of the circulatory system that delivers nutrient-rich blood to the body. The heart is composed of four chambers, the left ventricle being the chamber where the highest pressures are reached. The wall thickness of each chamber depends on the maximum pressure reached during normal function. The innermost layer of the heart wall is known as the endocardium; the outermost layer is known as the epicardium [20]. Myocardial muscle cells (myocytes) are electrically connected with gap junctions that allow the propagation of action potentials to occur. The propagation of the action potential causes rhythmic contraction of the myocytes. When the heart contracts blood is pumped out of the ventricle and into the aorta and coronary arteries, supplying blood to the entire body [21, 22].

The myocardium has a coronary circulation which provides oxygen and nutrients to the myocytes. If any portion of the coronary circulation is blocked, a population of the myocytes may be starved. Initially, when the coronary circulation is occluded, the production of adenosine triphosphate in the heart is changed from a natural aerobic mechanism to a compromised anaerobic mechanism. The reason for this change is simply an insufficient supply of glucose and oxygen to the tissue. The result of this change is a dramatic decrease in the production of adenosine triphosphate. Myocytes require adenosine triphosphate to function and this dramatic decrease results in an inability of the muscle to contract. The energy reserve for adenosine triphosphate production, creatine phosphate, is then depleted shortly thereafter. The intracellular pH of the myocytes decreases as anaerobic glycolysis persists because of the buildup of hydrogen ion byproduct [23]. Osmosis causes water to enter the myocytes and as the heart tissue swells, cell death occurs due to edema. After several weeks or even months, scar tissue forms over the damaged tissue because of the infiltration of collagen depositing fibroblasts into the infarction. Further migration of monocytes, neutrophils, and macrophages to the infarction zone occurs due to the inflammatory response. Matrix metalloproteinases (MMPs) that are released from the neutrophils cause myocyte collagen degradation and infarction expansion [1].

The leading cause of death in the United States is cardiovascular disease [24]. Nine hundred twenty thousand people in the United States annually suffer from myocardial infarction. Myocardial infarction and coronary heart disease cost patients in the United States over $156 billion a year [25]. After a myocardial infarction occurs, 22% of men and 46% of women are diagnosed with heart failure within six years. At this point, the heart is unable to pump a sufficient amount of blood to the body's organs, significantly altering a patient's ability to perform even basic physical tasks.

2.1.1: The Rat Heart

The rat heart has a similar coronary circulation as a healthy human heart (Figure 1). Blood first enters the heart from the right atrium via the vena cava, passes through the tricuspid valve into the right ventricle, passes through the pulmonary valve into the pulmonary artery. The blood then travels through the lungs and is oxygenated, returns to the left atrium from the pulmonary vein, passes through the mitral valve into the left ventricle, and finally exits the heart by passing through the aortic valve into the aorta which delivers oxygenated blood to the body [26]. The key difference between the rat and human heart, other than size, is heart rate. The average rat heart beats at a rate of 400 beats per minute, while a healthy human heart beats at a rate of 70 beats per minute [27]. Despite this difference, the physiological similarities between the human and rat heart are the reason that the rat was chosen as a suitable model for assessing cardiac stem cell therapy. Future studies will also focus on delivering hMSCs in a rat myocardial infarction model and assessing cardiac function post-delivery. The rat heart can be infarcted by coronary artery ligation and utilized to study the effects of hMSC therapy on heart function [28, 29].

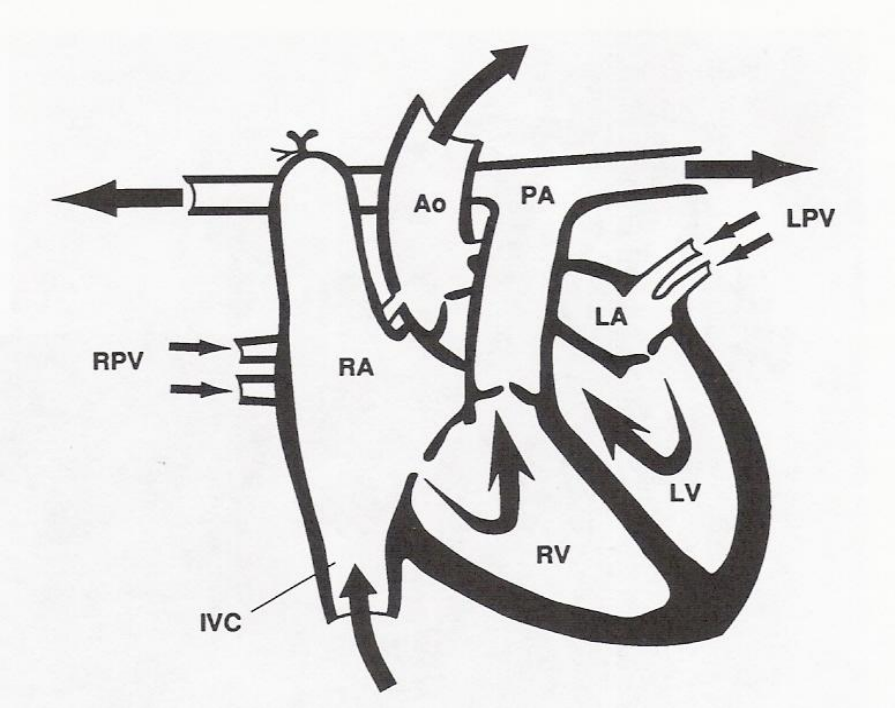

Figure 1: Rat heart blood circulation pathway [26]

2.2: Current Treatments for Myocardial Infarction

After a myocardial infarction, the heart cannot repair itself. Post-infarction scar tissue forms over the dead tissue where the cardiac myocytes perished. If the infarction is not treated, the scar tissue will begin to thin and the dimensions of the left ventricle start to change [30]. Myocardial infarction also has profound effects on the general function of the heart. Ejection fraction, the amount of blood in the ventricle that is ejected with each stroke of the heart, decreases depending on the size of the infarction. The normal stroke volume, the amount of blood ejected from the ventricle with each heart beat, is initially maintained despite the decrease in ejection fraction because of compensatory responses. The compensatory responses increase the stress in the ventricular wall because of the extra pressure and volume applied. The increase in stress can cause complications including aneurysms and rupture [30].

The current treatments for myocardial infarction only strive to treat the effects of infarction by performing bypass surgery or restoring the normal shape of the heart from a spherical shape to the natural, more efficient elliptical shape. A typical procedure that restores blood flow is coronary artery bypass grafting, or CABG. However, CABG does not actually treat the infarct [31]. Surgical ventricular restoration is a more recent procedure that is gaining popularity as clinical trials demonstrate its

effectiveness [32]. There are two possible procedures for ventricular restoration, endocardial patch plasty and direct linear closure [6].

Direct linear closure requires the surgeon to remove the infarcted myocardium and suture the heart tissue back together. The main goal of this surgery is to restructure the size and shape of the heart. Since a portion of the myocardium is being removed, the closure is not always perfect, resulting in less than optimal dimensions. If the infarction size exceeds a certain size, endocaridal patch plasty is performed instead of direct linear closure. Endocardial patch plasty requires a patch to be sutured in place of the infarcted tissue [33]. The specific procedure is known as the Dor procedure and requires the heart to be completely arrested. Coronary revascularization is required to allow blood flow to reach the epicardial layer of the heart wall and maintain the infarct thickness [31]. The infarction is then excised and a balloon is inflated in the left ventricle to guide the restoration of the heart. A suture is utilized to tighten the ventricle to the shape of the balloon. Once this step is completed, a biomaterial patch of polytetrafluoroethylene (PTFE) or polyethylene terephthalate (PET) is used to replace the excised tissue and close the remaining gap in the heart wall. The purpose of the patch is to prevent further changes in the shape and volume of the ventricle [33, 34].

The surgical techniques in this section focus on restoring the ventricular dimensions and pressures. None of them aim to regenerate the cells that are lost when a myocardial infarction occurs. There are several issues with the materials which are used for endocardial patch plasty that can affect the life of the patient. These materials have been shown to form large regions of fibrosis and are nearly four orders of magnitude stronger than the heart muscle, causing a large discrepancy in the mechanical properties. Despite all of the surgical effort required for these procedures, the overall function of the heart remains compromised because the infarcted tissue does not contribute.

2.3: Myocardial Cellular Therapy

Cardiac regeneration has become the focus of cardiac cellular therapy. Instead of excising the infarcted tissue, cellular therapy aims to restore the tissue back to its functional form. A variety of cell types, including bone marrow stem cells, skeletal myoblasts, embryonic stem cells, and cardiac stem cells have been employed for myocardial cellular therapy [35-38]. Embryonic stem cells are controversial and currently increase the risk of tumor formation. Skeletal myoblasts do not have the ability to electrically couple with cardiac myocytes. There is still no agreement in the scientific community about the existence of cardiac stems cells. Sufficient quantities of fetal cardiomyocytes cannot be obtained for effective clinical use [39-41]. Based on all of these factors, human mesenchymal stem cells (hMSCs) were chosen to pursue cardiac regeneration.

Human mesenchymal stem cells only represent 0.001% to 0.01% of the total nucleated cells in the bone marrow, where they are acquired [42]. They are able to differentiate into several different tissue types including fat, cartilage, and bone. They also are adherent and multipotent cells. In terms of tissue regeneration, these cells are ideal due to their relatively high proliferation rate, genetic stability, and ease of isolation [40, 42, 43]. For cardiac regeneration, hMSCs have been shown to induce angiogenesis, differentiate into a cardiac myocyte-like phenotype after being delivered to the heart, and are capable of being utilized allogeneically without causing an immune response [41, 42, 44].

Researchers have delivered hMSCs to the heart and discovered many improvements in cardiac function post-delivery. Improvements include an increase in ventricular performance and a decrease in infarction size [13, 35, 45-48]. Researchers have also shown the potential these cells may have to differentiate into myocytes and possibly release cytokines or growth factors, which could encourage the natural repair of the heart [13, 35, 48]. In 2009, Hare et al. completed clinical trials in which allogeneic hMSCs were delivered intravenously to humans. The trials were double-blind, placebo-controlled, dose-escalating, and multi-center. Fifty three patients were enrolled for the 6-month trial period from 10 different study centers. The trial concluded that hMSCs did not increase toxicity when compared to placebo, the hMSC treated group had four times fewer arrhythmia events, and the hMSC group had a significant increase in left ventricular ejection fraction [49].

Even though hMSCs have demonstrated their positive potential when delivered to the heart, the exact mechanism that is responsible for these improvements is not completely understood. There are several theories currently: differentiation of delivered hMSCs, cell fusion, a presence of passive cells in the myocardial wall, and paracrine signaling [50]. Despite the controversy surrounding the mechanism by which hMSCs improve cardiac function, researchers agree that hMSCs restore a portion of cardiac function. For this reason, hMSCs will be the cells delivered to the heart for this project.

2.3.1: Current Drawbacks of Cellular Therapy

As shown in this section, cellular therapy has a great deal of potential. However, there are limitations that hinder the extent of the positive impact that these cells are capable of. A majority of the limitations are due to the delivery method and include insufficient localization, cell retention, cell survival, and a lack of a matrix for cell attachment that can result in cell death [4, 39, 41, 51].

Intramyocardial injection requires the injection of a certain volume of cell suspension directly into a myocardial infarction. The limitation of this delivery method is that once the syringe needle is removed, the cells are pushed out due to the contraction of the heart [4]. The main problem with systemic delivery is the lack of localization. When cells are delivered systemically, a majority of the cells engraft in organs other than the heart including the liver, lungs, and spleen [47, 52]. For this delivery method the

cells are suspended in either media or phosphate buffered saline (PBS). After injection, there is low cell attachment and a high rate of cell death. These limitations strongly affect the myocardial engraftment rate, which ranges from 1 to 10% [4, 40].

Hou et al. injected peripheral blood mononuclear cells (PBMNCs) intramyocardially and determined delivery efficiency in the ischemic swine heart. It was determined that the delivery efficiency was 11 ± 3% and when compared to intracoronary (IC) and interstitial retrograde coronary venous (IRV) delivery, intramyocardial injection (IM) had the highest delivery variability and efficiency. It was also found that 43 ± 3% (IRV), 26 ± 3% (IM), and 47 ± 1% (IC) of the cells were found in the lungs for each of the respective delivery methods. These numbers are startlingly large and with certain cell types may cause unwanted consequences [53].

Since the engraftment rates of current hMSC delivery methods are so low, the number of cells delivered must be optimized to overcome these limitations. Researchers currently deliver between 500,000 to 50,000,000 cells to each animal subject [35, 44, 47, 52, 54]. Table 1 illustrates typical cardiac cell delivery numbers to rodent models with various scaffold types. The number of cells that engraft can be calculated using the percent engraftment reported by the researcher.

Type of cell	Animal Model	Cell Count	Scaffold	Reference
Bone marrow-derived mononuclear cells	Rat	8×10^6 cells/cm^2	PGCL polymer	[55]
Bone marrow MSCs	Rat	1×10^5 cells/cm^2	Bovine pericardium	[56]
Bone marrow MSCs	Mouse	1×10^6 cells/cm^2	Collagen matrix	[57]
Bone marrow MSCs	Rat	2.2×10^6 cells/cm^2	Type I collagen-GAG scaffold	[58]
Bone marrow cells	Rat	1×10^7 cells/cm^2	PGAC cloth	[59]
Bone marrow MSCs	Rat	1×10^6 cells/cm^2	PLCL scaffold	[60]
Bone marrow MSCs	Rat	5×10^4 cells/cm^2	Acellular bovine pericardium	[12]

Table 1: Scaffolds used for MSC delivery in rodent models and MSC seeding counts

2.4: Cardiac Regeneration with Biomaterials

The limitations of myocardial cellular therapy are largely due to inefficiency of the current cellular delivery methods including cellular cardiomyoplasty and systemic delivery. Biomaterials aim to improve cell delivery by allowing the control of the cellular microenvironment, which in turn allows researchers to command cell behavior [61]. When using biomaterials for the creation of a scaffold, several scaffold properties must be considered including degradation rate, porosity, cell adhesion, size, and compliance [10, 39, 61]. Numerous scaffold designs have been created for use in cardiac applications using gelatin, fibrin, collagen, and alginates in the form of gels or 3D scaffolds [9-12, 15, 62-66].

Alginate is a natural polysaccharide that is derived from brown seaweed. Alginate is used in gel and 3D sponge form for cell delivery to the infarcted heart [67]. Leor et al. was able to create a cardiac graft using a cell seeded alginate sponge. Other researchers have had similar success with alginate due to its hydrophilic nature, biocompatibility, neovascularization *in vivo*, and adjustable porosity [10, 67-69]. The drawback of alginate is its inability to interact with mammalian cells because of a lack of arginine-glycine-aspartic acid (RGD) ligands that allow cell adhesion. To overcome this limitation, alginate is often covalently modified with this ligand [67].

Gelatin sponges are biomaterials composed of purified porcine skin gelatin [70]. Li et al. and Akhyari et al. have utilized gelatin sponges for culturing and delivering cells to the heart. Gelatin sponges are biodegradable and support cell attachment and cell contraction. Gelatin sponges also have shortcomings including, natural thrombogenicity and a high level of porosity which make it unsuitable for blood contacting applications [70-72].

Collagen is the most abundant protein in mammals. It is also known as the primary component of connective tissue. Collagen has been used successfully in cardiac applications for cell delivery and contraction. Like alginate, collagen comes in many forms; gels or 3D sponges are most common [9, 62, 73]. Collagen has several properties that demonstrate its potential as a scaffold including cell attachment, cell proliferation, high hydrophilicity, and degradability. Veritas™ is an example of a 3D collagen matrix that can be utilized to deliver cells to the heart.

Fibrin is created during the wound healing process and serves as a provisional matrix for cell attachment and migration. Thrombin is produced at the site of a wound and fibrinogen naturally circulates in the blood. When fibrinogen and thrombin are combined, a fibrin clot is created to halt bleeding and assist in healing [74, 75]. Thrombin and fibrinogen are also available commercially and allow the creation of fibrin sealants and glues [37]. Fibrin naturally has RGD binding motifs that allow cell adhesion, can potentially be created with autologous thrombin and fibrinogen, is angiogenic, and is FDA approved for clinical use [11, 76, 77].

Currently, the biggest challenge for injectable gel mediated cell delivery is cell and gel retention. However, cell survival is improved with these gels [11, 37, 65]. 3D scaffolds used for infarction regeneration, on the other hand, have other shortcomings that include insufficient nutrient diffusion and vascularization [11, 13]. Since these 3D scaffolds are usually approximately 2-4 mm thick, nutrients cannot diffuse through the entire thickness. Nutrients can only diffuse through a maximum depth of 150 μm [4]. Since a majority of the scaffold will not contain nutrients, a large quantity of the cells seeded on the scaffold will not remain viable when implanted. For this reason, a new type of scaffold must be developed to improve cell viability and targeted cell delivery in a myocardial infarction. A new type of scaffold should degrade at a rate that allows cell engraftment while not interfering with cardiac function. Angiogenesis must also be induced to ensure proper nutrient flow via new blood vessels [61].

2.4.1: Collagen and Fibrin Microthreads

Type I collagen microthreads were originally developed to repair ligaments and tendons because of the similarities in mechanical properties. Type I collagen microthreads allow for cell attachment and proliferation to occur and do not lose strength after 20 days of cell culture. In fact, these collagen microthreads exhibited increased strength after being seeded with cells [78-82]. The main purpose of using collagen microthreads in the heart is mechanical reinforcement. When the suture needle pulls the microthread bundle through the wall of the heart it causes weaker materials to fail, like fibrin microthreads. For this reason, collagen microthreads were used.

Discrete fibrin microthreads, developed by Cornwell et al., are another novel scaffold type which was developed for tissue regeneration. Fibrin microthreads allow cell migration, control cell orientation, and provide cell signaling [19]. Fibrin microthreads were first evaluated by Cornwell et al., and were determined to have higher tensile strength than fibrin gels. Cornwell et al. also demonstrated that fibrin microthreads support fibroblast alignment, growth, viability, and migration after 7 days of cell culture. Murphy et al. showed that fibrin microthreads also support human mesenchymal stem cell (hMSC) viability and proliferation, and allow the hMSCs to retain their pluripotency [16]. Murphy et al. were also able to seed the fibrin microthreads with a physiologically relevant (to the heart) quantity of hMSCs. In addition, fibrin microthreads can also be modified by crosslinking to increase tensile strength and loaded with growth factors to alter cellular function [14, 19].

Fibrin and collagen microthreads are promising scaffolds for cell delivery. Combining these two scaffold types into a single bundle increases tensile strength, by using collagen, while maintaining the cell seeding properties of fibrin. When bundled together, this hybrid scaffold can be used as an effective, localized cell delivery method. Like intramyocardial injection, biological microthread mediated hMSC delivery strives to deliver cells directly into the myocardial infarction, and is therefore a localized delivery

method. Delivery methods such as intravenous infusion rely on hMSCs homing to the myocardial infarction, and are therefore non-localized. Fibrin and collagen are biodegradable. Fibrin can be loaded with growth factors and is angiogenic. In terms of structure, fibrin and collagen microthreads are shaped like suture, and therefore can be used in a manner similar to suture. When bundled together, fibrin and collagen microthreads can be attached to a suture needle and the microthreads can be delivered into the heart wall, much closer to the actual infarction when compared to other localized cell delivery methods.

2.5: Cell Tracking with Quantum Dots

Since hMSCs are being delivered to the rat heart, cell tracking must be employed to distinguish the delivered cells from the cells that already populate the heart. Cells can be labeled with particles in order to employ positron emission tomography (PET) or magnetic resonance imaging (MRI). However, these methods are relatively expensive due to the equipment they require and can only track greater than 10,000 cells [83]. Secondary staining (LacZ for example) is also an option, but false positives are too commonly generated [84]. In addition, secondary staining is time intensive.

Fluorescent cell tracking utilizes fluorescent proteins, polymethines, or inorganic/organic hybrids to emit light at a specific wavelength when exposed to ultraviolet light [85]. Fluorescent dyes and green fluorescent proteins are difficult to distinguish in the heart due to an abundance of autofluorescence [4]. An important advantage to using fluorescent cell tracking is the ability to track cells with any fluorescent microscope. Quantum dots, specifically, are fluorescent nanocrystals that are about 10-20 nm in size [86]. Rosen et al. determined that quantum dots enter hMSCs via endocytosis after 24 hours of incubation in quantum dot solution [87]. Quantum dot filters, which were used to view quantum dot signal under a fluorescent microscope, also elicit minimal heart tissue autofluorescence. Compared to other filters, which allow an excessive amount of autofluorescence to pass through, the quantum dot filter ensures that loaded cells are easily found.

Chapter 3: Hypothesis and Specific Aims

We hypothesize that biological microthreads will increase the efficiency of hMSC delivery to the beating rat heart compared to intramyocardial injection. The rat heart will be sectioned and histologically analyzed after the desired implantation time of the biological microthreads. We will implant biological microthreads and inject a bolus of hMSCs intramyocardially in different *in vivo* groups and compare the different methods. The biological microthread implantation group will also be analyzed to determine the location of the delivered hMSCs.

Specific Aim 1: Compare engraftment of hMSCs in the rat heart (intramyocardial injection vs. biological microthreads)

For this specific aim, we hypothesize that more hMSCs will engraft in the rat heart with biological microthread cell delivery versus intramyocardial injection. In order to test this specific aim, we bundled 8 fibrin microthreads with 4 collagen microthreads and attached this bundle to a suture needle. We first loaded our hMSCs with 655 ITK carboxyl quantum dots for cell tracking. We then seeded the biological microthreads with hMSCs and incubated them for 1 day. After incubation, the cell seeded microthreads were implanted in the rat heart for one hour. In the intramyocardial injection group, a bolus of 10,000 hMSCs was injected into the myocardial wall of the left ventricle. One hour after implantation, the rat was euthanized and the heart was removed for histological analysis. The heart was sectioned next after being frozen in O.C.T. into 8 µm thick sections. Three sections were histologically analyzed every 480 µm using Hoesct dye to visualize cell nuclei. Each microscope image was taken with two filters: the Hoechst and quantum dot filter. These two images were merged using ImageJ software to confirm that the images contained quantum dot loaded hMSCs. The quantum dot loaded cells were then manually counted. These counts were used to calculate hMSC delivery efficiency to the rat heart. Delivery efficiency illustrated the potential effectiveness of each delivery method.

Specific Aim 2: Determine localization of hMSCs in the rat heart for biological microthread delivery

For this specific aim, we hypothesize that the biological microthreads will uniformly deliver hMSCs throughout the length of the implant. We also hypothesize that the biological microthreads will deliver cells to the entire thickness of the left ventricular wall. To test this, we first seeded quantum dot loaded hMSCs on hybrid bundles of fibrin-collagen microthreads which were attached to suture needles. The hMSCs were then incubated on the microthreads for 1 day. After incubation, the cell seeded

microthreads were implanted in the rat heart for 1 hour and the rat was euthanized. After euthanization, the heart was removed for histological analysis. The rat heart was then sectioned into 8 μm thick sections after being frozen in O.C.T. Compound. One section was histologically analyzed every 480 μm using Masson's trichrome staining to determine the location of the biological microthread implantation. Each microscope image was taken at 5x magnification and Adobe Photoshop software was used to determine the distance of the biological microthread from the endocardium and the epicardium of the left ventricular wall in the rat heart. These distances were graphed to illustrate the location of the microthread in the left ventricular wall for the entire length of the implantation. The hMSC delivery distribution along the length of the microthread bundle was determined using the method described in Specific Aim 1 to determine the engraftment rate (three Hoechst dyed heart sections analyzed every 480 μm).

Chapter 4: Materials and Methods

In this section, the protocols used to accomplish our specific aims will be described. Collagen and fibrin microthread production and hMSC seeding on these microthreads will be detailed. The surgical procedure used to implant the biological microthread bundles as well as how the heart will be sectioned and histologically analyzed will also be discussed.

4.1: Collagen and Fibrin Microthread Production and Seeding

Collagen microthreads were created using a previously established protocol [88]. Type I collagen was first extracted from rat tails using a previously published procedure [89]. The type I collagen was then extruded through 0.86 mm diameter polyethylene tubing (Becton Dickinson, Inc., Franklin, NJ), using a syringe pump (KD Scientific, New Hope, PA), at a flow rate of 0.7 mL/min. The type I collagen threads were extruded into a fiber formation buffer bath (pH 7.42, 135 mM NaCl, 30 mM TrizmaBase (Tris), and 5 mM NaPO4 dibasic; Sigma, St. Louis, MO) which was maintained at a temperature of 37^0C. After 24 hours, the microthreads were moved into fiber incubation buffer (pH 7.42, 135 mM NaCl, 10 mM Tris, and 30 mM sodium phosphate dibasic, Sigma) which was maintained at a temperature of 37^0C. After 24 hours, the microthreads were moved into and kept in distilled water for 24 hours at 37^0C. Lastly, the microthreads were taken out of the water bath, air dried, and stored in a desiccator at room temperature before usage (see Figure 3).

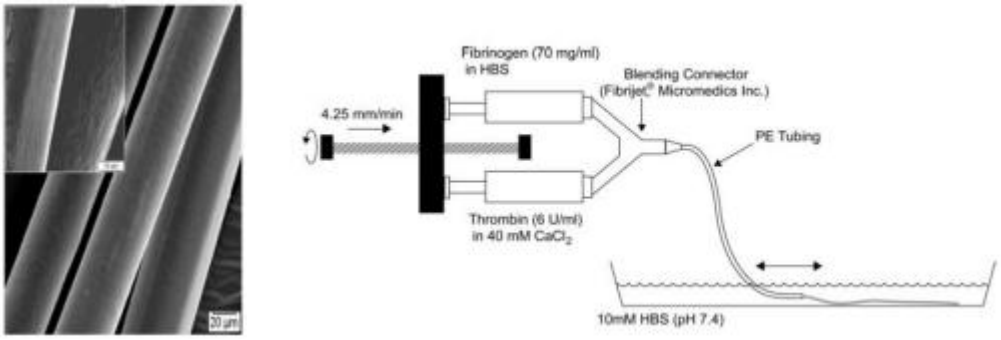

Figure 2: Fibrin microthread scanning electron micrograph (left) and extrusion diagram (right) [19]

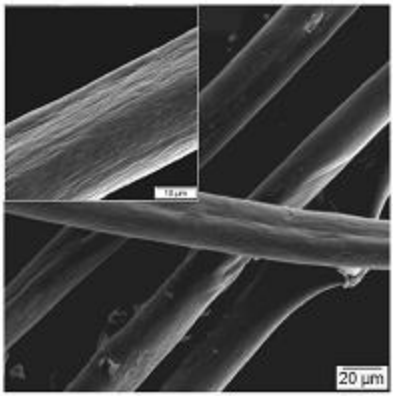

Figure 3: Collagen microthread scanning electron micrograph [19]

Fibrin microthreads were created using a previously established protocol [19]. Two separate 1 mL syringes were each filled with thrombin and fibrinogen taken from bovine plasma (Sigma Aldrich, St. Louis, MO). A blending application tip was used to combine the thrombin and fibrinogen and the combined solution was extruded through 0.38 mm polyethylene tubing (Beckton Dickinson, Franklin Lakes, NJ) into a 10 mM HEPES, 7.4 pH bath that was kept at room temperature (see Figure 2). After 15 minutes in the bath, the microthreads were taken out and air dried.

The mechanical properties of the individual fibrin and collagen microthreads were insufficient to be implanted in the rat heart. Fibrin microthreads that were bundled together also lacked the ability to be implanted in the rat heart due to insufficient mechanical properties. Individual fibrin and collagen microthreads also have very little surface area for cells to attach to. For these reasons, we grouped together the collagen and fibrin microthreads into a single microthread bundle. Bundling the microthreads was performed by placing eight fibrin and four collagen microthreads adjacent to each other and dragging a droplet of distilled water along the length of them until they formed a single bundle (see Figure 4). Bundling these microthreads increases total surface area which augments cell seeding capacity, increases the probability of successful implantation, and creates grooves in between the individual microthreads to improve initial cell attachment.

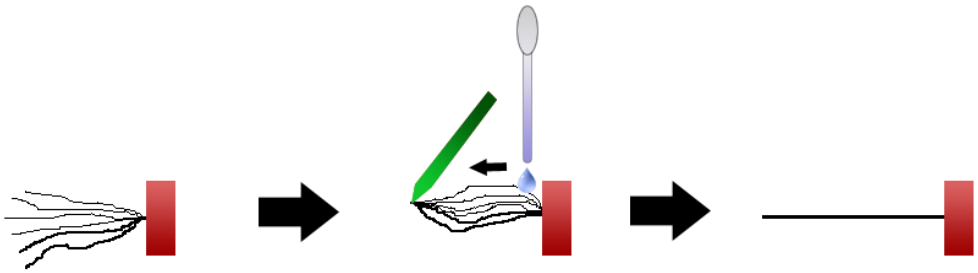

Figure 4: Microthread bundling

The day before seeding the microthread bundles, the hMSCs were quantum dot loaded for cell tracking. The quantum dot media was created by adding Qdot 655 ITK™ carboxyl quantum dots (1.025µL qdot solution per 1 mL media, Invitrogen Q2132MP, Carlsbad, CA) to Mesenchymal Stem Cell Growth Medium (MSCGM: 10% mesenchymal stem cell growth supplement, 2% L-glutamine, 0.1% gentamicin sulfate/amphotericin-B in mesenchymal stem cell basal medium, Lonza, Walkersville, MD). The next step was to remove the media from the flask of hMSCs and replace it with the quantum dot media. The hMSCs were then placed in a 37^0C, 5% CO_2 incubator for 24 hours and then rinsed with sterile PBS prior to seeding.

In order to seed the microthreads, the microthread bundles were first attached to suture needles then placed into a bioreactor that consisted of 1.98 mm I.D. Silastic tubing (Dow Corning, Midland, MI) sealed with side clamps (see Figure 5). A 27G needle was used as an inlet port to sterilize and eventually seed the microthread bundle. In order to prepare for sterilization, the microthreads were rehydrated by adding PBS, via the 27G needle, to the bioreactors for 15 minutes. The PBS was removed and replaced with 70% ethyl alcohol, via the 27G needle, for 1 hour. The final step was to rinse the microthreads for 15 minutes, three times with sterile PBS via the 27G needle.

Ten minutes after the removal of the sterile PBS, the biological microthread bundles were seeded with hMSCs. Seeding the microthreads involved first trypsinizing human mesenchymal stem cells (Lonza, Walkersville, MD) then centrifuging and suspending them at a concentration of 1,000,000 cells/mL in Mesenchymal Stem Cell Growth Medium (MSCGM: 10% mesenchymal stem cell growth supplement, 2% L-glutamine, 0.1% gentamicin sulfate/amphotericin-B in mesenchymal stem cell basal medium, Lonza, Walkersville, MD). For all mesenchymal stem cell based experiments, passage 4-9 cells were used. One hundred microliters of cell suspension was injected into the bioreactor with one side clamp removed to allow air to escape. Ten microliters of cell suspension was put on a 4 well chamber slide to ensure proper quantum dot loading of the hMSCs. The bioreactors were then put into 50 mL conical tubes with holes cut into them to allow oxygen to reach the cells. The conical tubes were then put

into a MACSmix™ rotisserie (Miltenyi Biotec, Bergisch Gladbach, Germany, see Figure 6) and the rotisserie was placed into a 37^0C, 5% CO_2 incubator for 24 hours while spinning the cells at 4 rpm. This allowed the cells to adhere to all sides of the microthread bundle. After 1 day of culture, the microthread bundles were removed from the incubator and implanted in the rat heart.

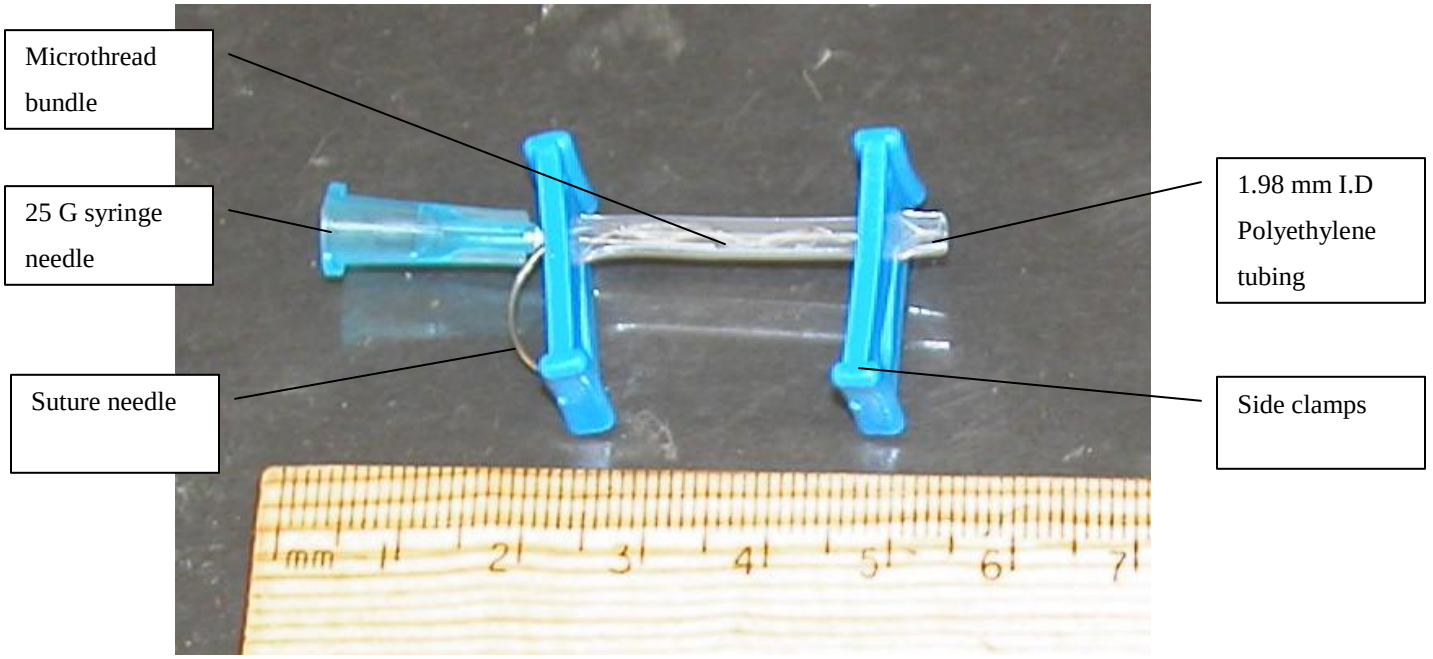

Figure 5: Biological microthread seeding diagram

Figure 6: Microthreads placed in tube rotator

4.2: Quantifying Cells Seeded on Biological Microthreads

Quantifying the number of cells on each microthread bundle allowed the calculation of cell delivery and seeding efficiency. After seeding the microthreads with hMSCs, one microthread bundle was stained with Hoechst (nuclear stain) and Phalloidin (f-actin filament) stain and two others were trypsinized in order to count the seeded cells with a hemocytometer. These two methods will be described in detail in this section.

4.2.1: Qualitative analysis of cell seeding using Hoechst dye and Phalloidin stain

After one day of culture, one microthread bundle was used for qualitatively analyzing cell seeding with Hoechst and Phalloidin staining. The microthreads were first removed from the bioreactors and suture needles and placed on glass slides. The microthreads were then rinsed with PBS, fixed in 4% paraformaldehyde (Boston Bioproducts, Worcester, MA), and rinsed with PBS twice for 5 minutes. The microthreads were then permeabilized with 0.25% Triton X-100 in PBS for 10 minutes, blocked with 1% bovine serum albumin in PBS for 10 minutes, and stained with Alexa Fluor 488 conjugated phalloidin (5µL stock solution in 200µL PBS, Invitrogen A12379, Carlsbad, CA) for 30 minutes to help discern the f-actin filaments in the cytoskeleton. The microthreads were then rinsed three times for 10 minutes with 1% bovine serum albumin in PBS and counterstained for 5 minutes with Hoechst dye (Cambrex Bio Science, Charles City, IO) at a 1:6000 concentration to help distinguish the cell nuclei (see Figure 7 for an example).

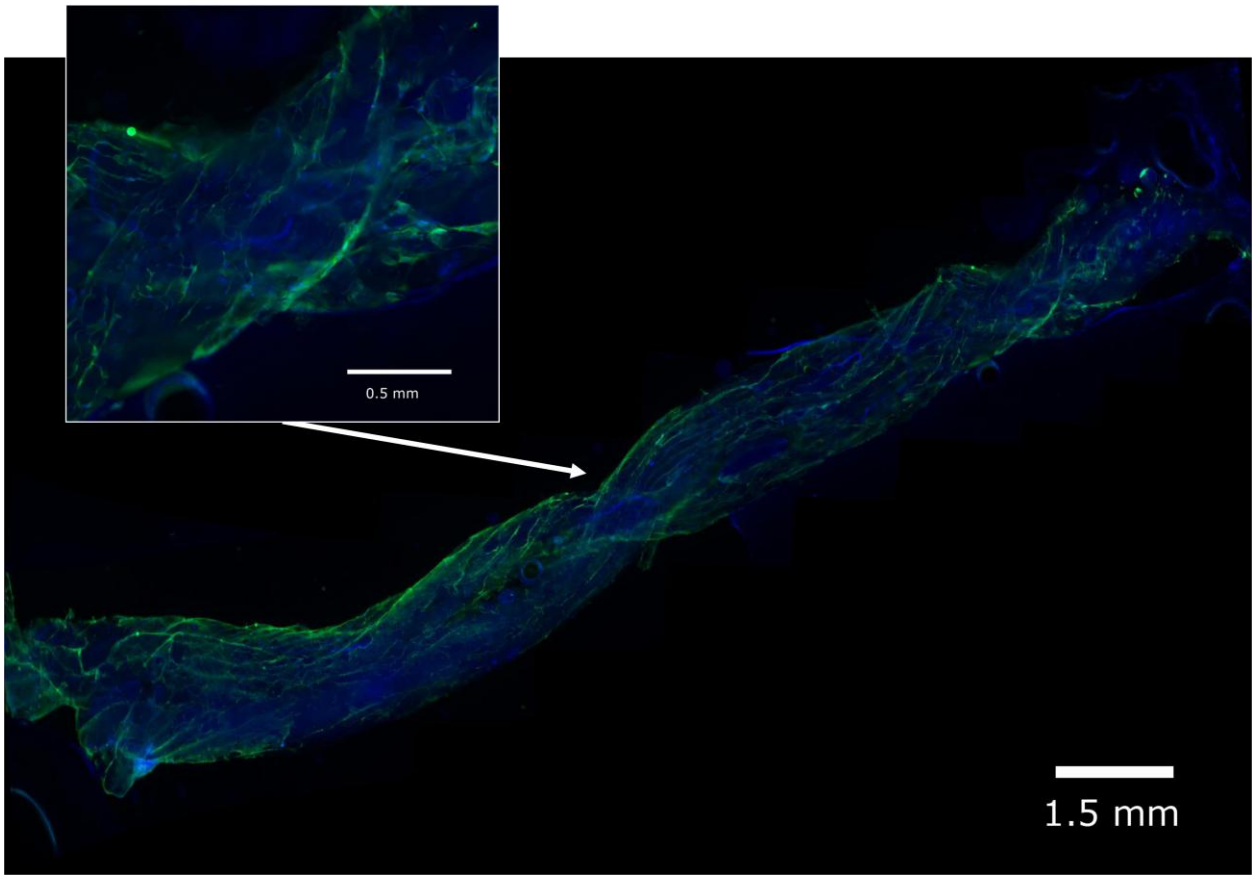

Figure 7: Whole 2 cm length of a biological microthread bundle after 1 day of seeding with hMSCs
(5x magnification for picture on top left, nine 5x pictures merged together for center picture, Hoechst dyed nuclei are blue, Phalloidin stained f-actin filaments are green).

Cell seeding was qualitatively analyzed by locating and imaging the cells on the microthread with a fluorescent Leica DM LB2 microscope (see Figure 7). In the next section, counting hMSCs after they have been trypsinized off of the biological microthreads will be described. However, on some occasions trypsinization was not 100% effective. Any biological microthreads that were not digested after trypsinization, usually collagen microthreads, were stained with Hoechst and Phalloidin staining to ensure that all cells have detached (see Figure 8).

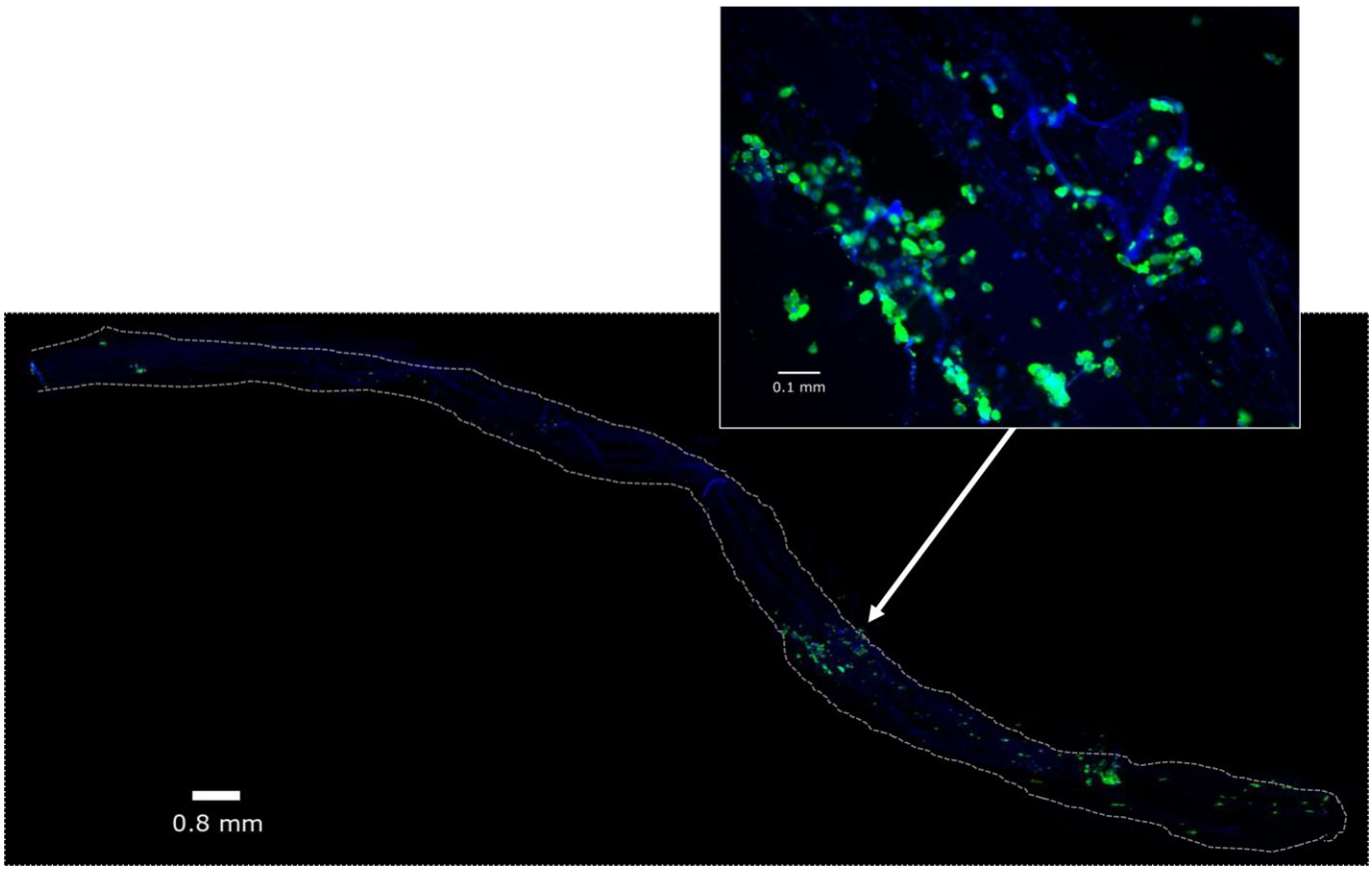

Figure 8: Trypsinized whole biological microthread bundle
(5x magnification for picture on top right, nine 5x pictures merged together for center picture, Hoechst dyed nuclei are blue, Phalloidin stained f-actin filaments are green). This image illustrates that on some occasions, hMSCs were still attached to the microthread bundles, usually collagen, after 30 minutes of trypsinization.

4.2.1: Quantification of cell seeding using a hemocytometer

Hoechst and phalloidin staining provide an excellent visual representation of cell seeding on biological microthreads, but was not utilized to quantify cell seeding due to several key limitations. One of the limitations is that the rat DNA, which is on the surface of the collagen microthreads that are used in the microthread bundle, emits positive signal when stained with Hoechst dye. Rat DNA is on the surface of the collagen microthreads because the type I collagen used to make the microthreads was isolated from rat tails. This signal makes it very difficult to locate and count the hMSC nuclei that the Hoechst dye stains, resulting in a time consuming process. Finally, all of the cells on the microthread bundles cannot be seen because of the three dimensional nature of the large 12 biological microthread bundle size. In addition to the limited depth of field, the 2D projection of the 3D microthread bundle limits accuracy. The microthread bundles overlap and therefore can potentially cover a large population of cells.

Since there are numerous limitations to manually counting cells on microthread bundles, including reproducibility, visibility of cells, and autofluorescence, this method was not utilized in this

project. Hemocytometers are commonly used to count human mesenchymal stem cells (as well as other cell types) in many applications, including passaging and seeding biomaterials. Since hemocytometers are well-established for counting cells, it was determined to utilize them to count cells that are trypsinized off of biological microthreads. The microthreads were first removed from the bioreactor and rinsed with PBS. They were then placed in a 1.7 mL microcentrifuge tube with trypsin (at 37^0C) for 30 minutes. While in trypsin, the microthreads were agitated every 5 minutes to maximize cell detachment. The trypsin was then inactivated with Mesenchymal Stem Cell Growth Medium (Lonza, Walkersville, MD) and the microthread bundle in solution was centrifuged at 10,000 rpm in the conical tube for 10 minutes. The supernatant was then removed and fresh Mesenchymal Stem Cell Growth Medium (Lonza, Walkersville, MD) was added to the cells. The cell suspension was added to Trypan blue solution (Invitrogen, Carlsbad, CA) and mixed. The combined Trypan blue/cell suspension was transferred into the hemocytometer and the cells were counted.

4.3: Delivering hMSCs to the Rat Heart

The delivery of hMSCs to the rodent heart was the main focus of this research. The novel method which we introduced, biological microthread implantation, was compared to intramyocardial injection. In order to compare these two methods, the delivery efficiency was quantified. Analysis of implantation position within the myocardium also helped define the surgical consistency of our microthread bundling design and determine whether the implantation procedure was reproducible. The best way to test the effectiveness of our microthread bundling design was to implant the microthread bundle into the beating, live rat heart. This section will describe the surgical procedure to implant seeded biological microthreads and inject a bolus of hMSCs into the rat heart.

All procedures that were performed on animal subjects were approved and overseen by Worcester Polytechnic Institute's Institutional Animal Care and Use Committee (IACUC). The IACUC protocol number was 08-01.

4.3.1: Biological Microthread Implantation and Intramyocardial injection

The surgical procedure to implant biological microthreads was relatively straightforward and was intended to be easily reproducible. First, the left lateral region of the rat was shaved, concentrating on the rib cage to ensure a clean incision surface. The Sprague-Dawley rat (Charles River Laboratories, Wilmington, MA) was then intubated with a 16 gauge catheter. The shaved area was then sterilized with three alternating applications of 70% ethanol and betadine. The catheter was then attached to a ventilator (Columbus Instruments, Columbus, OH) and the rat was covered with sterile surgical drapes. Isoflurane was administered (at 2%, titrated to effect) once the rat was connected to the ventilator via a vaporizer. An incision was made above the 5^{th} intercostal space to gain access to the muscle layer. The thoracic

cavity was reached by carefully cutting the muscle layer with iris scissors and impeding excessive bleeding with a cauterizer. Rib spreaders were used to maintain visibility of the thoracic cavity and ensure proper implantation of the microthreads or injection of the hMSCs. A cotton applicator was carefully used to move the lungs and gain access to the heart. The stem cell seeded biological microthread bundle was then passed through the anterior wall of the left ventricle (from just below the base of the heart to just above the apex) with a half-circle tapered size 18 suture needle (Securos Surgical, Fiskdale, MA). The biological microthreads were then cut from the suture needle and left implanted. Instead of implanting biological microthreads, intramyocardial injection required the injection of a bolus of hMSCs into the left ventricle of the rat heart. Thirty-five μL of cell suspension (10,000 hMSCs) was drawn into a 100 μL syringe (Hamilton Company, Reno, Nevada) with a 27 gauge syringe needle attached (Becton Dickinson and Co., Franklin Lakes, NJ) and then injected into the left ventricular wall of the rat heart. One hour later, the rat was euthanized and the heart was removed for histological analysis for both the intramyocardial injection and biological microthread implantation groups.

4.4: Histological Analysis of the Rat Heart Post-Implantation or Injection

The rat heart was histologically analyzed in order to determine the results of the surgical implantation experiments. The rat hearts utilized for both the intramyocardial injection and biological microthread implantation groups underwent the same histological analysis. Once the heart was removed from the rat it underwent fixation, sectioning, and staining. The histological analysis steps are detailed below.

4.4.1: Heart sectioning and preparation

At the conclusion of the surgical aspect of the experiment (1 hour after implantation) the rat heart was removed. Once the rat heart was removed it was cut in half, bisecting the microthread or injection site. The heart was rinsed with PBS to remove excess blood and then immediately placed in 4% paraformaldehyde for 24 hours to allow for proper fixation. After fixation, the rat heart was then placed in 30% sucrose for 24 hours. Each half of the rat heart was then placed (cut end of heart facing down) in a separate Peel-A-Way® Disposable Embedding Mold (Polysciences Inc., Warrington, PA) and covered with O.C.T. Compound (Sakura Finetek USA Inc., Torrance, CA). The two rat heart halves were then placed in a freezer and the O.C.T. compound was allowed to harden. Once the O.C.T. compound was completely frozen, the block containing half of the heart was placed in a Leica CM3050 cryostat (Leica Microsystems, Bannockburn, IL) and 8 μm thick heart sections were cut and placed on VWR® Micro Slides (VWR International, West Chester, PA). These microscope slides were stored in a freezer after sectioning in order to preserve the heart sections. A schematic of this process is shown below in Figure 9.

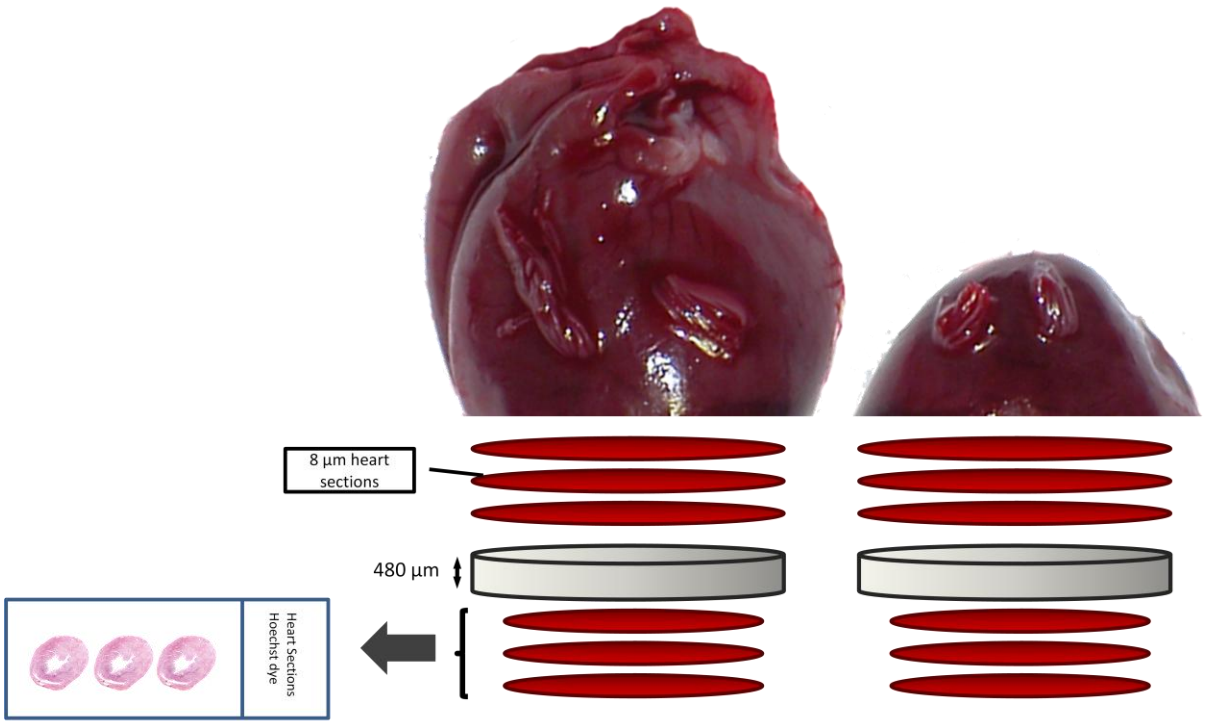

Figure 9: Bisecting and sectioning the rat heart

4.4.2: Heart section staining

In order to determine the results of the experiments, the heart sections that were cut had to be stained. Staining of the heart sections allowed the calculation of total cell delivery, cell delivery efficiency, and localization of cell delivery. The first step was to stain every twenty slides (from one end of the microthread implantation to the other) with Masson's trichrome to establish the location and orientation of the implanted microthread bundles. Masson's trichrome staining was not utilized for the intramyocardial injection experiments since only cells were delivered. Hoechst dye (Invitrogen, Carlsbad, CA) was used to stain the next set of heart sections. Specifically, three 8 µm thick sections were stained with Hoechst dye and sixty 8 µm thick sections were omitted until the next three 8 µm thick sections were stained. This pattern was continued until quantum dot loaded hMSCs were no longer visible in the heart sections. The same pattern was also used to stain the heart sections with α-Actinin (Sigma-Aldrich, St. Louis, MO) and Hoechst counter-stain. α-Actinin staining was utilized to confirm that the quantum dot loaded cells were hMSCs and not striated cardiac myocytes.

In order to stain the heart sections with Masson's Trichrome, the following steps were performed: The heart sections (on microscope slides) were first rinsed with distilled water and then put in Bouin solution (Sigma-Aldrich HT10-1-128, St. Louis, MO) for 1 hour at 56^0C. The heart sections were then allowed to cool and washed with running tap water until the yellow color disappeared. The heart sections were stained with Weigert hematoxylin (Sigma-Aldrich HT107 and HT109, St. Louis, MO) next for 10

minutes. The sections were then washed with warm running tap water for 10 minutes. The sections were then stained in Biebrich scarlet-acid fuchsin solution for 5 minutes. The sections were then rinsed in distilled water and placed in Phosphomoybdic/Phosphotungstic acid solution for 15 minutes. The sections were stained in aniline blue solution next for 3 minutes and rinsed in distilled water. The sections were then placed in 1% acetic acid solution for 3 minutes and finally rinsed several times with tap water. An example of a Masson's Trichrome-stained section is shown in Figure 10.

Staining the heart sections with sarcomeric α-actinin was performed with the following protocol: the heart sections were first rinsed with PBS twice for 5 minutes. The heart sections were then permeabilized with 0.25% Triton X-100 in PBS for 20 minutes, blocked with 1.5% normal rabbit serum in PBS for 30 minutes, and then the monoclonal sarcomeric anti-α-actinin primary antibody was placed on the heart sections for 24 hours at 4^0C in a humidity chamber (1:400 in 1.5% normal rabbit serum, Sigma A7811, St. Louis, MO). The heart sections were then rinsed three times for 5 minutes with PBS and the Alex Fluor 488 rabbit anti-mouse secondary antibody was applied for 45 minutes (1:400 in 1.5% normal rabbit serum, Invitrogen A11059, Carlsbad, CA). The heart sections were rinsed three times for 5 minutes with PBS and counterstained for 5 minutes with Hoechst dye (Cambrex Bio Science, Charles City, IO) at a 1:6000 concentration.

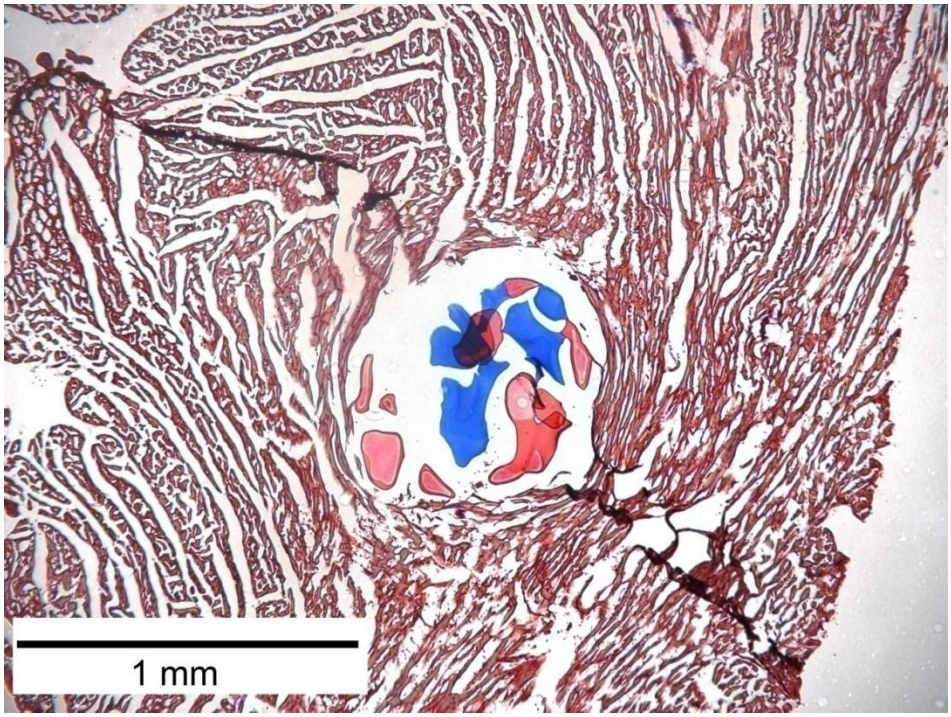

Figure 10: Masson's trichrome stained rat heart section
(5x magnification, collagen microthreads are blue, fibrin microthreads are red)

4.4.3: Counting and calculating cells delivered to the heart

Staining the heart sections allowed the visualization of the cell nuclei and microthread implant. Staining also confirmed that quantum dot loaded hMSCs were being delivered to the heart. However, quantum dot loaded cells were manually counted from the Hoechst dyed sections. Examples of quantum dot loaded hMSCs can be seen in Figure 11. In the microthread implantation section there are a total of 5 quantum dot loaded cells, while there are 4 quantum dot loaded cells in the intramyocardial injection section (arrows). Figure 11 illustrates some of the challenges that emerge when quantum dot loaded cells are in close proximity. When in close proximity, individual quantum dot loaded cells cannot be distinguished from each other. To reduce the possibility of double counting quantum dot loaded cells, whenever there was a strong signal around several nuclei, the number of quantum dot loaded cells, as counted, would be one cell. Properly quantum dot loaded hMSCs have quantum dots in the cytoplasm of the cell; therefore quantum dot signal should be in the immediate vicinity of the cell nuclei. Only cell nuclei with a 5 µm minimum diameter were counted to reduce the possibility of double counting the same cell if it spanned adjacent sections. In many cases, if a slice of a nucleus (with a diameter less than 5 µm) was seen in a section, either the previous or subsequent section would contain the full diameter of the same nucleus. Once three consecutive sections were analyzed for quantum dot loaded cells, 60 sections

were skipped and another three sections were analyzed. This pattern was continued until quantum dot loaded cells were no longer visible in the sections.

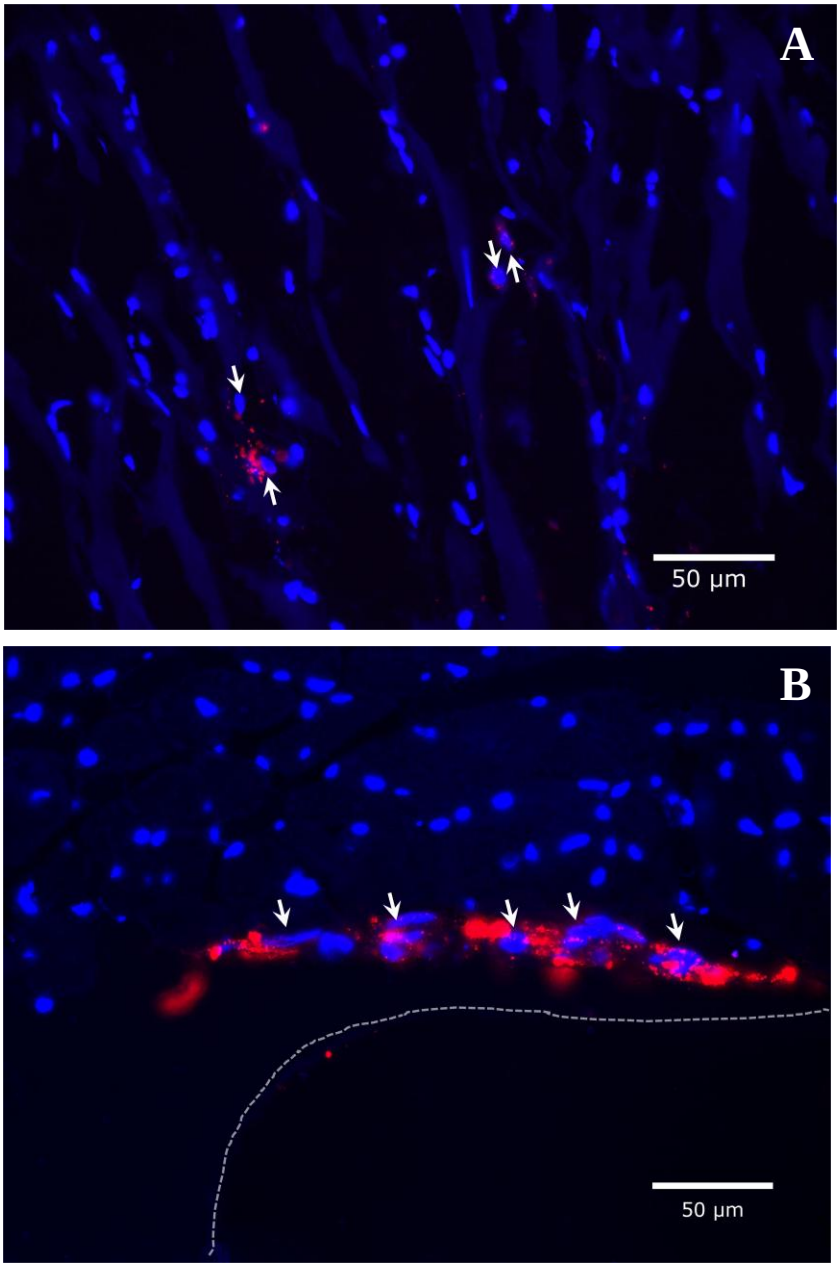

Figure 11: Quantum dot loaded hMSCs delivered to the rat heart
(40x magnification, Hoechst dyed nuclei are blue, Quantum dots are red). A: quantum dot loaded hMSCs injected into rat heart. B: quantum dot loaded hMSCs delivered to the rat heart with biological microthreads. Single quantum dot loaded hMSCs are indicated with arrows. The quantum dot loaded hMSC count is conservative because if there is more than one nucleus within a "cloud" of quantum dot signal, only a single cell was counted. The biological microthread bundle is outlined with a dotted white line.

Manually counting three sections every sixty sections obviously does not indicate the total number of cells delivered to the heart. Manually counting all heart sections, over 400 sections per experiment, would have been impractical because of the cost and time that it would require. Each counted section (3 sections per slide) was stained with Hoechst dye, coverslipped, and analyzed with a fluorescent microscope. Each of these steps was done with care to ensure that all sections were analyzed properly. In order to calculate the total number of cells delivered to the heart, some assumptions had to be made. It was assumed that there was a linear relationship between each of the slides (three rat heart sections per slide, see Figure 12). For example, the total number of cells delivered from slide 1 to slide 21 in EXP0214 would be calculated as follows: ((6 + 15) / 2) x 20 = 210.

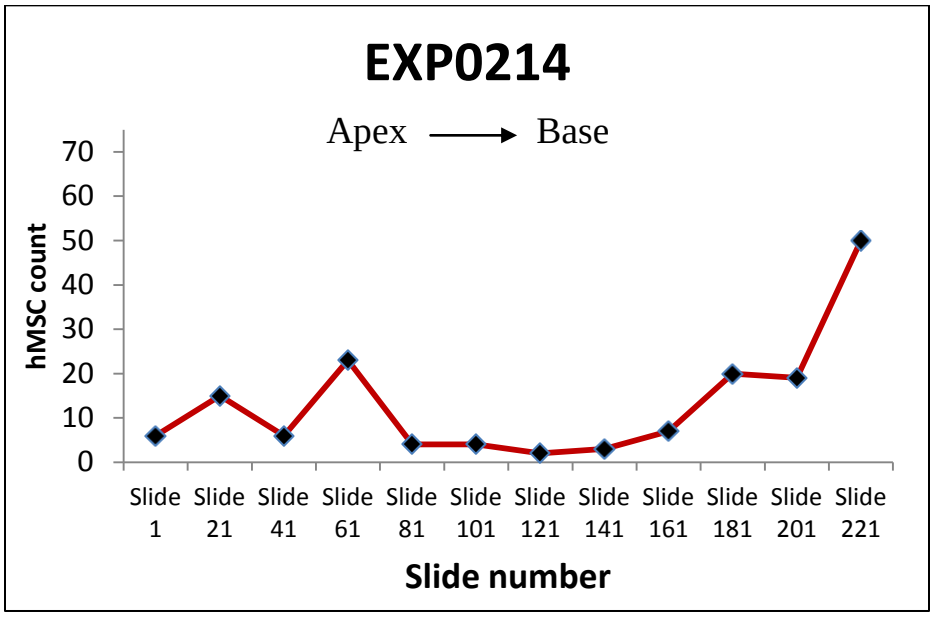

Figure 12: Counting hMSCs delivered to the rat heart

This graph illustrates how the number of quantum dot- positive hMSCs delivered to the rat heart was calculated. These numbers were taken from EXP0214, where the total number of hMSCs delivered to the rat heart was determined to be 2670. There are 3 rat heart sections on each slide.

Once the total number of cells delivered to the heart was calculated, the delivery efficiency could be determined. In order to determine the delivery efficiency, the biological microthread implant length and depth had to be measured. Equation 1 was used to determine the delivery efficiency of each microthread implantation:

$$\frac{hMSCs\ engrafted\ in\ heart\ wall}{\frac{Length\ of\ implanted\ microthread}{2\ cm\ initial\ microthread\ length} * hMSCs\ on\ microthread\ bundle}$$

Equation 1: Microthread implantation delivery efficiency calculation

The implant length was the distance between where the implanted biological microthread entered and exited the heart. The implant depth was the maximum distance from the outside of the heart that the microthread was implanted (this number was calculated by analyzing trichrome stained histological sections of the rat heart). The implant depth was usually not at the center point of the implantation length and therefore was the maximum implant depth. Based on this number, the total length of microthread implanted inside the heart could be calculated (see
Figure 13). The delivery efficiency of each intramyocardial injection was calculated using Equation 2:

$$\frac{hMSCs\ engrafted\ in\ heart\ wall}{10{,}000\ hMSCs\ initially\ injected\ into\ heart\ wall}$$

Equation 2: Intramyocardial injection delivery efficiency calculation

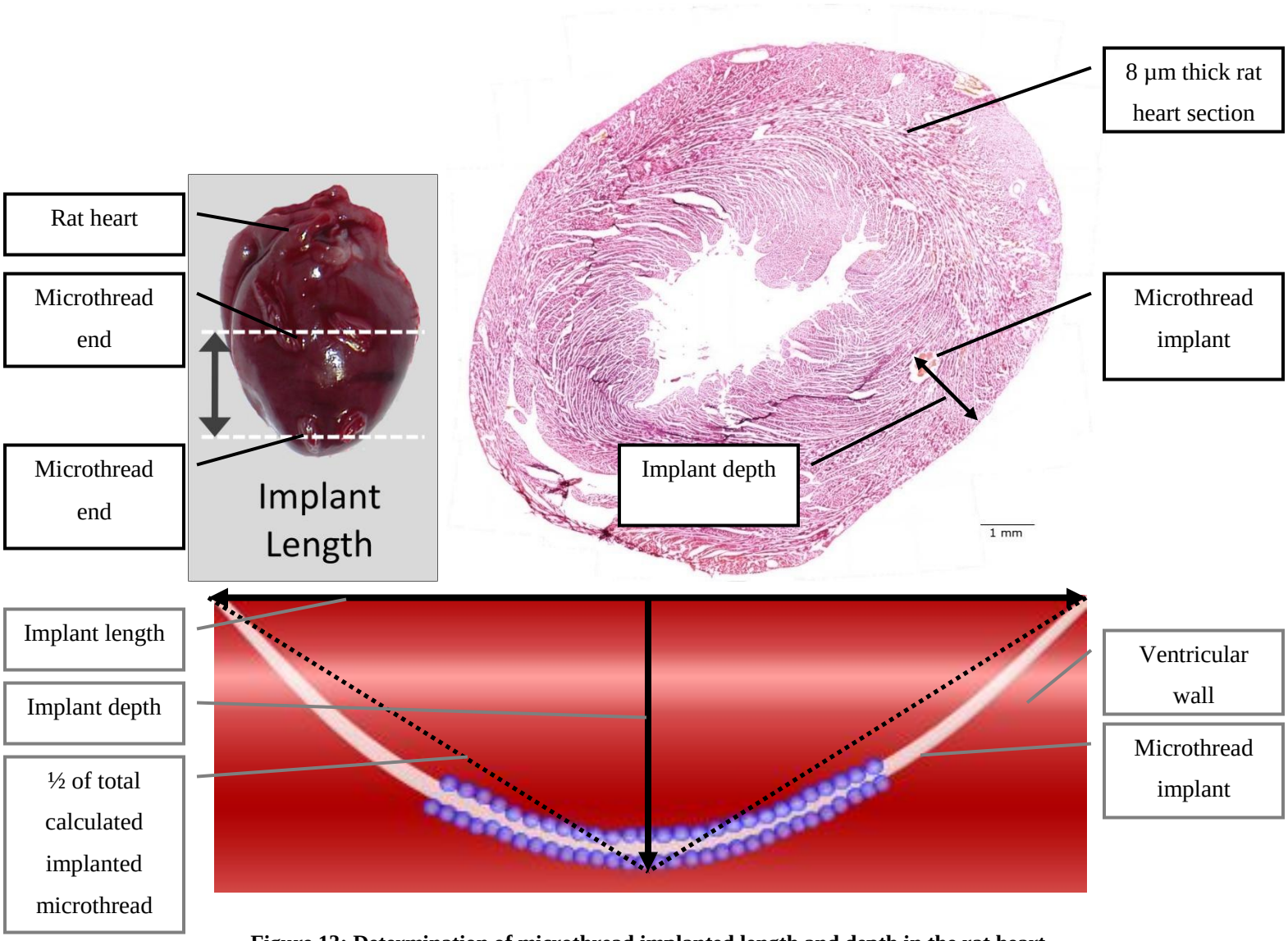

Figure 13: Determination of microthread implanted length and depth in the rat heart

This figure shows how implant length and depth are determined, and how the total implantation length is calculated. Once these values are determined in trichrome stained section, the lower image is drawn to make a triangle based on these values. The hypotenuse of ½ the implant length and implant depth (the two legs of the right triangle) is determined using the Pythagorean Theorem. The hypotenuse value is multiplied by two to represent the combination of the two hypotenuses, which is an estimate of the length of microthread implanted in the rat heart.

4.4.4: Tracking microthread implantation in the rat heart

In order to determine the location of the microthread in the rat heart (left ventricular wall) the heart sections were stained with Masson's trichrome stain as previously described. These stained heart sections were imaged (at 5x magnification) with a Leica DM LB2 microscope with a Leica DFC-480 digital camera attached. Adobe Photoshop software was utilized to determine the distance of the biological microthread implant from the innermost section of the endocardium. This procedure was done

from the base to the apex of the heart (every 60 heart sections) to track the entire microthread implantation. Figure 14 illustrates how the biological microthread implantation distance from the epicardium was calculated. The 0.5 mm scale bars were employed to determine the distance from the epicardium using Adobe Photoshop. The distances were determined by first determining the shortest distance from the outermost part of the epicardium to the innermost part of the endocardium, while crossing the centroid of the microthread. Once the endocardial distances were determined for the experiment, they were graphed (distance from endocardium vs. implantation distance).

4.5: Statistical Analysis

Statistics were performed in this project using Microsoft Excel 2007 with the Analysis ToolPak. Statistical differences were determined using unpaired, two-tail, unequal variance t tests for two groups. All data was reported in the following format unless otherwise noted: mean ± SEM (standard error of the mean). All experiments had a minimum of $n = 2$. A p-value < 0.05 indicated a statistically significant difference between groups.

BASE APEX

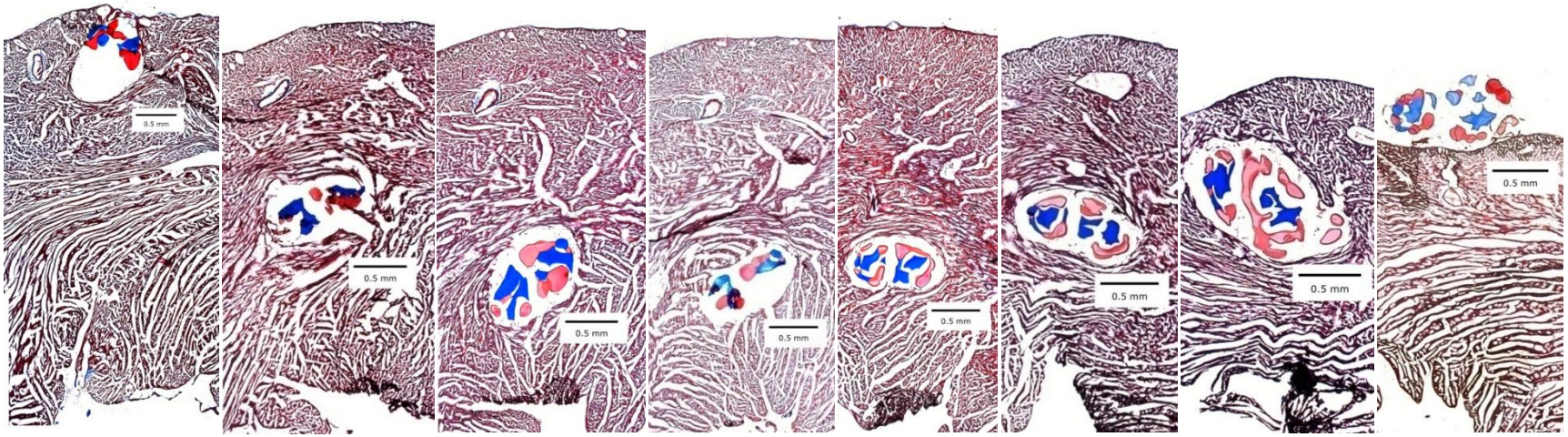

Figure 14: Microthread implantation tracking

(5x magnification, Masson's Trichrome staining, collagen microthreads are blue, fibrin microthreads are pink). The images are organized as follows: left (first): section containing biological microthread closest to base of the heart, right (last): section containing biological microthread closest to the apex of the heart. This figure illustrates how the biological microthread was implanted into the left ventricular wall of the rat heart. These images were used to determine the distance of the microthread from the innermost section of the endocardium. Each section is 480 µm apart.

4.4.5: Confocal microscopy

Confocal microscopy was utilized for some of the images in this thesis due to the thickness of the heart sections. Confocal microscopy was used to visualize α-actinin/Hoechst stained sections with quantum dot loaded cells delivered to the heart and to produce three dimensional recreations of the 8 µm tissue sections which could be rotated to analyze the location of quantum dot signal relative to hMSC nuclei. All of the confocal images were taken with 20x, 40x, or 63x oil objectives. The confocal images were taken with a Leica TCS SP5 II point scanning confocal microscope. Once the slide was in place, the biological microthread was found and the implantation area was scanned for quantum dots through the microscope's eyepiece. After a suitable area was found, the confocal system's lasers were used to excite the sample and an image was displayed on the computer screen.

Two lasers were utilized: a UV laser (405 nm) for the Hoechst dye and 655 ITK quantum dots and a 488 nm laser for the Alexa Fluor 488. Qdot 655 ITK quantum dots are excited from 400 - 650 nm and emit signal from 600 - 700 nm with maximum emission at 655 nm [86]. Hoechst 33342 dye is excited from 300 – 450 nm and emits signal from 355 – 650 nm, with maximum emission at 460 nm [90]. Alexa Fluor 488 is excited from 350-600 nm and emits signal from 488 – 650 nm, with maximum emission at 519 nm [91] (see Figure 17). Each channel (Hoechst, quantum dot, and Alexa Fluor 488) had to be adjusted for gain and offset until the image was properly displayed. If a z-stack was desired, the beginning and end of the stack had to be chosen so that a thickness of the tissue section would be scanned by the microscope. The confocal software would determine the number of scans required to recreate a thickness of the tissue section (usually 80-150 images). A z-stack would then allow several options including a 3D rotation of the tissue section and a maximum projection of the tissue section (all pictures merged into a single image, see Figure 15). Spectral analysis was also utilized on several sections to reduce the autofluorescence of the heart tissue (see Figure 16).

As described earlier, Alexa Fluor 488 and Hoechst 33342 dye have a wide spectral emission and therefore cause tissue autofluorescence and bleeding into other channels. Hoechst 33342 dye emits signal from 355-650 nm and Alexa Fluor 488 emits signal from 488-650 nm meaning that both stains emit signal from 488 – 650 nm (Figure 17). For spectral analysis, the entire potential emission spectrum was scanned by the microscope (5 nm per scan) and a spectral histogram was displayed and analyzed by the user. The desired spectral ranges were then chosen, and a majority of the autofluorescence was removed. This process was done for both the Hoechst and quantum dot channels (400 – 700 nm) and then the Alexa Fluor 488 channel (400-500 nm).

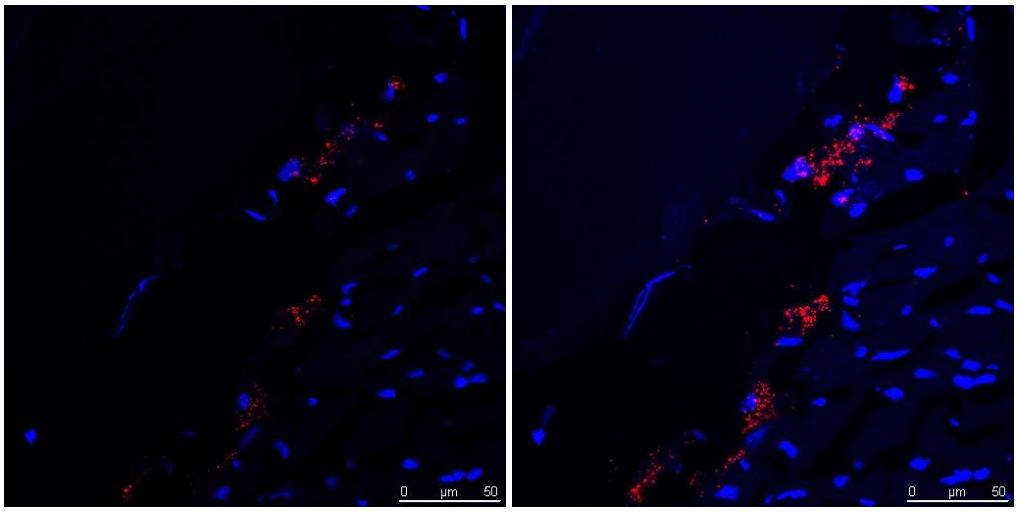

Figure 15: Confocal images before (left) and after (right) max projection
(63x magnification, Hoechst dyed nuclei are blue, quantum dots are red)

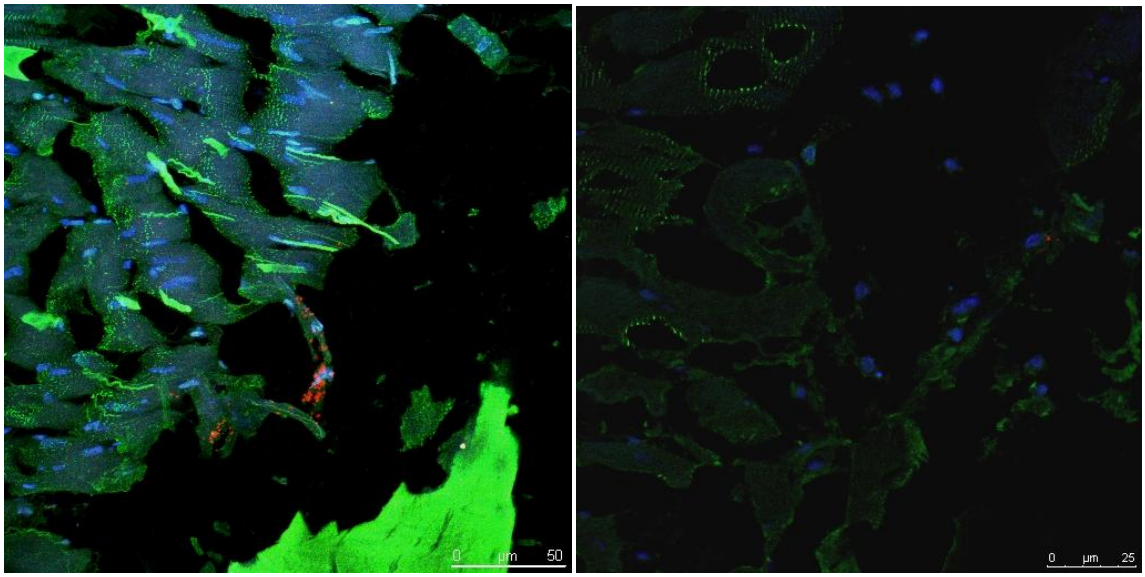

Figure 16: Confocal images before (left) and after (right) spectral analysis
(63x magnification, Hoechst dyed nuclei are blue, Alex Fluor 488 stained α-actinin is green, quantum dots are red)

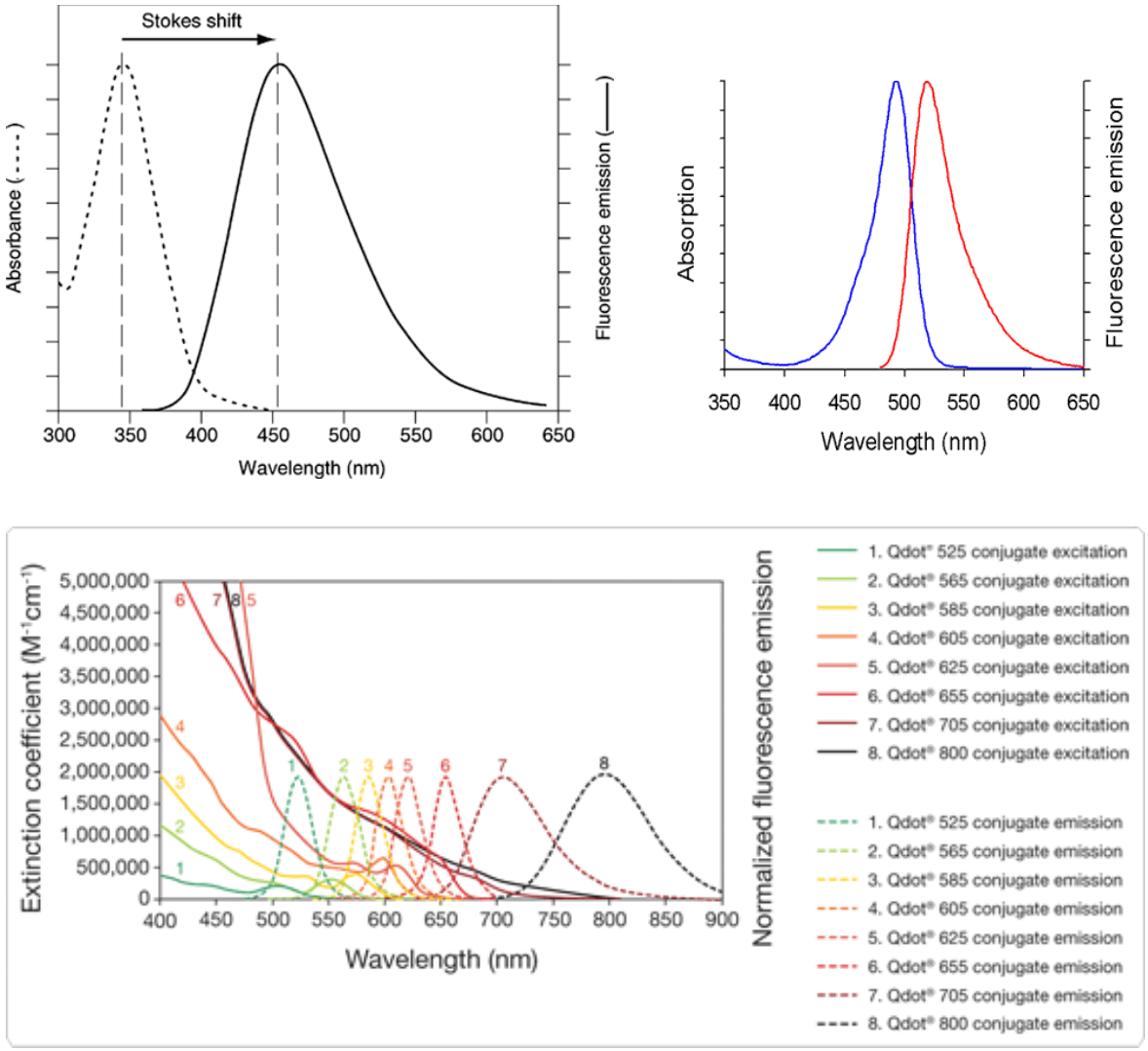

Figure 17: Spectral absorbance and emission curves for Hoechst 33342 (top left), Alexa Fluor 488 (top right), and Qdot 655 ITK quantum dots (bottom)

Chapter 5: Results

5.1: Quantifying hMSC seeding on biological microthreads

The quantification of hMSC seeding on biological microthreads was required to calculate the hMSC delivery efficiency of the biological microthread implantation. The biological microthreads were stained with Hoechst dye and Phalloidin to qualitatively assess hMSC seeding (see Figure 18). The hMSCs appear to cover nearly the entire surface of the 8 fibrin, 4 collagen microthread bundle after 24 hours of incubation in the bioreactor.

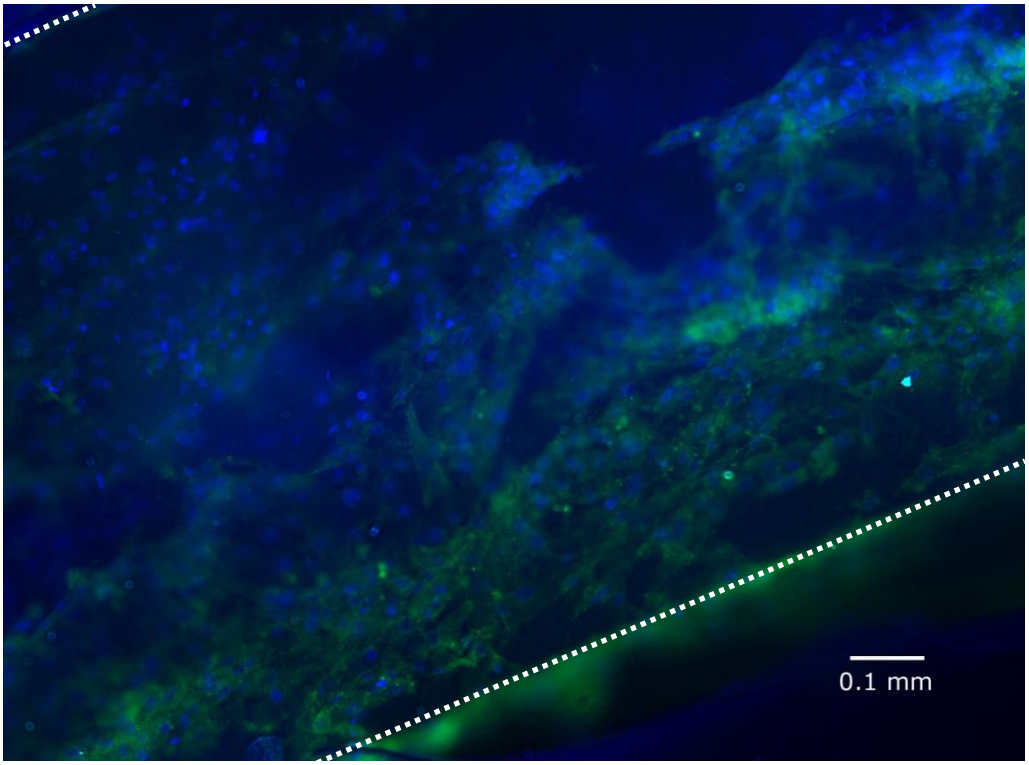

Figure 18: Biological microthread seeding after 24 hours
(10x magnification, Hoechst dyed nuclei are blue, Phalloidin stained f-actin filaments are green)

Qualitative assessment confirmed that the hMSCs were being seeded on the biological microthreads. Quantitative assessment was done by trypsinizing the biological microthreads and counting the dislodged hMSCs with a hemocytometer. Counting was performed one day after seeding to coincide with the surgical implantation of microthread bundles seeded within the same batch. The results of these counts are shown in Table 2a. However the results of these counts were not utilized as the denominator in the microthread implantation efficiency calculations for several reasons. For the first two experiments (EXP0214 and EXP0215) the microthreads were not analyzed for any remaining attached hMSCs after 30 minutes of trypsinization to ensure complete removal of cells from the microthread bundles prior to analysis. Also, in subsequent experiments, microthread bundles were agitated every 5 minutes during the

30 minutes trypsinization period to maximize hMSC detachment, which resulted in more consistent counts. Agitation and analysis of remaining microthread bundles was incorporated into the protocol and five additional microthread seeding experiments were performed. Although the same seeding conditions were used in EXP0214-EXP0219, the seeding experiments were not seeded at the same time as microthread implantation surgeries. The results of these seeding experiments are shown in Table 2b. These results were used to determine the average number of cells seeded on a 2 cm microthread bundle, which was subsequently used as the denominator for calculating the efficiency of biological microthread implantation. Based on these seeding experiments, it was determined that an average of 11,806 ± 3,932 (n = 20) hMSCs were seeded on the biological microthreads using the 24 hour bioreactor seeding technique. The implantation length and depth were utilized to estimate the total number of cells that were seeded on the length of microthread that was implanted in the rat heart (adjusted hMSC seeding, Table 3). The adjusted hMSC seeding count was always lower than the average microthread seeding count due to the fact that on average a 0.62 cm (out of a total microthread length of 2 cm) length of microthread was implanted into the rat heart. Adjusted hMSC seeding was calculated using Equation 3 as follows:

$$\frac{Implant\ \ lengt\ h}{2\ cm\ \ initial\ \ microt\ hread\ \ lengt\ h} * Average\ hMSCs\ on\ microthread\ bundle\ after\ 24\ hours$$

Equation 3: Adjusted hMSC seeding calculation

Experiment	Average Cell Number ± SD
EXP0214 (n=2)	7,320 ± 6,619
EXP0215 (n=2)	4,540 ± 2,517
EXP0217 (n=2)	18,119 ± 16,915
EXP0218 and EXP0219 (n=2)	15,951 ± 8,926
Average (n=8 total)	**11,483 ± 8,744**

Table 2a: Biological microthread hMSC seeding count (old counting protocol)

Experiment	Average Cell Number ± SD
Seeding Experiment 1 (n=4)	5,824 ± 2,457
Seeding Experiment 2 (n=4)	10,260 ± 4,817
Seeding Experiment 3 (n=4)	12,381 ± 4,313
Seeding Experiment 4 (n=4)	16,966 ± 3,695
Seeding Experiment 5 (n=4)	13,601 ± 4,377
Average (n=20 total)	**11,806 ± 3,932**

Table 2b: Biological microthread hMSC seeding count

Microthread implantation sample	Implant length (cm)	Implant depth (cm)	(Implant length / initial thread length) * hMSCs on threads
EXP0214	0.66	0.45	6,588
EXP0215	0.44	0.28	4,203
EXP0217	0.7	0.27	5,219
EXP0218	0.64	0.4	6,048
EXP0219	0.73	0.3	5,578
Average	**0.63**	**0.34**	**5,527**

Table 3: Adjusted number of hMSCs delivered on biological microthreads
This table shows the values of the measurements taken to estimate the total number of cells seeded on the length of microthread that was implanted in the rat heart. The implant length was divided by 2 cm (the original length of the seeded microthread bundle) and multiplied by 11,806 (the average number of hMSCs on microthread bundles after 24 hours of seeding).

5.2: Quantifying hMSC delivery to the ventricular wall

One of the main objectives of this thesis was to maximize the delivery of hMSCs to the left ventricular wall in the rat heart. A method was developed to estimate the number of hMSCs delivered to the rat heart as previously described. All experiments were histologically analyzed and the hMSC delivery distribution and efficiency were determined. The biological microthread implantation group (n = 5) had a delivery efficiency of 63.6 ± 10.6% (see Table 4) and the intramyocardial injection group (n = 4) had a delivery efficiency of 11.8 ± 6.25% (see Table 5). Biological microthread implantation was significantly more efficient ($p < 0.05$, see Figure 19). The total number of cells engrafted in each group was also calculated (see Figure 20). The average number of cells engrafted for each biological microthread implantation was 3,527 ± 624. The average number of cells engrafted for each intramyocardial injection was 1,146 ± 547. Biological microthread implantation delivered significantly more hMSCs ($p < 0.05$). It should be noted that for the final intramyocardial injection surgery, there were no quantum dot loaded hMSCs engrafted in the ventricular wall. For this reason, there were only four

intramyocardial injection experiments analyzed. In terms of rat weight, the intramyocardial injection group rats had an average weight of 569 g and the microthread implantation group rats had an average weight of 576 g (see appendix D for data). Heart rate prior to euthanasia was also determined for the rats in the two groups. However, for the first two microthread implantation experiments a pulse oximeter was not available so no data was acquired. The average heart rate for the intramyocardial injection group was 196 beats per minute. The average heart rate for the microthread implantation group was 220 beats per minutes (see appendix D for data).

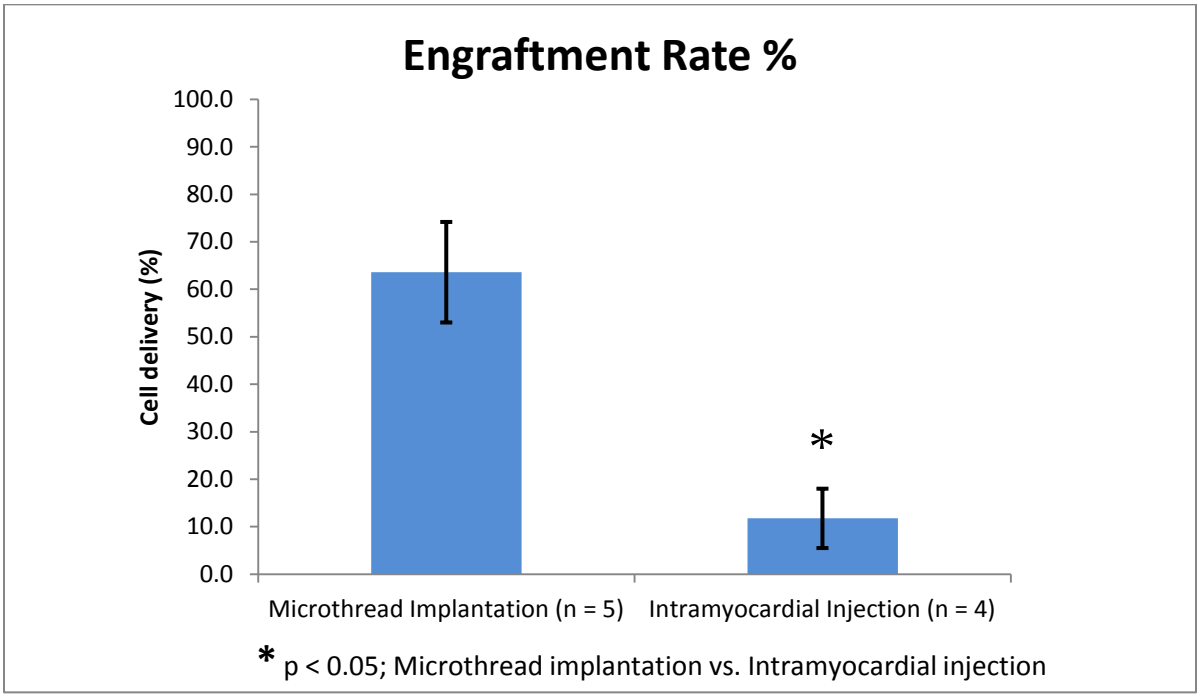

Figure 19: hMSC engraftment rate (%): microthread implantation vs. intramyocardial injection

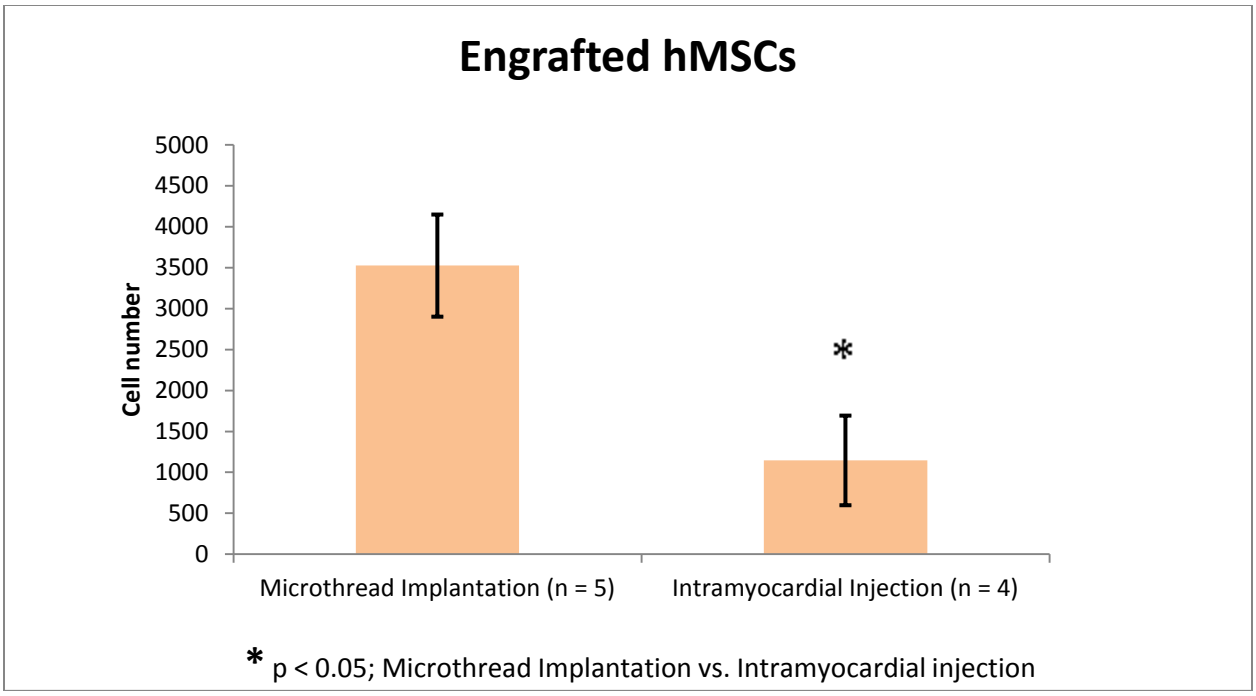

Figure 20: hMSC engraftment number comparison: microthread implantation vs. intramyocardial injection

The hMSC delivery length, the length of heart tissue from base to apex to which hMSCs were delivered, was compared between the intramyocardial injection and microthread implantation groups next. Quantum dot loaded hMSCs were delivered to an average length of 0.55 ± 0.06 cm for the microthread implantation group (see Table 4) and 0.33 ± 0.13 cm for the intramyocardial injection group (see Table 5). Human mesenchymal stem cells were delivered to a significantly longer length with the microthread implantation group ($p < 0.05$, see Figure 21).

Experiment	Total hMSCs Delivered	Engraftment Rate
EXP0214	2,670	41%
EXP0215	1,828	43%
EXP0217	3,709	71%
EXP0218	3,896	64%
EXP0219	5,526	99%
Average	**3,527**	**64%**

Table 4: Microthread implantation experiment cell delivery results

This table shows the total number of hMSCs delivered to the rat heart and the total delivery efficiency for each biological microthread implantation as a percentage of cells delivered per microthread bundle implanted (see Table 3).

Experiment	Total hMSCs Delivered	Delivery Efficiency
EXP0220	752	7.52%
EXP0221	2,779	27.8%
EXP0224	461	4.61%
EXP0225	591	5.91%
Average	**1,146**	**11.8%**

Table 5: Intramyocardial injection experiment cell delivery results

This table shows the total number of hMSCs delivered to the rat heart and the total delivery efficiency for each intramyocardial injection experiment. Delivery efficiency was calculated as a percentage of 10,000 hMSCs injected per heart sample.

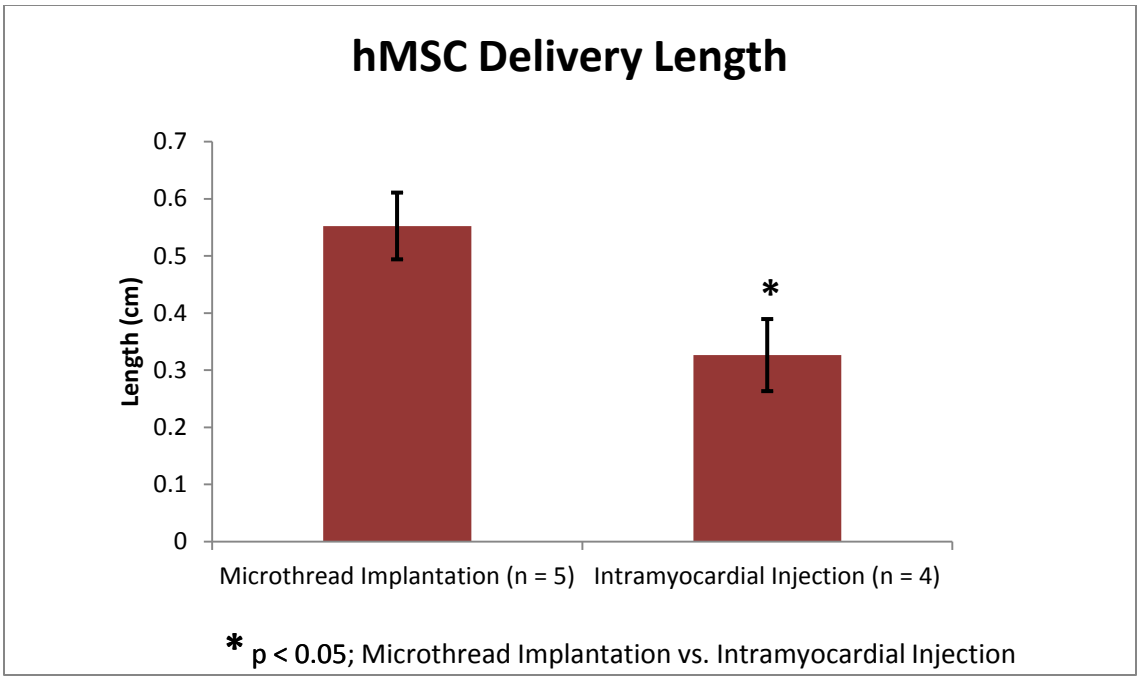

Figure 21: hMSC delivery length comparison: microthread implantation vs. intramyocardial injection

5.3: hMSC delivery distribution

The hMSC delivery distribution was determined by counting the number of hMSCs delivered in three consecutive rat heart sections every sixty sections after histology and staining were completed. In some cases (EXP0218) the microthread bundle entered the ventricular cavity due to surgical error and resulted in several sections not containing delivered cells (see Figure 22 for histology). Despite this imperfect implantation, cell delivery efficiency was still relatively high (64%). The hMSC delivery distribution graphs for EXP0214-EXP0219 (microthread bundle implantation, Figure 23) demonstrate a larger number of cells delivered to the base, where the suture needle was initially inserted for surgical implantation. Despite some shearing, cell delivery throughout the implantation length was still observed. The hMSC delivery distributions of the intramyocardial injections varied considerably from experiment to experiment (in terms of the number of cells delivered per 24 μm of heart tissue and total delivery length, see Figure 24).

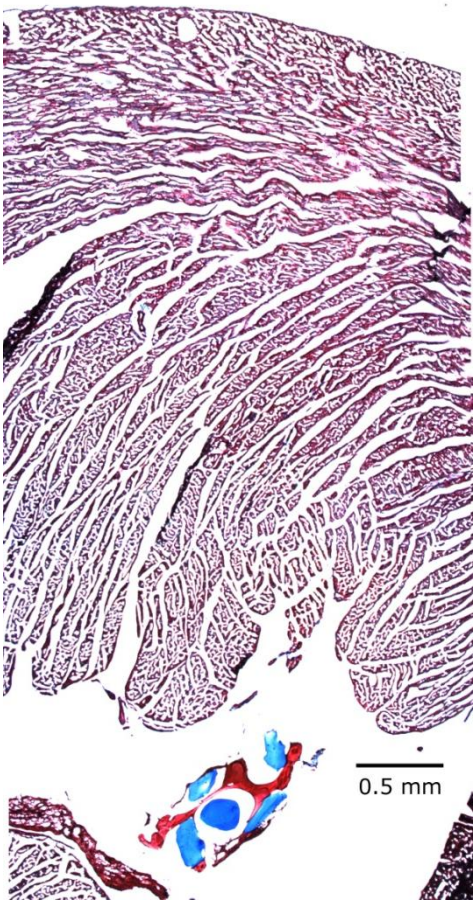

Figure 22: Biological microthread bundle delivered to ventricular cavity

Figure 23: hMSC delivery distributions – microthread implantations

The following graphs show the distribution of delivered hMSCs to the rat heart for the five individual hMSC-seeded microthread bundle implantation surgeries (EXP0214-EXP0219). The implantation distance (x axis) starts from the section of the biological microthread implanted closest to the base of the heart (where the microthread entered the heart) and ends at the biological microthread implanted closest to the apex of the heart (where the microthread exited the heart).

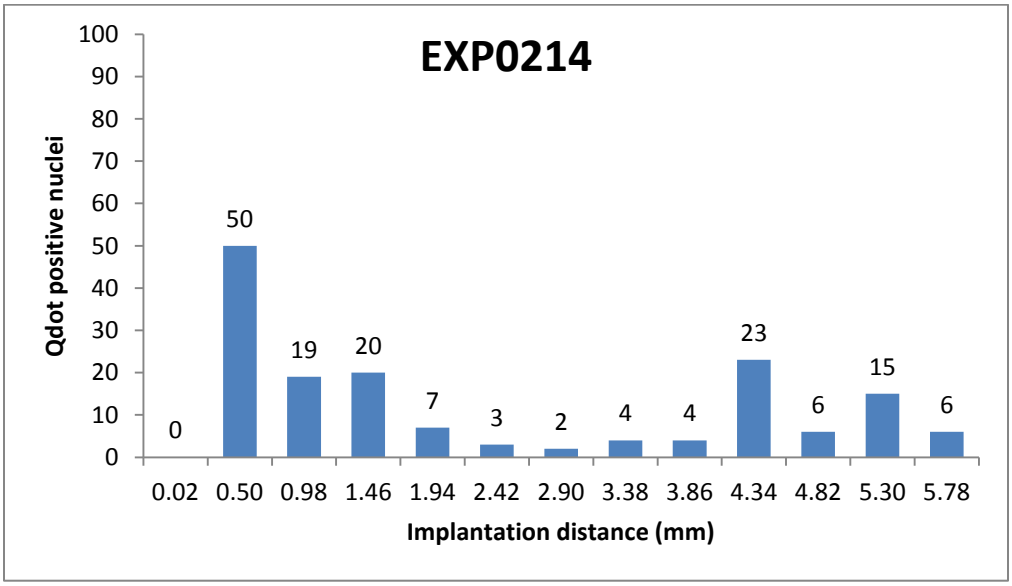

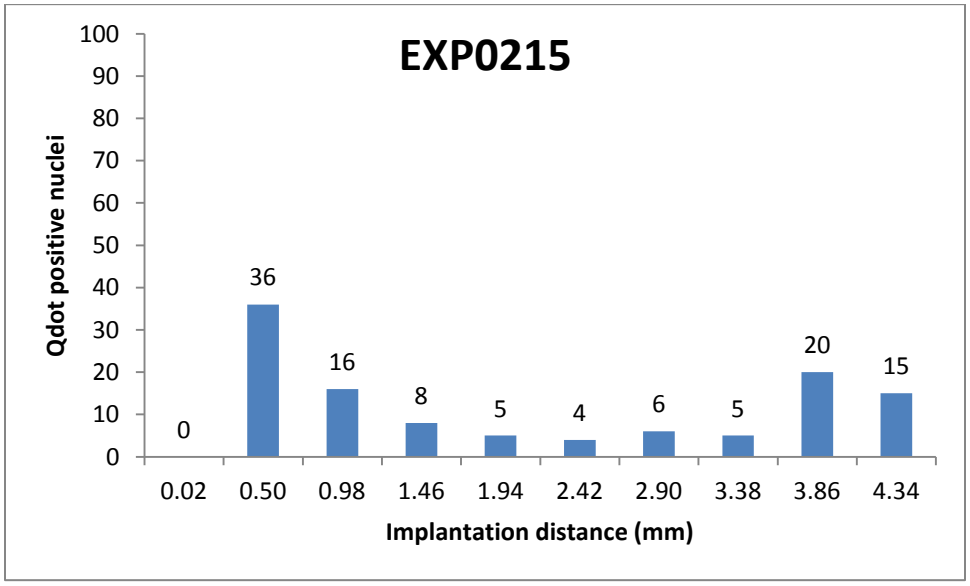

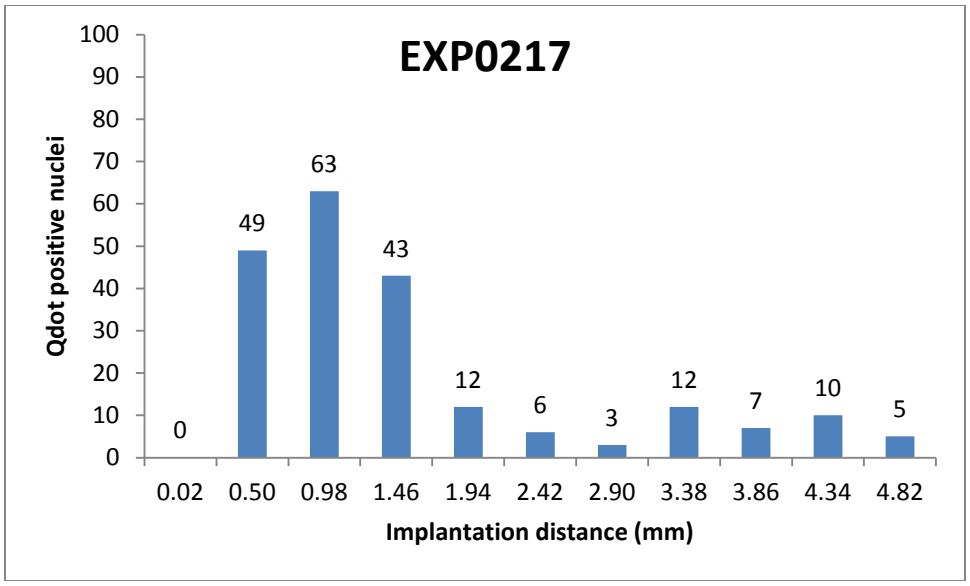
EXP0217
Qdot positive nuclei
100
90
80
70
60
50
40
30
20
10
0
0
49
63
43
12
6
3
12
7
10
5
0.02
0.50
0.98
1.46
1.94
2.42
2.90
3.38
3.86
4.34
4.82
Implantation distance (mm)

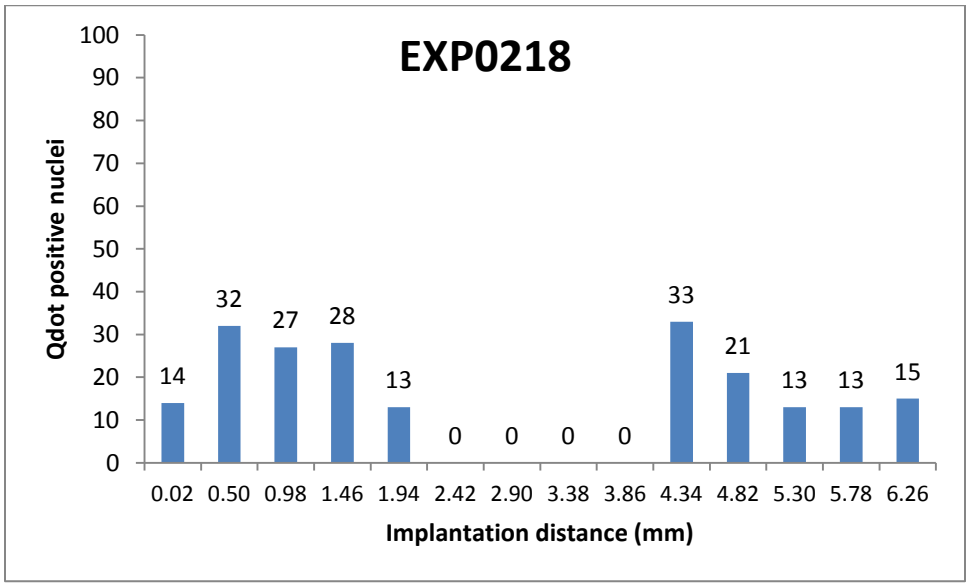
EXP0218
Qdot positive nuclei
100
90
80
70
60
50
40
30
20
10
0
14
32
27
28
13
0
0
0
0
33
21
13
13
15
0.02
0.50
0.98
1.46
1.94
2.42
2.90
3.38
3.86
4.34
4.82
5.30
5.78
6.26
Implantation distance (mm)

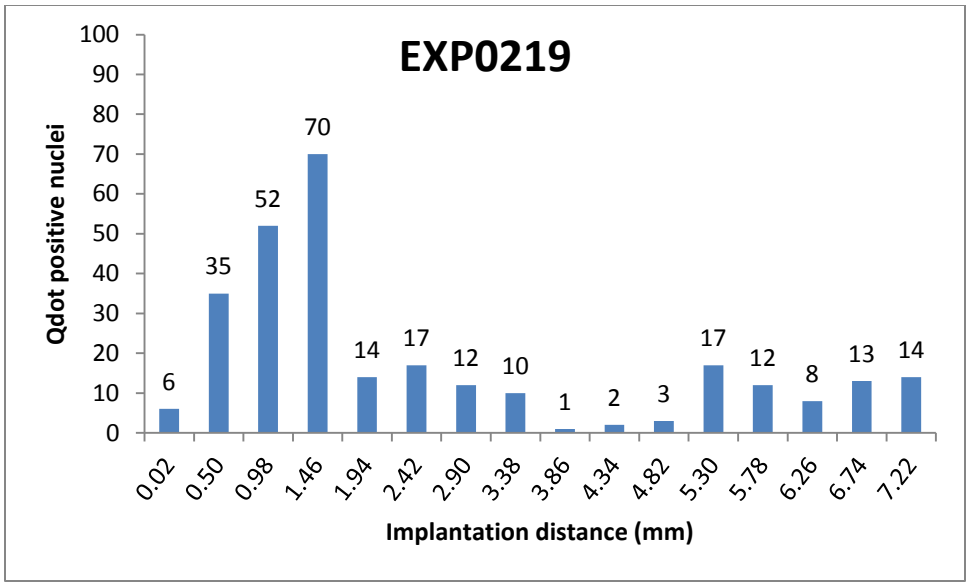
EXP0219
Qdot positive nuclei
100
90
80
70
60
50
40
30
20
10
0
6
35
52
70
14
17
12
10
1
2
3
17
12
8
13
14
0.02
0.50
0.98
1.46
1.94
2.42
2.90
3.38
3.86
4.34
4.82
5.30
5.78
6.26
6.74
7.22
Implantation distance (mm)

Figure 24: hMSC delivery distributions – intramyocardial injections

The following graphs show the distribution of delivered hMSCs to the rat heart for the four intramyocardial injections (EXP0220, 221, 224, 225). The implantation distance (x axis) starts from where the quantum dot loaded hMSCs were delivered closest to the base of the heart and ends where the final quantum dot loaded hMSCs were delivered, closest to the apex of the heart.

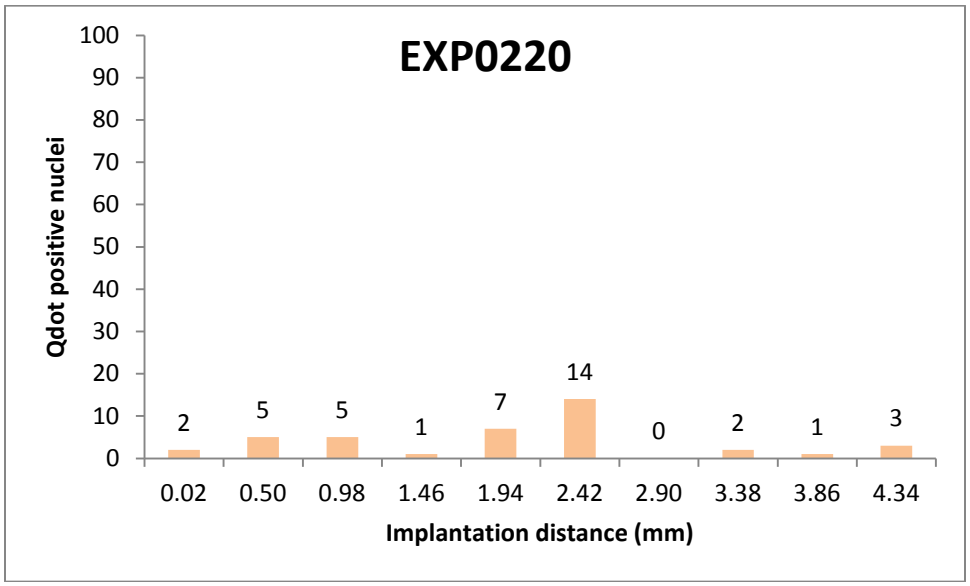

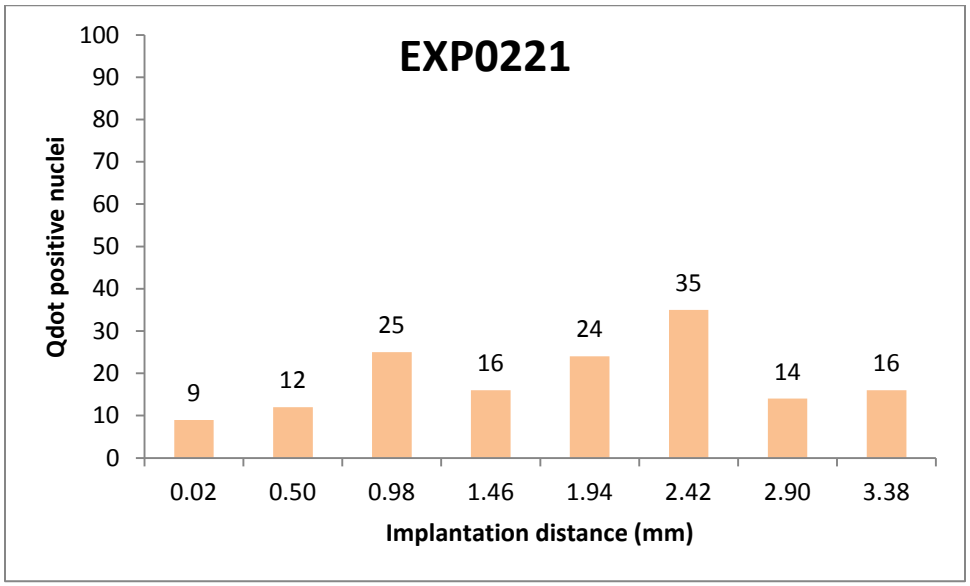

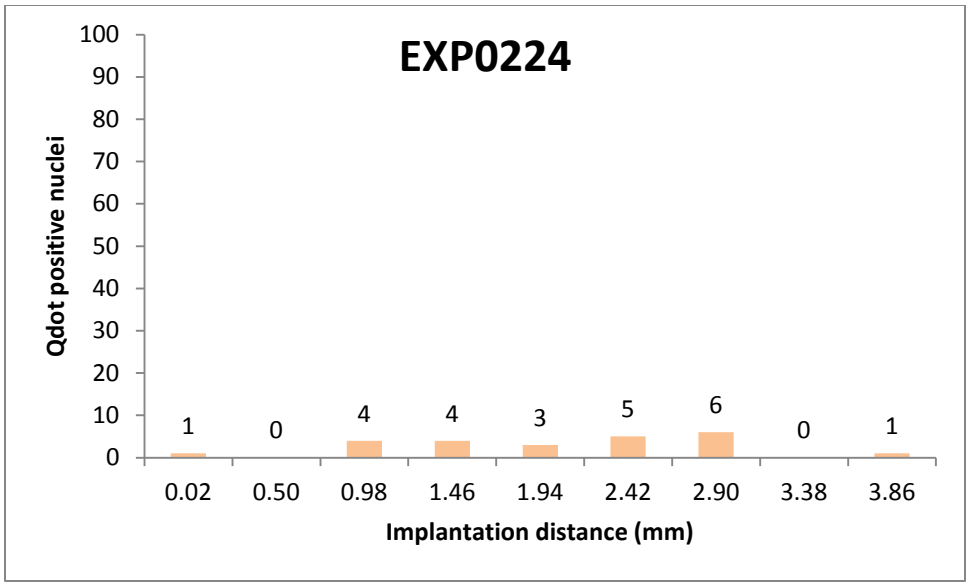

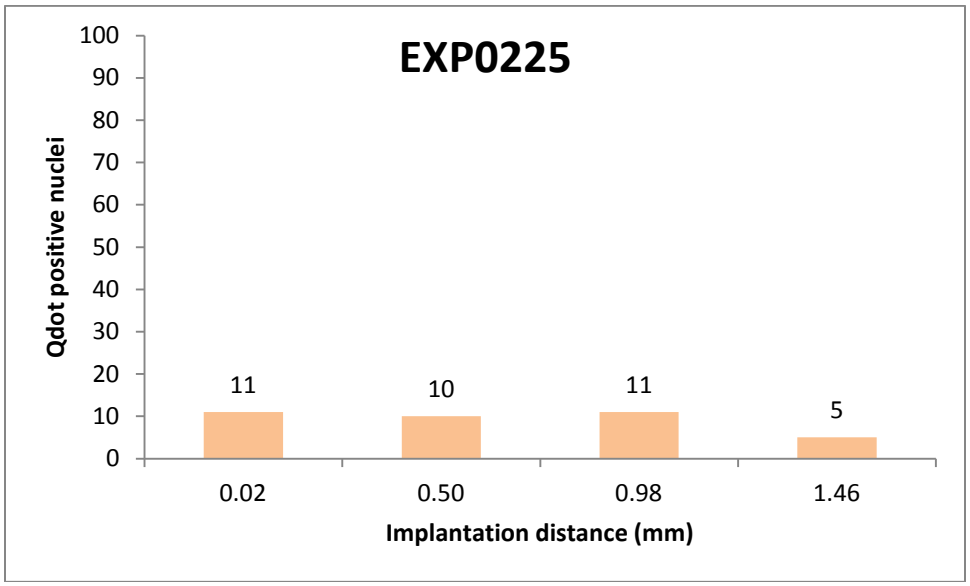

The combined delivery distributions of the microthread implantation and intramyocardial injection groups illustrated the average number of cells delivered along the implantation length: at the 0%, 25%, 50%, 75%, and 100% points of the total delivery length. These graphs demonstrate the cell delivery patterns of the two groups. As shown in Figure 25, a high percentage of the cells were delivered close to the entry point of the microthread bundle. At the 50% point, there was a steep reduction in the cell delivery percentage because the microthread bundle entered the ventricular cavity on several surgeries. Figure 26 shows the combined delivery distribution of the intramyocardial injection group. A majority of the cells were delivered at the 50% point, where the syringe needle released the hMSC suspension into the heart wall. Fewer cells were delivered towards the apex and the base of the heart (from the 50% point).

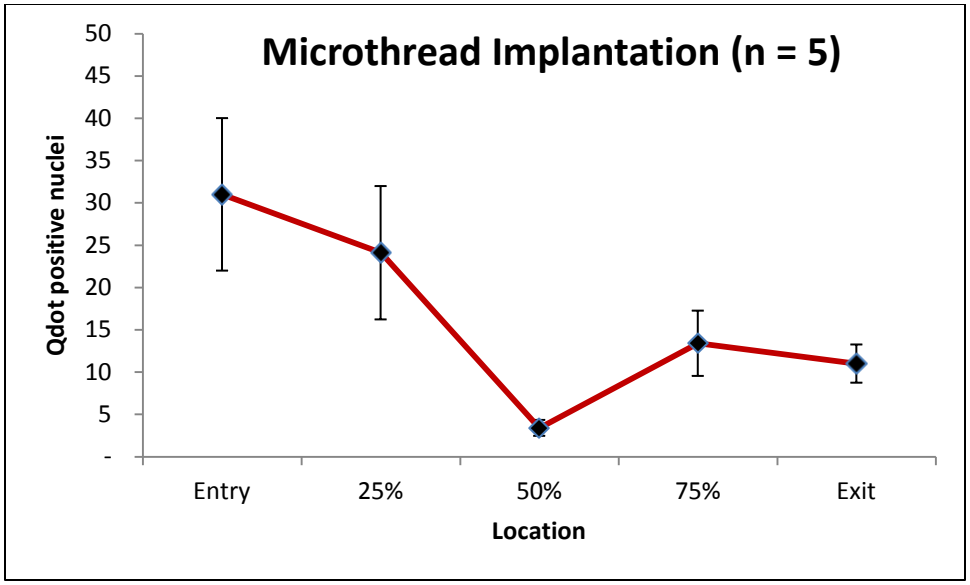

Figure 25: Microthread Implantation – Combined Delivery Distribution

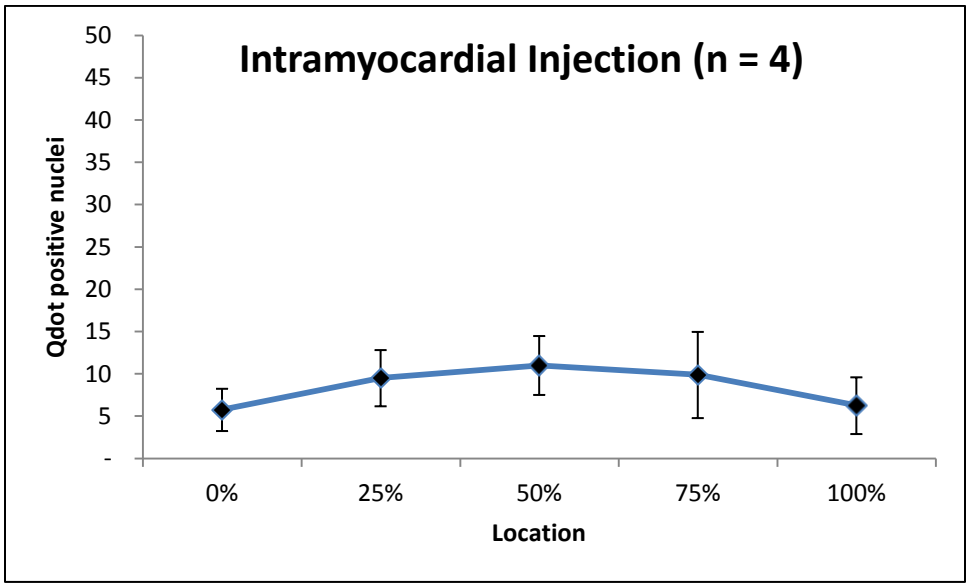

Figure 26: Intramyocardial Injection – Combined Delivery Distribution

5.3.1 Biological microthread implantation tracking

Implantation tracking allowed the estimation of the location of the delivered hMSCs for the biological microthread implantation experiments. The implantation tracking graphs depict the location of the biological microthread bundles within the rat myocardium (in the Masson's Trichrome stained heart sections) at 480 µm increments and the number of quantum dot loaded nuclei counted at each of these 480 µm increments. The Masson's Trichrome stained sections were taken directly adjacent to the Hoechst dye stained sections so that the location of the delivered cells could be estimated. Implantation tracking also quantitatively illustrated the success (in terms of localization) of an implantation experiment. Figure 27 demonstrates the differences between each microthread implantation experiment. The distance from the endocardium is shown as a percentage of the left ventricular wall thickness in these figures. One hundred percent distance means the microthread bundle is entirely out of the epicardium and 0% distance means the microthread bundle is in the innermost part of the endocardium. In some cases the biological microthread bundle entered the left ventricular cavity. In these cases, the distance from the endocardium was still considered 0%.

Figure 27: Microthread implantation tracking

The following five graphs (EXP0214-0219) show the location (in the left ventricular wall) of the biological microthread implantations and the number of delivered hMSCs in each location. The red line illustrates the distance of the biological microthread from the innermost part of the endocardium of the left ventricular wall.

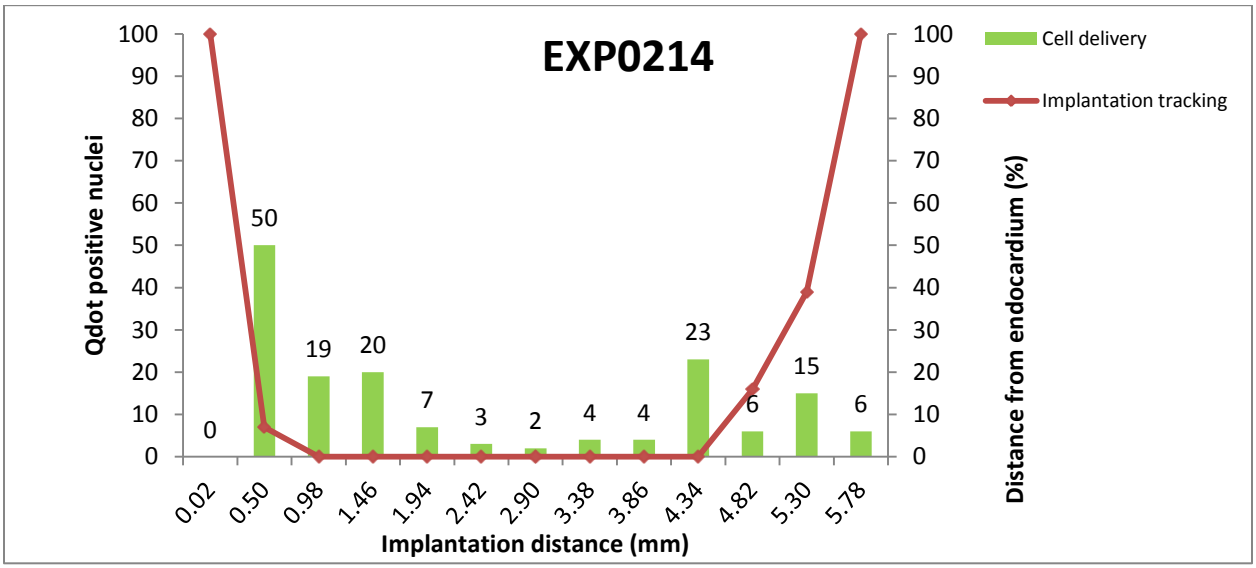

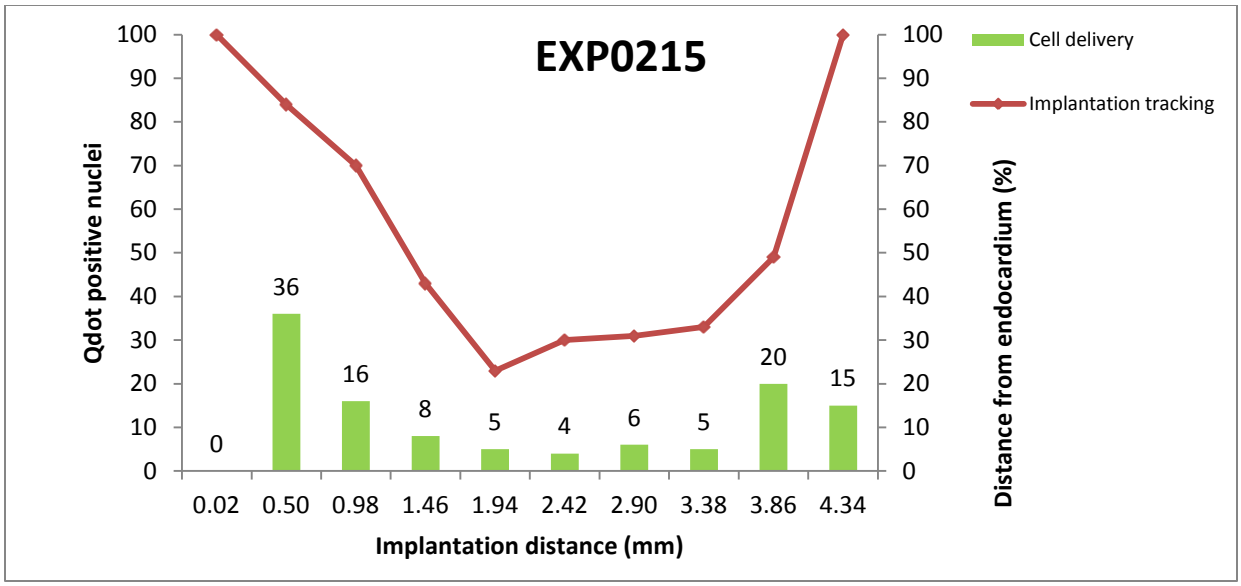
EXP0215
Qdot positive nuclei
Distance from endocardium (%)
Implantation distance (mm)
Cell delivery
Implantation tracking
0
36
16
8
5
4
6
5
20
15
0.02
0.50
0.98
1.46
1.94
2.42
2.90
3.38
3.86
4.34

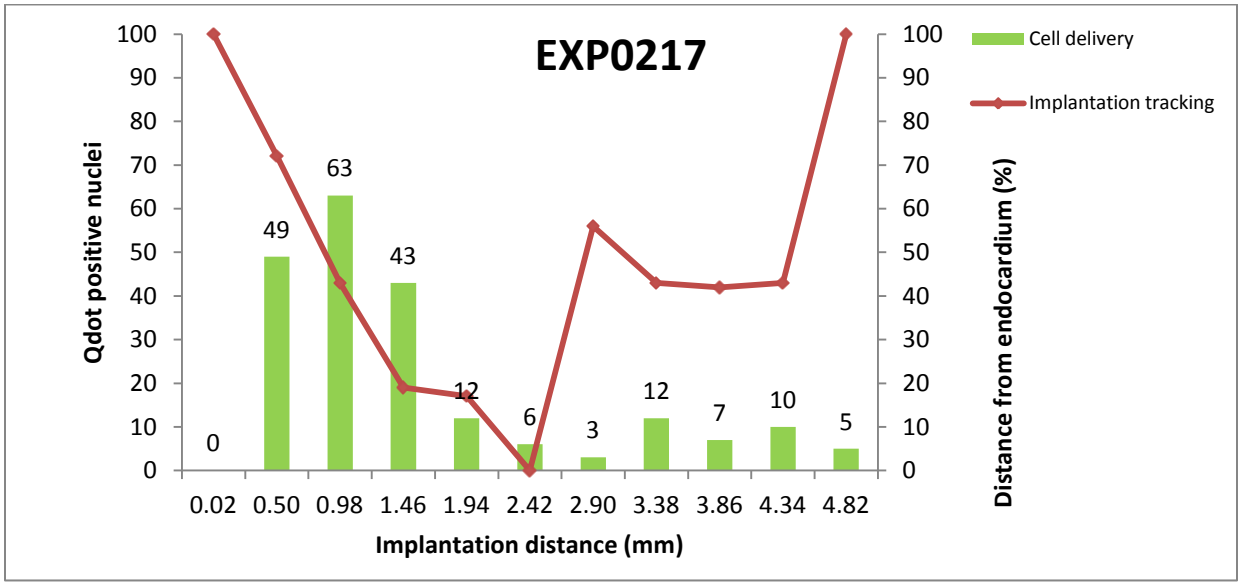
EXP0217
Qdot positive nuclei
Distance from endocardium (%)
Implantation distance (mm)
Cell delivery
Implantation tracking
0
49
63
43
12
6
3
12
7
10
5
0.02
0.50
0.98
1.46
1.94
2.42
2.90
3.38
3.86
4.34
4.82

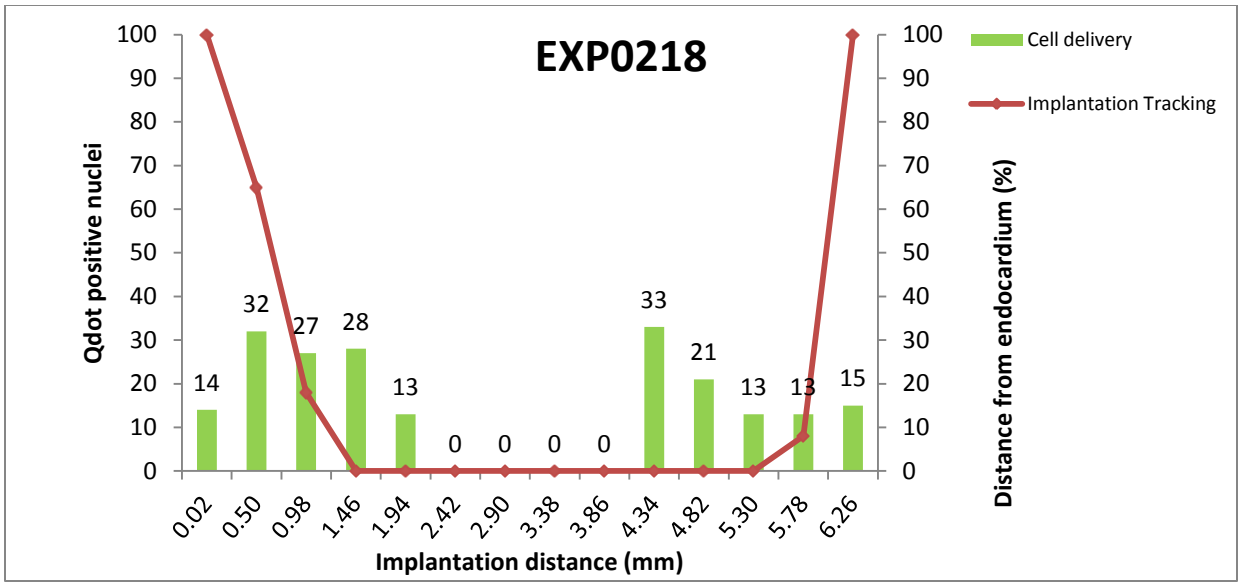

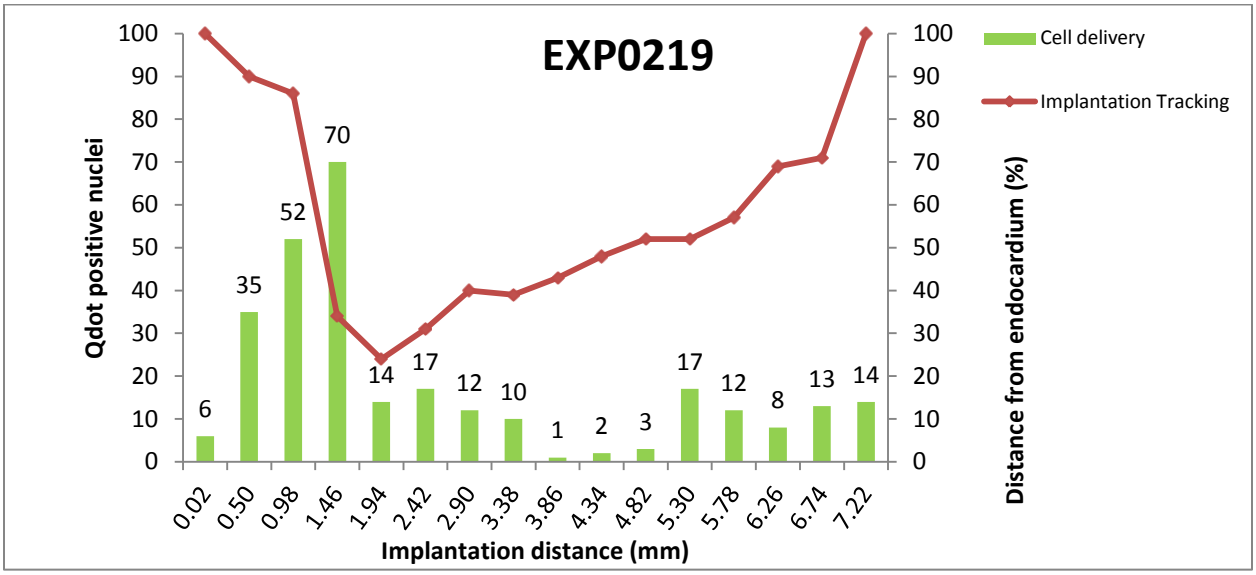

Table 6 illustrates the number of cells delivered to the endocardium, myocardium, and epicardium of the left ventricular wall for each biological microthread implantation experiment. The endocardium was defined as the region spanning 0 to 33.3% of the distance from the innermost part of the left ventricular wall. The myocardium was defined as the region spanning 33.4 to 66.6% of the distance from the innermost part of the left ventricular wall. The epicardium was defined as the region spanning 66.7 to 100% of the distance from the innermost part of the left ventricular wall.

The implantation tracking graphs illustrated the differences between each of the biological microthread implantations. The first noticeable trend was that only two out of the five biological microthread implantations had similar implantation tracking graphs (EXP0214 and EXP0218). These two

experiments maximized biological microthread implantation to the endocardium. EXP0217, perhaps the most puzzling experiment, had the most unexpected implantation tracking graph. Toward the center of the implantation, after the biological microthread entered the innermost part of the endocardium, the biological microthread bundle traveled 56% of the left ventricular wall thickness towards the epicardium over the course of 0.36 mm of heart tissue. The biological microthread bundle then traveled back towards the endocardium and then continued to exit the heart. This unexpected "zig-zag" pattern may have been the result of a surgical mistake during the implantation - the surgeon not passing the microthread bundle through the heart in a steady motion.

The percentage of hMSCs delivered to the endocardium, myocardium, and epicardium determined how effectively the biological microthread bundles can target transmural hMSC delivery. A goal of this project was to establish the ability of the biological microthread bundles to deliver hMSCs to the endocardium. There were 1,691 ± 448 hMSCs delivered to the endocardium for each biological microthread implantation. There were 1,152 ± 391 hMSCs delivered to the myocardium per biological microthread implantation and 683 ± 352 hMSCs delivered to the epicardium for each biological microthread implantation (see Figure 28).

Experiment	hMSCs Delivered to Endocardium (%)	hMSCs Delivered to Myocardium (%)	hMSCs Delivered to Epicardium (%)
EXP0214	1,930 (72.3%)	690 (25.8%)	50 (1.9%)
EXP0215	445 (24.3%)	477 (26.1%)	906 (49.6%)
EXP0217	1,790 (48.3%)	1,720 (46.4%)	199 (5.4%)
EXP0218	3,142 (80.6%)	460 (11.8%)	294 (7.5%)
EXP0219	1,150 (20.8%)	2,410 (43.6%)	1,966 (35.6%)
Average	**1,691 (49.3%)**	**1,152 (30.8%)**	**683 (20%)**

Table 6: Localization of delivered hMSCs

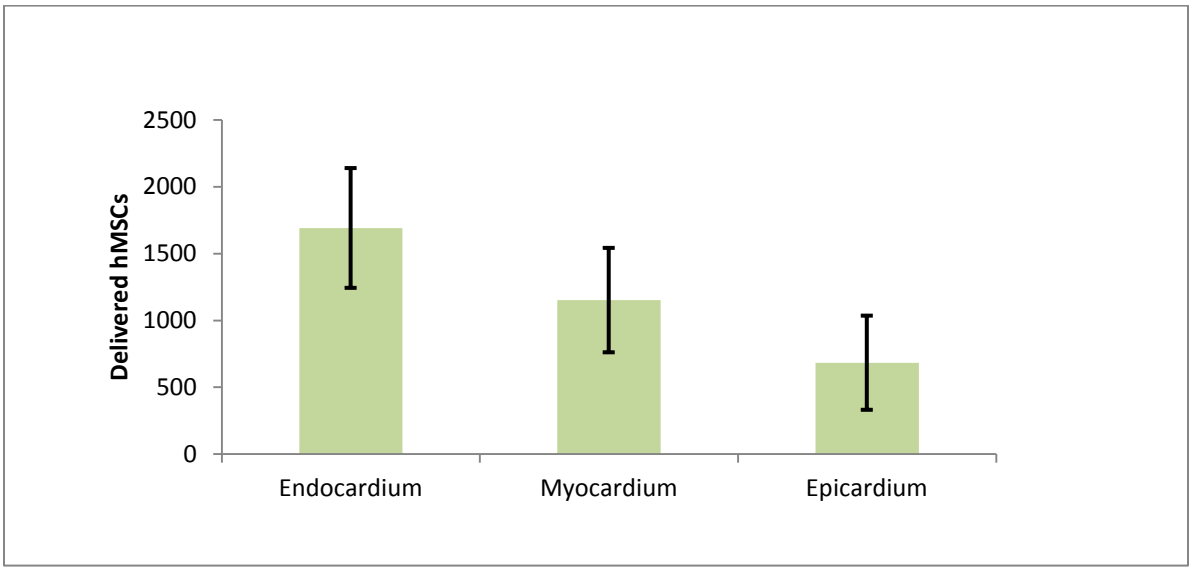

Figure 28: hMSC delivery localization to endocardium, myocardium, and epicardium

Chapter 6: Discussion

The experiments completed during this project have illustrated that biological microthreads can be seeded with over 11,000 hMSCs and implanted successfully in the rat heart. It has also been established that hMSCs can be delivered to the myocardium or endocardium with biological microthreads. Biological microthreads have also been shown to deliver cells consistently along the entire length of the implantation, despite some cell loss at the entry point. Finally, biological microthread mediated hMSC delivery has been shown to be more efficient than intramyocardial injection after one hour of implantation. The importance of these results will be discussed in this section.

6.1 Biological Microthread Cell Seeding

Determining how many cells were being seeded on the biological microthread bundles was more difficult than initially anticipated. Murphy et al. were able to estimate the number of hMSCs seeded on a bundle of four fibrin microthreads by staining with Hoechst dye followed by microscopy to analyze cell number [16]. However, with a larger bundle size (eight fibrin and four collagen microthreads) several complications became apparent. The first problem was the diameter of the larger microthread bundle. Since the bundle of 12 biological microthreads had an average diameter of 0.7 mm, counting all of the cells on the surface of the bundle was nearly impossible due to the substantial depth of field. Since the microthreads were bundled, they also overlapped each other and covered large populations of cells. Coverslipping such a large specimen was difficult and usually resulted in an excessive amount of air under the coverslip which degraded the sample over time. Due to these difficulties a different method was utilized, as discussed earlier (hemocytometer method), to count the number of cells seeded on the biological microthread bundles.

On average, 11,806 cells were seeded on 2 cm long biological microthread bundles utilized for this project. In the future, a larger seeding number may be desired to further increase the improvement of cardiac function post-MI. Murphy et al. demonstrated a nearly three-fold increase in cells seeded per microthread bundle after five days, when compared to the one day time point (3,344 versus 9,644 cells) [16]. If it is assumed that the same would occur with the microthread bundles seeded with hMSCs for this project, 30,000 cells could potentially be seeded on a single microthread bundle (this has been done after a single day of seeding but only for one sample). Since only a part of the microthread bundle was actually implanted into the rat heart, 12,000 cells could potentially be delivered to the rat heart with the increased seeding time ([5,527 / 11,803] x 30,000). Another method to increase the number of cells delivered with biological microthreads could be to implant more seeded biological microthread bundles. This method would also increase the area of myocardial tissue that receives hMSCs. However, this method would most likely be more effective in a larger animal model (dog, pig, etc.) due to the size of the injury that would be

created in a small rodent heart. A final potential method of increasing cell delivery would be to increase the number of fibrin microthreads and decrease the number of collagen microthreads used in the microthread bundle. This could potentially increase hMSC seeding on the microthread bundle.

Qualitative analysis of the Hoechst and phalloidin stained biological microthread bundle illustrated several important points. The first observation was that the entire length of the biological microthread bundle was seeded with hMSCs (although the hMSCs did not cover the entire surface area of the biological microthread bundle). Other methods that were attempted include the PDMS (Polydimethylsiloxane) v-well method and post method (the post method was used to seed Murphy et al.'s fibrin microthread bundles). The post method was attempted first because of its simplicity and effectiveness with the smaller fibrin microthread bundles. The post method required the microthread bundle to be attached to a suture needle and then glued onto a stainless steel washer. The washer was then placed in a 6 well plate and a 12 mm diameter Thermanox coverslip glued onto a PDMS post was placed underneath the center of the microthread bundle. The post was a Thermanox coverslip glued onto a PDMS cylindrical post that raised the coverslip to the level of the microthread bundle. After placement, 100 μL of cell suspension was pipetted directly onto the microthread bundle, which rested on the Thermanox coverslip. The PDMS v-well seeding method was designed so that a microthread bundle could be split into several smaller bundles to maximize the surface area exposed for seeding. The twelve equally sized v-shaped orifices in the PDMS v-well allowed the microthread bundle to be split into up to twelve separate microthreads or small microthread bundles. The protocol for seeding the v-well method was identical to the post method except for the use of the v-well. Both methods had the same critical flaws. As shown in Figure 29, only the center of the microthread bundle was actually seeded for both methods. Also, more than half of the surface of the microthread bundle was not being utilized because of the seeding design (the bottom half was covered with either a v-well or post, see Figure 30).

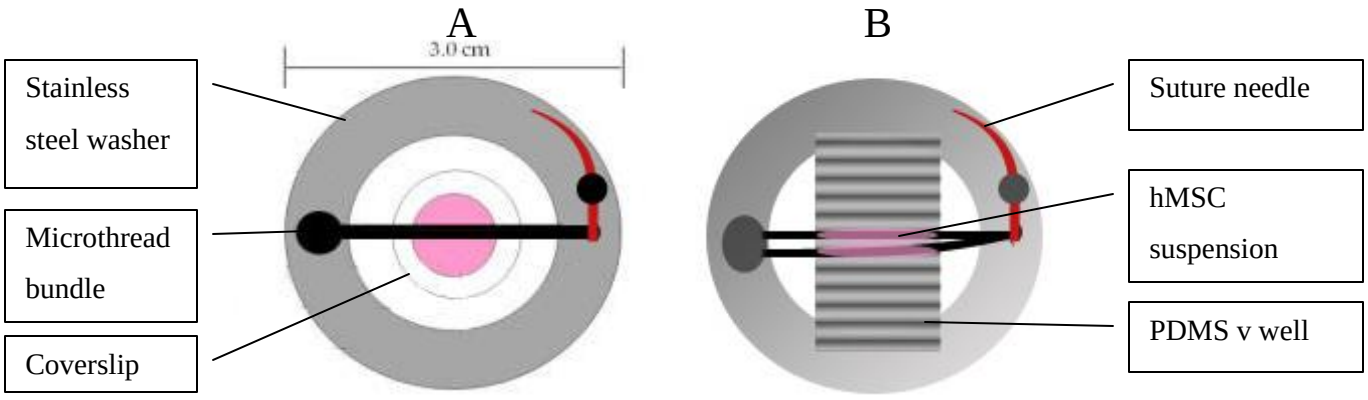

Figure 29: Previously attempted microthread seeding methods: post method (A) and v-well method (B).

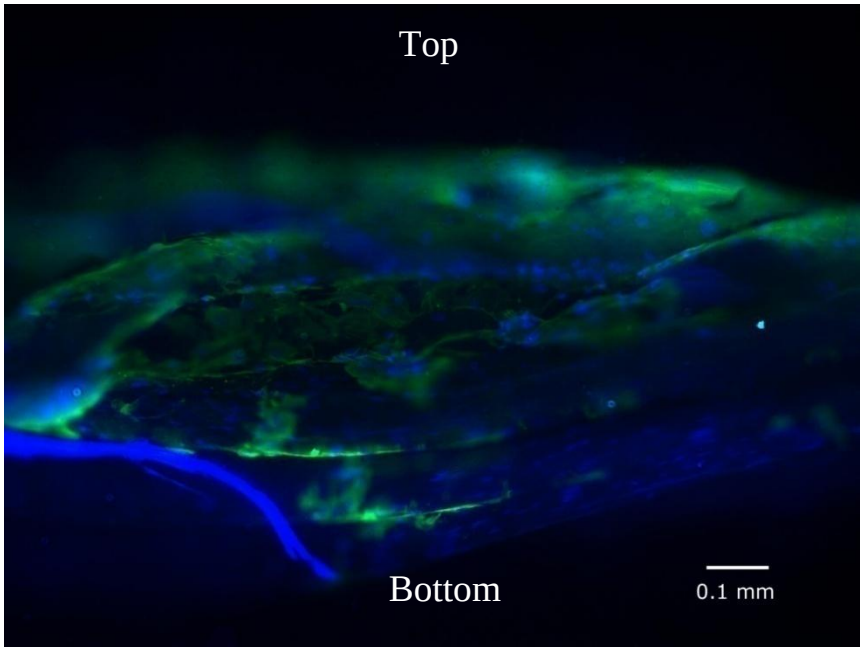

Figure 30: Biological microthread seeding after 24 hours – PDMS v-well method
(10x magnification, Hoechst dyed nuclei are blue, Phalloidin stained f-actin filaments are green). This picture illustrates the imaging difficulty when working with a bundle of 12 microthreads. Half of the image is clearly out of focus and the microthreads are stacked on top of one another, making it impossible to see all of the seeded cells. In terms of seeding, the bottom half of the microthread bundle has very few cells attached compared to the top half.

6.2 hMSC Delivery to the Heart

6.2.1 hMSC delivery efficiency

The main objective of this project was to develop a more efficient means of delivering hMSCs to the heart. As discussed in the background, current delivery methods have low cell engraftment rates. While improving delivery efficiency, the new delivery method had to facilitate surgical simplicity and reproducibility. Biological microthread implantation was chosen as a novel approach to cardiac cell delivery because of its relative surgical simplicity, similarity to suture, and ability to deliver cells near the endocardium. Intramyocardial injection was chosen as a comparison hMSC delivery method since it is widely utilized by researchers. In terms of protocol, 10,000 hMSCs were injected into the rat heart for intramyocardial injection because that was the estimated number of cells that could be delivered with seeded biological microthreads. However, since only 0.63 cm of microthread (out of 2 cm) was actually implanted into the heart on average, the adjusted microthread-mediated cell delivery was 5,527.

Each group (intramyocardial injection and biological microthread) was intended to have a sample size of 5. However, on the final intramyocardial injection experiment (EXP0226) there were no quantum dot loaded hMSCs found in the heart. This was most likely due to intracavitary injection of the hMSCs

(into the left ventricle) which resulted in the cells being washed away into the blood circulation. The ejection of the hMSC suspension due to ventricular contraction was also possible. Since the final experiment had a delivery efficiency of 0%, we did not include it in our statistical analysis because it was most likely due to surgical error. The intramyocardial injection group had a sample size of 4, while the biological microthread group had a sample size of 5. However, the experimental results illustrate an important point. Intramyocardial injection was more difficult to perform successfully than biological microthread implantation. Five out of five of our microthread implantations were successful, while four out of five intramyocardial injections were successful. The intramyocardial injections often lead to excessive bleeding due to puncturing a major blood vessel or entering the ventricular cavity with the syringe needle. The 80% success rate was mostly due to swift actions by the surgeon to minimize bleeding. Biological microthread implantation also resulted in the microthread entering the ventricular cavity or puncturing a major blood vessel on some occasions but did not cause excessive bleeding. This may be due to the fact that fibrin serves as a blood clot during the natural wound healing process and therefore halted the bleeding almost immediately.

The surgical implantation of biological microthread bundles in the rat heart was evaluated by comparing the engraftment rate of each microthread implantation. For EXP0214 and EXP0218, the surgeon attempted to implant the biological microthread bundle directly into the endocardium. In both cases, the biological microthread bundle entered the ventricular cavity and reduced the number of hMSCs engrafted into the heart wall. For the biological microthread implantation that had the highest engraftment rate, EXP0219, the surgeon attempted to implant the microthread bundle into the mid-myocardium. Therefore, future biological microthread implantation surgeries should focus on delivering the maximum length of microthread to the heart wall and not enter the ventricular cavity. Different suture needle sizes and shapes can be utilized to reduce microthread delivery to the ventricular cavity. The microthread bundles in this project were attached to size 18 tapered half-circle suture needles. A smaller suture needle (size 20 or above) that is 3/8 circle could potentially reduce delivery to the ventricular cavity.

Several complications with sectioning nearly the entire heart for each experiment (to calculate delivery efficiency) became apparent. The first issue was the amount of time required to histologically section a single heart. Four hundred eighty to 903 sections were cut per biological microthread implantation sample, while 183 to 543 sections were cut per intramyocardial injection sample. On some occasions it took several weeks before the results of a single surgery were completely analyzed. The analysis included histological sectioning, Hoechst staining, Masson's trichrome staining, α-actinin staining, and analyzing three sections every sixty sections for hMSC delivery count and biological microthread location in the heart wall. This meant that the surgeon did not know whether or not they had successfully implanted a biological microthread until several weeks passed. Another issue with sectioning

the entire heart was analyzing the sections after staining. The cryostat that was used for histologically sectioning the rat hearts occasionally cut sections of inconsistent thickness (if optimal cutting temperature was not maintained by the cryostat). Acquiring images of these sections usually resulted in a time consuming balancing act, focusing on the region of interest while a large portion of the section remained out of focus. Radiolabeled hMSCs [53] and MRI-labeled hMSCs [92] could have been utilized to reduce the time required for the complete analysis of hMSC delivery efficiency. However, both methods require a substantial initial investment of time and funding.

Quantum dots were chosen for hMSC tracking, when determining cell engraftment rate in the rat heart, for several reasons. Quantum dot loading hMSCs was a straightforward protocol and was easily reproducible (with 98% loading efficiency); involving simply adding quantum dots to the hMSC media and waiting 24 hours. Quantum dots do not affect hMSC differentiation or prevent proliferation *in vitro* [87]. Quantum dots are also not taken up by adult cardiac myocytes *in vitro* and cardiac cells *in vivo* and do not transfer to nearby cells. Quantum dot labeled hMSCs also retain quantum dots for more than six weeks *in vitro*. One of the most important advantages of quantum dots is the relatively large Stokes shift. Since there is a large gap between the maximum excitation and emission wavelengths, quantum dots are easily spotted in the heart tissue, due to minimal tissue autofluorescence and bright concentrated emission. When the three rules of counting are applied (see materials and methods section), quantum dots can be utilized to estimate cell engraftment rate. These rules are required because the most apparent disadvantage of quantum dots is the inability to see the exact outline of individual quantum dot loaded cells. This disadvantage is especially limiting when quantum dot loaded cells are in close proximity, and individual cells cannot be deciphered. In such cases, the number of quantum dot loaded cells counted must be conservative to eliminate the chances of counting non-quantum dot loaded cells.

Other methods of hMSC tracking are available that have some distinct advantages and could potentially help distinguish individual hMSC nuclei. Anti-NuMA (Nuclear Mitotic Apparatus Protein) human specific primary antibody could have been utilized to stain the hMSCs in our rat heart sections [93]. Using anti-NuMA would have allowed identification of individual hMSC nuclei and could have potentially improved counting accuracy in areas where hMSCs were in close proximity. Anti-NuMA would have also shown that the hMSCs that were delivered were in fact human cells. The disadvantages of using anti-NuMA include potential difficulty finding positive signal due to the autofluoresence of the heart tissue (if using a fluorescent secondary antibody such as Alexa Fluor 488) and an increase in the time required to complete tissue analysis (counting hMSCs delivered to the rat heart) due to the addition of another staining protocol.

Despite delivering fewer cells initially, significantly more cells were engrafted in the biological microthread group. It should be noted that the average of 3,527 hMSCs engrafted for the biological

microthread implantations could potentially be improved by simply increasing the seeding time on the biological microthreads. If the increased seeding time is not successful, new approaches to implantation could be employed, including implanting multiple biological microthreads bundles. The intramyocardial injection group exhibited an engraftment rate of 11.8%, which was comparable to the engraftment rate reported by other researchers (11%) [53]. Since only 1,180 hMSCs engrafted in the intramyocardial injection group on average, a higher concentration of cells could be injected to increase the cell engraftment number.

The number of hMSCs delivered to the rat heart was determined by manually counting quantum dot loaded hMSC nuclei in 24 μm of tissue every 480 μm. This meant that only 5% of the total heart length (from base to apex) was analyzed for each microthread implantation and intramyocardial injection sample. Future studies could focus on analyzing a single section (8 μm of tissue) at shorter intervals to decrease the distance between each of the analyzed tissue sections while not greatly increasing the percentage of tissue analyzed. The assumption that there was a linear relationship between each of the 480 μm increments was not validated. This aspect of this research should be pursued and the relationship between each of these points could potentially be determined by analyzing the heart sections at shorter intervals (40 μm for example).

Cardiac functional analysis (left ventricular ejection fraction, stroke volume, etc.) must be performed on the biological microthread implantation subjects to evaluate the effect of microthread bundle delivery to the myocardium (the left ventricular defect would be caused by ligating the left anterior descending coronary artery). The occlusion would then be removed and the blood flow would be restored prior to biological microthread implantation. The infarcted myocardium would be analyzed with or without hMSC delivery to analyze the effect of hMSCs and delivery method on cardiac function. The biological microthread bundles would be implanted in Sprague-Dawley rats with induced myocardial infarctions. The biological microthread bundle will initially be passed through the infarction to maximize hMSC delivery. However, this strategy may have to be altered due to reduced blood flow in the infarction zone and a reduction in the thickness of the heart wall with myocardial infarction. The implantation location will be an important factor in the effectiveness of biological microthread mediated hMSC delivery.

High Density Mapping (HDM) would be utilized to determine regional systolic function of the myocardial infarction before and after hMSC therapy. HDM allows the analysis of a small region (less than 10 mm^2) of the heart, by acquiring images of the beating heart and then allowing the user to pick a region of interest for software analysis [94]. The software then outputs regional stroke work which can be utilized to determine cardiac function in the region of interest [95-98]. The HDM method has been

utilized to calculate the regional function in the *in vivo* porcine model, isolated rabbit heart, and canine *in vivo* model [50, 99, 100].

6.2.2 hMSC delivery distribution

Another major goal of this project was to determine if hMSCs were being delivered throughout the length of the heart where the biological microthread was implanted or cells injected intramyocardially. If cells were being delivered to a narrow area of the heart but at a high efficiency, the delivery method was considered inefficient. The goal was to deliver a consistently high number of cells across an extensive length of heart tissue (from apex to base). Biological microthread implantation delivers hMSCs more efficiently, over a longer length in the heart tissue, and more hMSCs per 24 µm of heart tissue than intramyocardial injection.

The intramyocardial injection delivery distribution graphs demonstrate some of the characteristics of this delivery method. The cell delivery distribution appeared to be random and the surgical procedure was difficult to improve. The delivery distributions had random areas with no cell delivery in some cases (EXP0220 and EXP0224). The hMSC delivery length varied a great deal, 1,464 – 4,344 µm for the intramyocardial injections. The biological microthread implantation, in contrast, allowed the surgeon to customize the delivery length by implanting more or less of the biological microthread bundle.

The biological microthread implantation delivery distributions exhibited some important characteristics. The first characteristic was found in all of the biological microthread delivery distributions: more cells were delivered near the implantation entry site at the base of the heart (especially close to the initial insertion area, initial 24 – 1,464 µm of heart tissue). This trend may have been the result of cell shearing when the biological microthread first entered the cardiac tissue. The biological microthread was first inserted into the base-side of the heart and then removed from the apex-side of the heart. A second notable characteristic was an increase in the number of cells delivered on the end of the apex-side (usually the final 960 µm) of the implantation for some of the experiments. This trend may have been the result of cell shearing when the biological microthread exited the tissue. The final characteristic was a lack of cell engraftment in the heart wall in the center of the biological microthread implantation (1,920 µm of tissue for a single microthread implantation sample). This single occurrence was due to the biological microthread entering the ventricular cavity.

The intramyocardial injection delivery distributions were more difficult to analyze than the biological microthread implantations. The first issue was not knowing where the hMSCs were initially injected into the heart. Despite an effort to determine the injection location, the exact location could not be determined for each experiment. In terms of searching for delivered quantum dot loaded hMSCs in the heart wall, such efforts were very time consuming due to the random location of delivered hMSCs. The

entire rat heart was scanned with a fluorescent microscope for every analyzed section. The hMSCs were delivered to the endocardium, myocardium, and epicardium, with no discernable trend. In some cases there were no quantum dot loaded hMSCs present in one set of heart sections, but several present in the next set (480 μm apart). This random trend required excessive sectioning of the rat heart, even when there were no quantum dot loaded hMSCs present in several previous sets of sections. EXP0226, the failed intramyocardial injection experiment, illustrated all of the difficulties of analyzing the intramyocardial injection experiments. Four hundred eighty sections were cut for this experiment and all were analyzed, section by section, for delivered hMSCs. We did not find a single quantum dot loaded hMSC in all of these sections. The cell delivery length also varied greatly, despite an equal volume of injected cell suspension for each injection, and did not always dictate the delivery efficiency of an experiment. Cell delivery length could potentially be improved by passing a suture needle through the heart wall and injecting hMSCs into the cavity that was created to increase the amount of space available for the hMSC to engraft. EXP0221 had the highest delivery efficiency (27.8%) but did not deliver cells to the longest length of tissue (0.34 cm). EXP0220 and EXP0224 delivered hMSCs to a longer length of tissue, 0.43 cm and 0.39 cm respectively, but had lower delivery efficiencies of 7.5% and 4.6%.

Cell shearing can potentially be avoided by developing a sheath (biomaterial or polymer) to protect the cell-seeded biological microthread. The sheath would serve as a protective barrier for the hMSC seeded biological microthread bundle during the process of implantation into the left ventricular wall. The sheath could either be used in the seeding process as a bioreactor or placed over the biological microthread after seeding. The sheath would also have to be firmly attached to the suture needle without adversely affecting the seeded biological microthreads. After implantation, the sheath would be removed to ensure cell viability, minimize immune response, and ensure efficient cell delivery to the ventricular wall. A material such as polytetrafluoroethylene (PTFE) could potentially be utilized to sheath the biological microthread after seeding due to its low coefficient of friction. The low coefficient of friction would aid in the removal of the sheath post-implantation, reducing cell shearing when the sheath is removed, and decreasing the difficultly of implanting a sheathed biological microthread bundle. If the sheath was not used as a bioreactor, the current bioreactor seeding method could be employed to seed the biological microthreads with hMSCs. If the sheath was used as a bioreactor, new seeding experiments would be required to ensure proper hMSC seeding on the biological microthread (and not on the sheath). The inner and outer diameter of the sheath would also have to be an optimal size to minimize injury to the heart, minimize cell shearing during the removal of the sheath, and maximize cell seeding on the biological microthread. The sheathed biological microthread bundle has potential to be an efficient hMSC delivery method that can consistently deliver cells to the infarcted myocardium.

6.2.3 Microthread implantation tracking

Microthread implantation tracking established the location of the biological microthread bundle relative to the epicardium (outer third) and endocarium (inner third) of the left ventricular wall. Since the delivered hMSCs were found in close proximity of the biological microthread implantation (see Figure 31), Masson's trichrome stained sections were analyzed for the location of the implanted microthread. It was assumed that the location of the biological microthread indicated the location of hMSC delivery (see Figure 31). The distance from the epicardium and endocardium was stated as a percentage of the left ventricular wall thickness. When the implantation tracking graph was combined with the delivery distribution graph for a given experiment, the number of cells delivered to each third of the left ventricular thickness could be determined.

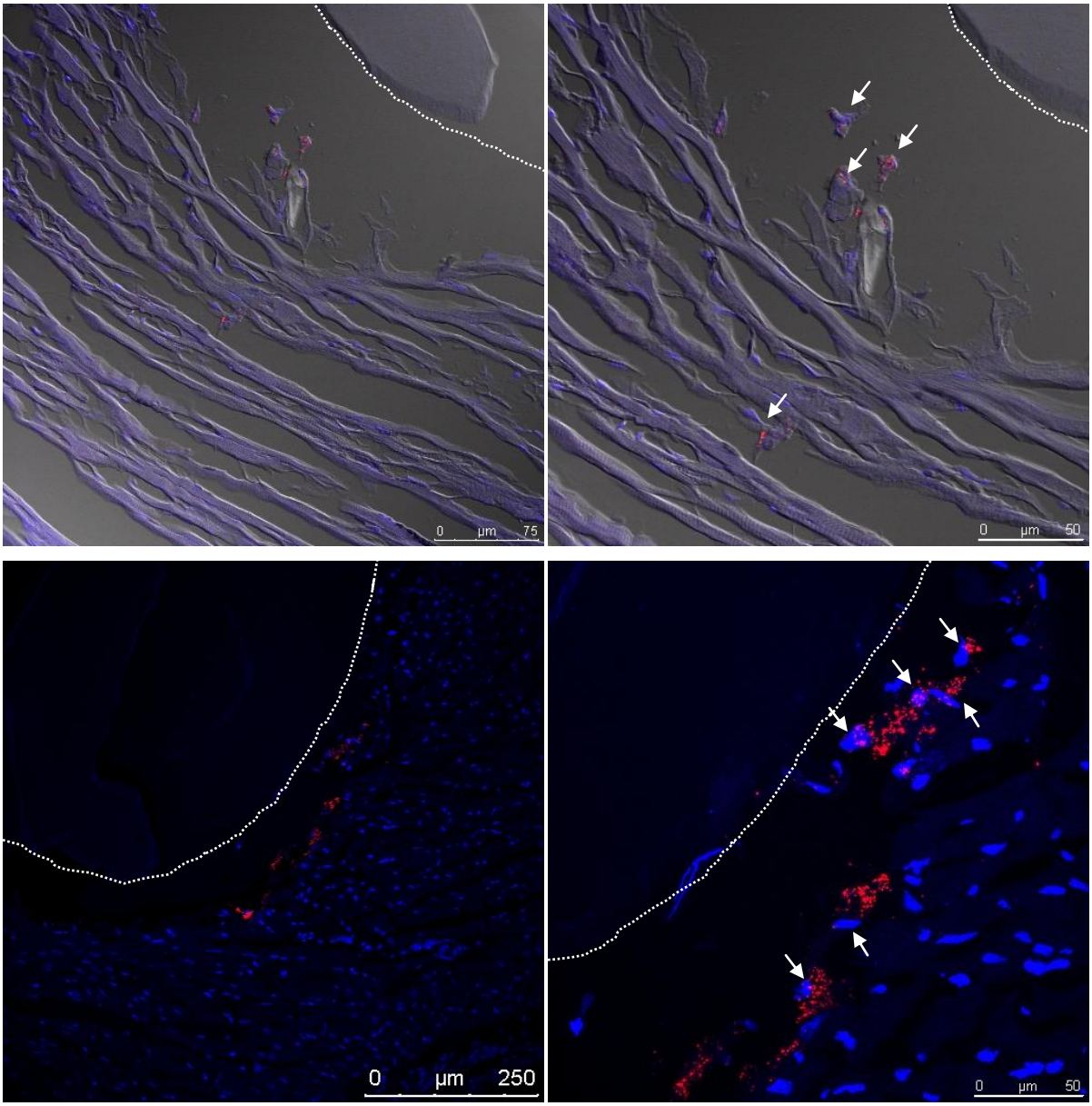

Figure 31: hMSCs delivered in close proximity to biological microthread bundle
(40x magnification [top left], 63x magnification [top right], Hoechst dyed nuclei are blue, quantum dots are red, DIC overlay). (20x magnification [bottom left], 63x magnification [bottom right], Hoechst dyed nuclei are blue, quantum dots are red). White arrows indicate the location of quantum dot loaded cells. White dashed outlines indicate the location of the biological microthread bundles.

Several complications arose as the heart sections were being analyzed. Some heart sections were smaller than others even when they were only 480 µm apart. This inconsistency can be attributed to the cryostat, which on occasion has cut sections of varying thickness (in some cases up to 3 µm more or less than the intended 8 µm thickness). Some heart sections also detached from the microscope slides during

staining (partially and fully), which resulted in the tissue folding on itself or complete tissue loss. These tissue sections were never used for analysis. The implanted biological microthread bundles also moved during sectioning on some of the heart sections. Since there were three heart sections on each slide, at least one section (out of the three) always had a biological microthread bundle that did not move during sectioning. On other occasions, the biological microthread bundle entered the ventricular cavity. When this occurred, the biological microthread bundle occasionally could not be found and it was assumed that the bundle was located 100% of the left ventricular wall thickness from the epicardium and 0% of the wall thickness from the endocardium. One of the implantation tracking graphs (EXP0217) also depicted the biological microthread bundle moving out and into the ventricular wall for a length of the implantation. This unexpected occurrence may have been due to several factors including: the cryostat cutting heart sections of various thicknesses and potentially not cutting the entire surface of the heart or difficulty passing the biological microthread bundle through the ventricular wall. Embedding the heart in paraffin may have prevented many of these complications, but was not done because of incompatibility with quantum dots. The quantum dots located in the loaded hMSCs faded several days after being embedded in paraffin.

6.3 Microscopy

Microscopy played a pivotal role in the completion of this project. Several different microscope types were used for different reasons throughout the project: an inverted microscope was used to ensure that hMSCs were quantum dot loaded prior to seeding a microthread bundle or trypsinizing hMSCs prior to injection; an upright microscope was used to count the number of hMSCs delivered to the heart wall, determine the location of the microthread implant, and acquire images of the hMSC seeded biological microthreads; and a confocal microscope was used to further study quantum dot loaded cells that were delivered to the heart. Each microscope type had its limitations. The upright and inverted microscopes could only focus on a narrow depth of field, which complicated acquiring images of quantum dot loaded hMSCs on some occasions. The upright and inverted microscopes also could not perform spectral analysis, which meant that tissue/microthread autofluorescence was nearly impossible to overcome. Only the inverted microscope could be used to acquire images of live cells since they were on the bottom of T75 flasks. The point scanning confocal microscope usually required a much longer time investment, especially when performing a z-stack or spectral analysis, than the upright and inverted microscopes, which resulted in fewer acquired images. Performing a z-stack on anything over 150 µm (at 40x magnification) was also not possible due to the limitations of the confocal microscope and software. Therefore a confocal image of the entire depth of the hMSC seeded biological microthread (over 700 µm diameter) was not possible with any oil objective (20x-63x).

The z-stacks, acquired with a confocal microscope, illustrated several points about quantum dots: quantum dots may look like they are in the cell's nucleus, but are actually in the cytoplasm on top of the nucleus; quantum dots can be on a completely different plane than the same cell's nucleus, making it look like a cell is or is not quantum dot loaded under a non-confocal microscope; quantum dots can span over nearly a an 8 µm thickness, which means that all quantum dots in a cell cannot be captured with a single image (a z-stack is required). Since the images used to perform the hMSC delivery count to the heart were taken with an upright microscope, some quantum dot loaded cells may not have been detected due to the limitations of the microscope. The lack of detection could have been due to several reasons including: only a faint part of the quantum dot signal being in focus, the visible signal not being adjacent to the loaded nucleus due to focal plane, and difficulty analyzing three dimensional "quantum dot clouds" with an upright microscope, causing an overly conservative count of quantum dot loaded cells (z-stack is required for a 3D image). Most of these problems were anticipated but could not be overcome due to time limitations (hundreds of images were taken for the analysis of all nine surgeries). The quantum dot counting rules, as discussed earlier, were established to minimize the chances of over-estimating the number of cells delivered to the heart. The actual number of cells delivered to the heart wall could have been higher than reported in this thesis for each experiment.

Conclusion

Biological microthreads were developed into a novel cardiac delivery method that is surgically simple to implant and can be seeded with hMSCs. We have demonstrated that biological microthread mediated hMSC delivery is more efficient and can deliver cells over a longer length of tissue than intramyocardial injection. We were also able to deliver a higher quantity of hMSCs to the endocardium and myocardium, effectively targeting those layers of the ventricular wall with biological microthread hMSC delivery. This delivery system may lead to improved treatment for millions of patients suffering from myocardial infarction or heart failure.

References

1. Sutton, M. and N. Sharpe, *Left ventricular remodeling after myocardial infarction: pathophysiology and therapy.* Circulation, 2000. **101**(25): p. 2981-8.
2. Bergmann, O., et al., *Evidence for cardiomyocyte renewal in humans.* Science, 2009. **324**(5923): p. 98-102.
3. Beltrami, A.P., et al., *Evidence that human cardiac myocytes divide after myocardial infarction.* N Engl J Med, 2001. **344**(23): p. 1750-7.
4. Laflamme, M. and C. Murry, *Regenerating the heart.* Nat Biotechnol, 2005. **23**(7): p. 845-56.
5. Cicala, R., *The Heart Disease Sourcebook*. 1997: RGA Publishing Group. 316.
6. Buckberg, G., *Ventricular structure and surgical history.* Heart Fail Rev, 2004. **9**(4): p. 255-68; discussion 347-51.
7. Liu, J., et al., *Human mesenchymal stem cells improve myocardial performance in a splenectomized rat model of chronic myocardial infarction.* J Formos Med Assoc, 2008. **107**(2): p. 165-74.
8. Grauss, R., et al., *Mesenchymal stem cells from ischemic heart disease patients improve left ventricular function after acute myocardial infarction.* Am J Physiol Heart Circ Physiol, 2007. **293**(4): p. H2438-47.
9. Simpson, D., et al., *A tissue engineering approach to progenitor cell delivery results in significant cell engraftment and improved myocardial remodeling.* Stem Cells, 2007. **25**(9): p. 2350-7.
10. Leor, J., et al., *Bioengineered cardiac grafts: A new approach to repair the infarcted myocardium?* Circulation, 2000. **102**(19 Suppl 3): p. III56-61.
11. Christman, K., et al., *Injectable fibrin scaffold improves cell transplant survival, reduces infarct expansion, and induces neovasculature formation in ischemic myocardium.* J Am Coll Cardiol, 2004. **44**(3): p. 654-60.
12. Wei, H.J., et al., *Bioengineered cardiac patch constructed from multilayered mesenchymal stem cells for myocardial repair.* Biomaterials, 2008. **29**(26): p. 3547-56.
13. Hou, M., et al., *Transplantation of mesenchymal stem cells from human bone marrow improves damaged heart function in rats.* Int J Cardiol, 2007. **115**(2): p. 220-8.
14. Cornwell, K., *Collagen and Fibrin Biopolymer Microthreads for Bioengineered Ligament Generation*, in *Biomedical Engineering*. 2007, WPI: Worcester.
15. Christman, K., et al., *Fibrin glue alone and skeletal myoblasts in a fibrin scaffold preserve cardiac function after myocardial infarction.* Tissue Eng. **10**(3-4): p. 403-9.
16. Murphy, M.K., *Fibrin Microthreads Promote Stem Cell Growth for Localized Delivery in Regenerative Therapy*, in *Biomedical Engineering*. 2008, WPI: Worcester.
17. Masuda, S., et al., *Cell sheet engineering for heart tissue repair.* Adv Drug Deliv Rev, 2008. **60**(2): p. 277-85.
18. Shimizu, T., et al., *Cell sheet engineering for myocardial tissue reconstruction.* Biomaterials, 2003. **24**(13): p. 2309-16.
19. Cornwell, K. and G. Pins, *Discrete crosslinked fibrin microthread scaffolds for tissue regeneration.* 2007: Journal of Biomedical Materials Research. p. 104-112.
20. Humphrey, J., *Cardiovascular Solid Mechanics: Cells, Tissues and Organs*. 2001.

21. Marieb, E.N. and K. Hoehn, *Human Anatomy & Physiology*. 2007: Pearson.
22. Sherwood, L., *Human physiology : from cells to systems*. 4th ed. 2001, Pacific Grove, Calif.: Brooks/Cole. xx, 766 p.
23. Wiley InterScience (Online service), *Wiley encyclopedia of biomedical engineering*. 2006, Wiley-InterScience: Hoboken, N.J.
24. Miniño, A., et al., *Deaths: final data for 2004.* Natl Vital Stat Rep, 2007. **55**(19): p. 1-119.
25. Thom, T., et al., *Heart disease and stroke statistics--2006 update: a report from the American Heart Association Statistics Committee and Stroke Statistics Subcommittee.* Circulation, 2006. **113**(6): p. e85-151.
26. Cramer, D., L. Podesta, and L. Makowka, *Handbook of Animal Models in Transplantation Research*. 1994: CRC Press, Inc.
27. Lee, T.M., M.S. Lin, and N.C. Chang, *Effect of pravastatin on sympathetic reinnervation in postinfarcted rats.* Am J Physiol Heart Circ Physiol, 2007. **293**(6): p. H3617-26.
28. Zakharova, L., et al., *Transplantation of cardiac progenitor cell sheet onto infarcted heart promotes cardiogenesis and improves function.* Cardiovasc Res.
29. Gaballa, M.A., et al., *Grafting an acellular 3-dimensional collagen scaffold onto a non-transmural infarcted myocardium induces neo-angiogenesis and reduces cardiac remodeling.* J Heart Lung Transplant, 2006. **25**(8): p. 946-54.
30. Braunwald, E. and M. Pfeffer, *Ventricular enlargement and remodeling following acute myocardial infarction: mechanisms and management.* Am J Cardiol, 1991. **68**(14): p. 1D-6D.
31. Athanasuleas, C., et al., *Surgical ventricular restoration in the treatment of congestive heart failure due to post-infarction ventricular dilation.* J Am Coll Cardiol, 2004. **44**(7): p. 1439-45.
32. Hernandez, A., et al., *Contemporary performance of surgical ventricular restoration procedures: data from the Society of Thoracic Surgeons' National Cardiac Database.* Am Heart J, 2006. **152**(3): p. 494-9.
33. Fang, J. and C. GS, *Surgical Management of Congestive Heart Failure*. 2005, Humana Press Inc.: Totowa, NJ.
34. Tønnessen, T. and C. Knudsen, *Surgical left ventricular remodeling in heart failure.* Eur J Heart Fail, 2005. **7**(5): p. 704-9.
35. Orlic, D., et al., *Mobilized bone marrow cells repair the infarcted heart, improving function and survival.* Proc Natl Acad Sci U S A, 2001. **98**(18): p. 10344-9.
36. Taylor, D.A., et al., *Regenerating functional myocardium: improved performance after skeletal myoblast transplantation.* Nat Med, 1998. **4**(8): p. 929-33.
37. Kolossov, E., et al., *Engraftment of engineered ES cell-derived cardiomyocytes but not BM cells restores contractile function to the infarcted myocardium.* J Exp Med, 2006. **203**(10): p. 2315-27.
38. Beltrami, A.P., et al., *Adult cardiac stem cells are multipotent and support myocardial regeneration.* Cell, 2003. **114**(6): p. 763-76.
39. Christman, K. and R. Lee, *Biomaterials for the treatment of myocardial infarction.* J Am Coll Cardiol, 2006. **48**(5): p. 907-13.
40. Schuldt, A., et al., *Repairing damaged myocardium: evaluating cells used for cardiac regeneration.* Curr Treat Options Cardiovasc Med, 2008. **10**(1): p. 59-72.
41. Reffelmann, T. and R. Kloner, *Cellular cardiomyoplasty--cardiomyocytes, skeletal myoblasts, or stem cells for regenerating myocardium and treatment of heart failure?* Cardiovasc Res, 2003. **58**(2): p. 358-68.
42. Pittenger, M. and B. Martin, *Mesenchymal stem cells and their potential as cardiac therapeutics.* Circ Res, 2004. **95**(1): p. 9-20.
43. Barry, F. and J. Murphy, *Mesenchymal stem cells: clinical applications and biological characterization.* Int J Biochem Cell Biol, 2004. **36**(4): p. 568-84.

44. Toma, C., et al., *Human mesenchymal stem cells differentiate to a cardiomyocyte phenotype in the adult murine heart.* Circulation, 2002. **105**(1): p. 93-8.
45. Piao, H., et al., *Effects of bone marrow derived mesenchymal stem cells transplantation in acutely infarcting myocardium.* Eur J Heart Fail, 2005. **7**(5): p. 730-8.
46. Mangi, A., et al., *Mesenchymal stem cells modified with Akt prevent remodeling and restore performance of infarcted hearts.* Nat Med, 2003. **9**(9): p. 1195-201.
47. Barbash, I., et al., *Systemic delivery of bone marrow-derived mesenchymal stem cells to the infarcted myocardium: feasibility, cell migration, and body distribution.* Circulation, 2003. **108**(7): p. 863-8.
48. Tang, J., et al., *Mesenchymal stem cells participate in angiogenesis and improve heart function in rat model of myocardial ischemia with reperfusion.* Eur J Cardiothorac Surg, 2006. **30**(2): p. 353-61.
49. Hare, J.M., et al., *A randomized, double-blind, placebo-controlled, dose-escalation study of intravenous adult human mesenchymal stem cells (prochymal) after acute myocardial infarction.* J Am Coll Cardiol, 2009. **54**(24): p. 2277-86.
50. Azeloglu, E.U., et al., *High resolution mechanical function in the intact porcine heart: mechanical effects of pacemaker location.* J Biomech, 2006. **39**(4): p. 717-25.
51. Müller-Ehmsen, J., et al., *Survival and development of neonatal rat cardiomyocytes transplanted into adult myocardium.* J Mol Cell Cardiol, 2002. **34**(2): p. 107-16.
52. Wolf, D., et al., *Dose-dependent effects of intravenous allogeneic mesenchymal stem cells in the infarcted porcine heart.* Stem Cells Dev, 2009. **18**(2): p. 321-9.
53. Hou, D., et al., *Radiolabeled cell distribution after intramyocardial, intracoronary, and interstitial retrograde coronary venous delivery: implications for current clinical trials.* Circulation, 2005. **112**(9 Suppl): p. I150-6.
54. Zhang, M., et al., *Cardiomyocyte grafting for cardiac repair: graft cell death and anti-death strategies.* J Mol Cell Cardiol, 2001. **33**(5): p. 907-21.
55. Piao, H., et al., *Effects of cardiac patches engineered with bone marrow-derived mononuclear cells and PGCL scaffolds in a rat myocardial infarction model.* Biomaterials, 2007. **28**(4): p. 641-649.
56. Wei, H., et al., *Porous acellular bovine pericardia seeded with mesenchymal stem cells as a patch to repair a myocardial defect in a syngeneic rat model.* Biomaterials, 2006. **27**(31): p. 5409-19.
57. Derval, N., et al., *Epicardial deposition of endothelial progenitor and mesenchymal stem cells in a coated muscle patch after myocardial infarction in a murine model.* Eur J Cardiothorac Surg, 2008. **34**(2): p. 248-54.
58. Xiang, Z., et al., *Collagen-GAG scaffolds grafted onto myocardial infarcts in a rat model: a delivery vehicle for mesenchymal stem cells.* Tissue Eng, 2006. **12**(9): p. 2467-78.
59. Fukuhara, S., et al., *Bone marrow cell-seeded biodegradable polymeric scaffold enhances angiogenesis and improves function of the infarcted heart.* Circ J, 2005. **69**(7): p. 850-7.
60. Jin, J., et al., *Transplantation of mesenchymal stem cells within a poly(lactide-co-epsilon-caprolactone) scaffold improves cardiac function in a rat myocardial infarction model.* Eur J Heart Fail, 2009. **11**(2): p. 147-53.
61. Davis, M., et al., *Custom design of the cardiac microenvironment with biomaterials.* Circ Res, 2005. **97**(1): p. 8-15.
62. Kofidis, T., et al., *A novel bioartificial myocardial tissue and its prospective use in cardiac surgery.* Eur J Cardiothorac Surg, 2002. **22**(2): p. 238-43.
63. Thompson, C., et al., *Percutaneous transvenous cellular cardiomyoplasty. A novel nonsurgical approach for myocardial cell transplantation.* J Am Coll Cardiol, 2003. **41**(11): p. 1964-71.

64. Zhang, P., et al., *Artificial matrix helps neonatal cardiomyocytes restore injured myocardium in rats.* Artif Organs, 2006. **30**(2): p. 86-93.
65. Zhang, G., et al., *Enhancing efficacy of stem cell transplantation to the heart with a PEGylated fibrin biomatrix.* Tissue Eng Part A, 2008. **14**(6): p. 1025-36.
66. Park, H., et al., *A novel composite scaffold for cardiac tissue engineering.* In Vitro Cell Dev Biol Anim, 2005. **41**(7): p. 188-96.
67. Rowley, J., G. Madlambayan, and D. Mooney, *Alginate hydrogels as synthetic extracellular matrix materials.* Biomaterials, 1999. **20**(1): p. 45-53.
68. Perets, A., et al., *Enhancing the vascularization of three-dimensional porous alginate scaffolds by incorporating controlled release basic fibroblast growth factor microspheres.* J Biomed Mater Res A, 2003. **65**(4): p. 489-97.
69. Stevens, M., et al., *A rapid-curing alginate gel system: utility in periosteum-derived cartilage tissue engineering.* Biomaterials, 2004. **25**(5): p. 887-94.
70. Ponticiello, M., et al., *Gelatin-based resorbable sponge as a carrier matrix for human mesenchymal stem cells in cartilage regeneration therapy.* J Biomed Mater Res, 2000. **52**(2): p. 246-55.
71. Akhyari, P., et al., *Mechanical stretch regimen enhances the formation of bioengineered autologous cardiac muscle grafts.* Circulation, 2002. **106**(12 Suppl 1): p. I137-42.
72. Li, R., et al., *Survival and function of bioengineered cardiac grafts.* Circulation, 1999. **100**(19 Suppl): p. II63-9.
73. Eschenhagen, T., et al., *Three-dimensional reconstitution of embryonic cardiomyocytes in a collagen matrix: a new heart muscle model system.* FASEB J, 1997. **11**(8): p. 683-94.
74. Cox, S., M. Cole, and B. Tawil, *Behavior of human dermal fibroblasts in three-dimensional fibrin clots: dependence on fibrinogen and thrombin concentration.* Tissue Eng. **10**(5-6): p. 942-54.
75. Ratner, B., et al., *Biomaterials Science: An Introduction to Materials n Medicine*. 2004, San Diego: Elsevier.
76. Ryu, J., et al., *Implantation of bone marrow mononuclear cells using injectable fibrin matrix enhances neovascularization in infarcted myocardium.* Biomaterials, 2005. **26**(3): p. 319-26.
77. Mol, A., et al., *Fibrin as a cell carrier in cardiovascular tissue engineering applications.* Biomaterials, 2005. **26**(16): p. 3113-21.
78. Dunn, M., et al., *Development of fibroblast-seeded ligament analogs for ACL reconstruction.* J Biomed Mater Res, 1995. **29**(11): p. 1363-71.
79. Bellincampi, L.D., et al., *Viability of fibroblast-seeded ligament analogs after autogenous implantation.* J Orthop Res, 1998. **16**(4): p. 414-20.
80. Koob, T.J., T.A. Willis, and D.J. Hernandez, *Biocompatibility of NDGA-polymerized collagen fibers. I. Evaluation of cytotoxicity with tendon fibroblasts in vitro.* J Biomed Mater Res, 2001. **56**(1): p. 31-9.
81. Gentleman, E., et al., *Mechanical characterization of collagen fibers and scaffolds for tissue engineering.* Biomaterials, 2003. **24**(21): p. 3805-13.
82. Gentleman, E., et al., *Development of ligament-like structural organization and properties in cell-seeded collagen scaffolds in vitro.* Ann Biomed Eng, 2006. **34**(5): p. 726-36.
83. Bulte, J.W. and D.L. Kraitchman, *Monitoring cell therapy using iron oxide MR contrast agents.* Curr Pharm Biotechnol, 2004. **5**(6): p. 567-84.
84. Kraitchman, D.L., et al., *Dynamic imaging of allogeneic mesenchymal stem cells trafficking to myocardial infarction.* Circulation, 2005. **112**(10): p. 1451-61.
85. Frangioni, J.V., *In vivo near-infrared fluorescence imaging.* Curr Opin Chem Biol, 2003. **7**(5): p. 626-34.
86. Invitrogen, *Qdot Nanocrystal Technology Overview.* 2008.

87. Rosen, A.B., et al., *Finding fluorescent needles in the cardiac haystack: tracking human mesenchymal stem cells labeled with quantum dots for quantitative in vivo three-dimensional fluorescence analysis.* Stem Cells, 2007. **25**(8): p. 2128-38.
88. Pins, G. and F. Silver, *A self-assembled collagen scaffold suitable for use in soft and hard tissue replacement.* Materials Science and Engineering, 1995: p. 101-107.
89. Elsdale, T. and J. Bard, *Collagen substrata for studies on cell behavior.* J Cell Biol, 1972. **54**(3): p. 626-37.
90. Invitrogen, *Hoechst 33342, trihydrochloride, trihydrate - Manual.* 2010.
91. Invitrogen, *Alexa Fluor Dye Series - Technical Notes and Product Highlights.* 2010.
92. Amado, L.C., et al., *Cardiac repair with intramyocardial injection of allogeneic mesenchymal stem cells after myocardial infarction.* Proc Natl Acad Sci U S A, 2005. **102**(32): p. 11474-9.
93. Huang, N.F., et al., *A rodent model of myocardial infarction for testing the efficacy of cells and polymers for myocardial reconstruction.* Nat Protoc, 2006. **1**(3): p. 1596-609.
94. Kelly, D.J., et al., *Accuracy and reproducibility of a subpixel extended phase correlation method to determine micron level displacements in the heart.* Med Eng Phys, 2007. **29**(1): p. 154-62.
95. Vinten-Johansen, J., et al., *Reversal of dyskinesis by increased end diastolic segment length in ischaemic-reperfused myocardium.* Cardiovasc Res, 1989. **23**(9): p. 810-9.
96. Bufkin, B.L., et al., *Preconditioning during simulated MIDCABG attenuates blood flow defects and neutrophil accumulation.* Ann Thorac Surg, 1998. **66**(3): p. 726-31; discussion 731-2.
97. Cohen, M.V., et al., *Favorable remodeling enhances recovery of regional myocardial function in the weeks after infarction in ischemically preconditioned hearts.* Circulation, 2000. **102**(5): p. 579-83.
98. Morris, J.J., 3rd, et al., *Quantification of the contractile response to injury: assessment of the work-length relationship in the intact heart.* Circulation, 1987. **76**(3): p. 717-27.
99. Gaudette, G.R., et al., *Determination of regional area stroke work with high spatial resolution in the heart.* Cardiovascular Engineering: An International Journal, 2002. **2**(4): p. 129-137.
100. Kochupura, P.V., et al., *Tissue-engineered myocardial patch derived from extracellular matrix provides regional mechanical function.* Circulation, 2005. **112**(9 Suppl): p. I144-9.

Appendix A: Microthread Seeding Counts

Experiment	Hemacytometer count	Trypsinized thread cell count	Total cell seeding
0214	12,000		12,000
	2,640		2,640
0215	6,320		6,320
	2,760		2,760
0217	30,080		30,080
	4,032	2,127	6,159
0218 and 0219	22,200	63	22,263
	9,120	520	9,640
Seeding Experiment 1	7,560	60	7,620
	1,050	1,149	2,199
	6,400	145	6,545
	6,560	370	6,930
Seeding Experiment 2	3,533	30	3,563
	14,896	32	14,928
	11,777	170	11,947
	10,577	26	10,603
Seeding Experiment 3	15,200	51	15,251
	15,333	18	15,351
	6,066	101	6,167
	12,720	33	12,753

Seeding Experiment 4	12,740	77	12,817
	15,360	44	15,404
	18,200	38	18,238
	21,312	92	21,404
Seeding Experiment 5	11,250	22	11,272
	16,100	50	16,150
	8,700	19	8,719
	18,200	61	18,261
Average		**230**	**11,685**

Appendix B: hMSC Delivery Number Calculation

EXP0214	Counted hMSCs		Average of 2 adjacent counted slides	Average * # Slides Inbetween
Slide 1	6		10.5	210
Slide 21	15		10.5	210
Slide 41	6		14.5	290
Slide 61	23		13.5	270
Slide 81	4		4	80
Slide 101	4		3	60
Slide 121	2		2.5	50
Slide 141	3		5	100
Slide 161	7		13.5	270
Slide 181	20		19.5	390
Slide 201	19		34.5	690
Slide 221	50		50	50
Total cells delivered				**2670**

EXP0215	Counted hMSCs		Average of 2 adjacent counted slides	Average * # Slides Inbetween
Slide 1	15		17.5	350
Slide 21	20		12.5	237.5
Slide 40	5		5.5	115.5
Slide 61	6		5	100
Slide 81	4		4.5	99
Slide 103	5		6.5	130
Slide 123	8		12	240
Slide 143	16		26	520
Slide 163	36		36	36
Total cells delivered				**1828**

EXP0217	Counted hMSCs		Average of 2 adjacent counted slides	Average * # Slides Inbetween
Slide 1	5		7.5	150
Slide 21	10		8.5	170
Slide 41	7		9.5	190
Slide 61	12		7.5	150
Slide 81	3		4.5	90
Slide 101	6		9	180
Slide 121	12		27.5	550
Slide 141	43		53	1060
Slide 161	63		56	1120
Slide 181	49		49	49
Total cells delivered				**3709**

EXP0218	Counted hMSCs		Average of 2 adjacent counted slides	Average * # Slides Inbetween
Slide 1	15		14	280
Slide 21	13		13	260
Slide 41	13		17	340
Slide 61	21		27	486
Slide 81	33		16.5	330
Slide 101	0		0	0
Slide 121	0		0	0
Slide 141	0		0	0
Slide 161	0		6.5	175.5
Slide 188	13		20.5	410
Slide 208	28		27.5	550
Slide 228	27		29.5	590
Slide 248	32		23	460
Slide 268	14		14	14
Total cells delivered				**3895.5**

EXP0219	Counted hMSCs		Average of 2 adjacent counted slides	Average * # Slides Inbetween
Slide 1	14		13.5	270
Slide 21	13		10.5	210
Slide 41	8		10	200
Slide 61	12		14.5	290
Slide 81	17		10	200
Slide 101	3		2.5	50
Slide 121	2		1.5	30
Slide 141	1		5.5	110
Slide 161	10		11	220
Slide 181	12		14.5	290
Slide 201	17		15.5	310
Slide 221	14		42	840
Slide 241	70		61	1220
Slide 261	52		43.5	870
Slide 281	35		20.5	410
Slide 301	6		6	6
Total cells delivered				**5526**

EXP0220	Counted hMSCs		Average of 2 adjacent counted slides	Average * # Slides Inbetween
Slide 1	3		2	40
Slide 21	1		1.5	30
Slide 41	2		1	20
Slide 61	0		7	140
Slide 81	14		10.5	210
Slide 101	7		4	80
Slide 121	1		3	60
Slide 141	5		5	100
Slide 161	5		3.5	70
Slide 181	2		2	2
Total cells delivered				**752**

EXP0221	Counted hMSCs		Average of 2 adjacent counted slides	Average * # Slides Inbetween
Slide 1	16		15	300
Slide 21	14		24.5	490
Slide 41	35		29.5	590
Slide 61	24		20	400
Slide 81	16		20.5	410
Slide 101	25		18.5	370
Slide 121	12		10.5	210
Slide 141	9		9	9
Total cells delivered				**2779**

EXP0224	Counted hMSCs		Average of 2 adjacent counted slides	Average * # Slides Inbetween
Slide 1	1		0.5	10
Slide 21	0		3	60
Slide 41	6		5.5	110
Slide 61	5		4	80
Slide 81	3		3.5	70
Slide 101	4		4	80
Slide 121	4		2	40
Slide 141	0		0.5	10
Slide 161	1		1	1
Total cells delivered				**461**

EXP0225	Counted hMSCs		Average of 2 adjacent counted slides	Average * # Slides Inbetween
Slide 1	5		8	160
Slide 21	11		10.5	210
Slide 41	10		10.5	210
Slide 61	11		11	11
Total cells delivered				**591**

Appendix C: Microthread Implantation Tracking Measurements

Exp 214					
Slide Number	**Endocardial distance (mm)**	**Epicardial distance (mm)**	**Left ventricular wall thickness (mm)**	**Endo distance/wall thickness (%)**	**Epi distance/wall thickness (%)**
Slide 241	2.03	0	2.03	100	0
Slide 221	1.096	1.744	2.84	38.6	61.4
Slide 201	0.457	2.342	2.799	16.3	83.7
Slide 181	0	3.09	3.09	0	100
Slide 161	0	3.09	3.09	0	100
Slide 141	0	3.09	3.09	0	100
Slide 121	0	4.715	4.715	0	100
Slide 101	0	4.33	4.33	0	100
Slide 81	0	4.248	4.248	0	100
Slide 61	0	4.017	4.017	0	100
Slide 41	0	4.343	4.343	0	100
Slide 21	0.249	3.432	3.681	6.8	93.2
Slide 1	4.149	0	4.149	100	0

Exp 215					
Slide Number	**Endocardial distance (mm)**	**Epicardial distance (mm)**	**Left ventricular wall thickness (mm)**	**Endo distance/wall thickness (%)**	**Epi distance/wall thickness (%)**
Slide 1	4.95	0	4.95	100	0
Slide 21	4.136	0.78	4.916	84.1	15.9
Slide 40	2.71	1.135	3.845	70.5	29.5
Slide 61	1.49	1.98	3.47	42.9	57.1
Slide 81	0.82	2.82	3.64	22.5	77.5
Slide 103	1.2	2.76	3.96	30.3	69.7
Slide 123	1.24	2.73	3.97	31.2	68.8
Slide 143	0.96	1.95	2.91	33.0	67.0
Slide 163	1.39	1.47	2.86	48.6	51.4
Slide 183	2.77	0	2.77	100	0

Exp 217					
Slide Number	**Endocardial distance (mm)**	**Epicardial distance (mm)**	**Left ventricular wall thickness (mm)**	**Endo distance/wall thickness (%)**	**Epi distance/wall thickness (%)**
Slide 201	1.556	0	1.556	100	0
Slide 181	1.305	1.7	3.005	43.4	56.6
Slide 161	1.337	1.8711	3.2081	41.7	58.3
Slide 141	1.8	2.33	4.13	43.6	56.4
Slide 121	1.33	1.67	3	55.7	44.3
Slide 101	0	2.62	2.62	0	100
Slide 81	0.559	2.796	3.355	16.7	83.3
Slide 61	0.577	2.436	3.013	19.2	80.8
Slide 41	1.36	1.79	3.15	43.2	56.8
Slide 21	2.23	0.88	3.11	71.7	28.3
Slide 1	2.601	0	2.601	100	0

Exp 218					
Slide Number	**Endocardial distance (mm)**	**Epicardial distance (mm)**	**Left ventricular wall thickness (mm)**	**Endo distance/wall thickness (%)**	**Epi distance/wall thickness (%)**
Slide 268	1.61	0	1.61	100	0
Slide 248	0.2381	2.789	3.0271	7.9	92.1
Slide 228	0	3.268	3.268	0	100
Slide 208	0	3.296	3.296	0	100
Slide 188	0	4.147	4.147	0	100
Slide 161	0	3.34	3.34	0	100
Slide 141	No Thread	No Thread	3.629	0	100
Slide 121	No Thread	No Thread	3.66	0	100
Slide 101	No Thread	No Thread	3.66	0	100
Slide 81	No Thread	No Thread	2.156	0	100
Slide 61	0	3.786	3.786	0	100
Slide 41	0.664	3.1	3.764	17.6	82.4
Slide 21	2.713	1.477	4.19	64.7	35.3
Slide 1	2.581	0	2.581	100	0

Exp 219					
Slide Number	**Endocardial distance (mm)**	**Epicardial distance (mm)**	**Left ventricular wall thickness (mm)**	**Endo distance/wall thickness (%)**	**Epi distance/wall thickness (%)**
Slide 301	4.84	0	4.84	100	0
Slide 281	3.11	1.27	4.38	71.1	28.9
Slide 261	3.673	1.677	5.35	68.7	31.3
Slide 241	3.077	2.341	5.418	56.8	43.2
Slide 221	2.307	2.09	4.397	52.5	47.5
Slide 201	1.321	1.198	2.519	52.4	47.6
Slide 181	0.821	0.886	1.707	48.1	51.9
Slide 161	0.89	1.175	2.065	43.1	56.9
Slide 141	1.1	1.73	2.83	38.9	61.1
Slide 121	1.47	2.25	3.72	39.5	60.5
Slide 101	1.09	2.41	3.5	31.1	68.9
Slide 81	0.93	3.01	3.94	23.6	76.4
Slide 61	1.28	2.46	3.74	34.2	65.8
Slide 41	3.64	0.594	4.234	86.0	14.0
Slide 21	3.74	0.41	4.15	90.1	9.9
Slide 1	3.89	0	3.89	100	0

Appendix D: Surgical Notes

Experiment number	EXP0214
Experiment date	09/09/2009
Rat sex	Male
Rat type	Sprague Dawley
Rat weight	690 grams
Drugs administered (volume)	Ketamine (1.04 mL), Xylazine (0.05 mL), Isoflurane (2% vaporized)
Implantation type	8 fibrin, 4 collagen microthread bundle seeded with hMSCs
hMSC passage number	Passage 7
Target survival time	1 hour
Time anesthetized	9:25 am
Time intubated, isoflurane administered	9:50 am
First incision	10:02 am
Microthread implantation time	10:21 am
Euthanasia time	11:27 am
Rat heart rate and $Sp0_2$ prior to euthanasia	Equipment not available

Experiment number	EXP0215
Experiment date	09/16/2009
Rat sex	Male
Rat type	Sprague Dawley
Rat weight	442 grams
Drugs administered (volume)	Ketamine (0.64 mL), Xylazine (0.03 mL), Isoflurane (2% vaporized)
Implantation type	8 fibrin, 4 collagen microthread bundle seeded with hMSCs
hMSC passage number	Passage 8
Target survival time	1 hour
Time anesthetized	9:05 am
Time intubated, isoflurane administered	9:15 am
First incision	9:30 am
Microthread implantation time	9:48 am
Euthanasia time	10:58 am
Rat heart rate and $Sp0_2$ prior to euthanasia	Equipment not available

Experiment number	EXP0217
Experiment date	10/07/2009
Rat sex	Male
Rat type	Sprague Dawley
Rat weight	540 grams
Drugs administered (volume)	Ketamine (0.57 mL), Xylazine (0.03 mL), Isoflurane (2% vaporized)
Implantation type	8 fibrin, 4 collagen microthread bundle seeded with hMSCs
hMSC passage number	Passage 9
Target survival time	1 hour
Time anesthetized	8:39 am
Time intubated, isoflurane administered	9:12 am
First incision	9:28 am
Microthread implantation time	9:38 am
Euthanasia time	10:45 am
Rat heart rate and $Sp0_2$ prior to euthanasia	224 beats per minute, 99% $Sp0_2$

Experiment number	EXP0218
Experiment date	10/21/2009
Rat sex	Male
Rat type	Sprague Dawley
Rat weight	593 grams
Drugs administered (volume)	Ketamine (0.75 mL), Xylazine (0.04 mL), Isoflurane (2% vaporized)
Implantation type	8 fibrin, 4 collagen microthread bundle seeded with hMSCs
hMSC passage number	Passage 9
Target survival time	1 hour
Time anesthetized	8:40 am
Time intubated, isoflurane administered	9:20 am
First incision	9:25 am
Microthread implantation time	9:45 am
Euthanasia time	10:45 am
Rat heart rate and $Sp0_2$ prior to euthanasia	227 beats per minute, 94% $Sp0_2$

Experiment number	EXP0219
Experiment date	10/21/2009
Rat sex	Male
Rat type	Sprague Dawley
Rat weight	616 grams
Drugs administered (volume)	Ketamine (0.68 mL), Xylazine (0.04 mL), Isoflurane (2% vaporized)
Implantation type	8 fibrin, 4 collagen microthread bundle seeded with hMSCs
hMSC passage number	Passage 9
Target survival time	1 hour
Time anesthetized	10:40 am
Time intubated, isoflurane administered	10:50 am
First incision	11:07 am
Microthread implantation time	11:20 am
Euthanasia time	12:20 am
Rat heart rate and $Sp0_2$ prior to euthanasia	210 beats per minute, 96% $Sp0_2$

Experiment number	EXP0220
Experiment date	10/28/2009
Rat sex	Male
Rat type	Sprague Dawley
Rat weight	655 grams
Drugs administered (volume)	Ketamine (0.67 mL), Xylazine (0.04 mL), Isoflurane (2% vaporized)
Implantation type	Intramyocardial injection of hMSCs
hMSC passage number	Passage 9
Target survival time	1 hour
Time anesthetized	8:45 am
Time intubated, isoflurane administered	9:25 am
First incision	9:33 am
hMSC injection time	10:22 am
Euthanasia time	11:25 am
Rat heart rate and $Sp0_2$ prior to euthanasia	182 beats per minute, 92% $Sp0_2$

Experiment number	EXP0221
Experiment date	11/02/2009
Rat sex	Male
Rat type	Sprague Dawley
Rat weight	462 grams
Drugs administered (volume)	Ketamine (0.68 mL), Xylazine (0.05 mL), Isoflurane (2% vaporized)
Implantation type	Intramyocardial injection of hMSCs
hMSC passage number	Passage 6
Target survival time	1 hour
Time anesthetized	8:40 am
Time intubated, isoflurane administered	9:10 am
First incision	9:32 am
hMSC injection time	9:51 am
Euthanasia time	11:00 am
Rat heart rate and $Sp0_2$ prior to euthanasia	227 beats per minute, 96% $Sp0_2$

Experiment number	EXP0224
Experiment date	01/06/2010
Rat sex	Male
Rat type	Sprague Dawley
Rat weight	572 grams
Drugs administered (volume)	Ketamine (1.36 mL), Xylazine (0.13 mL), Isoflurane (2% vaporized)
Implantation type	Intramyocardial injection of hMSCs
hMSC passage number	Passage 7
Target survival time	1 hour
Time anesthetized	9:40 am
Time intubated, isoflurane administered	9:46 am
First incision	10:00 am
hMSC injection time	10:32 am
Euthanasia time	11:35 am
Rat heart rate and $Sp0_2$ prior to euthanasia	205 beats per minute, 91% $Sp0_2$

Experiment number	EXP0225
Experiment date	01/13/2010
Rat sex	Male
Rat type	Sprague Dawley
Rat weight	588 grams
Drugs administered (volume)	Ketamine (0.61 mL), Xylazine (0.03 mL), Isoflurane (2% vaporized)
Implantation type	Intramyocardial injection of hMSCs
hMSC passage number	Passage 8
Target survival time	1 hour
Time anesthetized	8:40 am
Time intubated, isoflurane administered	9:15 am
First incision	10:10 am
hMSC injection time	10:35 am
Euthanasia time	11:27 am
Rat heart rate and $Sp0_2$ prior to euthanasia	170 beats per minute, 96% $Sp0_2$

Appendix E: Surgical Procedure

Materials: 70% ethanol, betadine solution, saline solution, sterile q-tips, sterile gauze, non-sterile gauze, sterile surgical drape, sterile no. 10 scalpel blade, 6-0 Prolene suture, rat intubation kit, non-sterile gauze, 16 gauge catheter, catheter guide, (3) sterile 1 cc syringes, surgical stapler, (3) 27 gauge syringe needles, proper sized sterile surgeon's gloves, non-sterile drapes, (2) towel clamps, sterile scalpel, Hamilton 100 µL glass syringe, protective rat handling glove, surgical scissors, iris scissors, rib spreader, plastic tub, forceps, cauterizer with sterile head, needle holders (large and small), Xylazine, Isoflurane, Ketamine, Lidocaine, Pentobarbital, Plexiglass rat intubation container, ventilator, tubing to connect ventilator to isoflurane dispenser to the rat, isoflurane dispenser, digital scale, electric shaver, surgical tape, suture needle with quantum dot loaded hMSC seeded fibrin thread attached, pulse oximeter

Procedure:

1. Put plastic tub on digital scale and re-calibrate
2. Grab the base of the rat's tail and put on scale
3. Record weight and return rat to cage
4. Calculate the necessary concentrations of Xylazine and Ketamine to sedate the rat
    a. Drug concentration of Ketamine: 100 mg/kg
    b. Drug concentration of Xylazine: 10 mg/kg
5. Use a 1 cc syringe with a 27 gauge needle to inject the calculated drug concentrations into the rat
6. Put rat back in cage for 5 minutes or until completely sedated
    a. Check if rat is completely sedated by gently touching the eye and looking for the rat to flinch
    b. If rat does not become completely sedated inject an additional 10% (of the initial calculated concentration) of both drugs into the rat and wait 5 minutes after each injection to test sedation
7. Put the rat on non-sterile drapes and position the rat so that the left side is facing up, allowing access to the abdominal region
8. Shave all fur between the front and hind legs
9. Put rat on top of the intubation container and intubate
10. Ensure intubation by putting a mirror in front of the catheter and checking for condensation
11. Gently move rat onto new non-sterile drapes (left side facing up)

12. Use surgical tape to tape one front and hind leg (the ones closest to the drapes) to the drapes on the table
13. Connect to ventilator tubing to the 16 gauge catheter that was intubated earlier
14. Use the isoflurane dispenser to add 2.0% isoflurane to the air reaching the rat
15. Ensure ventilator function by checking chest for expansion and contraction in correlation with ventilator
16. Rinse shaved area with betadine and 70% ethanol 3x with non-sterile gauze (rinse with betadine first)
17. Put on sterile surgical gloves
18. Put sterile drapes over the rat and cut a hole with blunt-end surgical scissors over the area of incision
19. Use scalpel, iris scissors, and cauterizer to gain access to abdominal cavity, making sure not to puncture any organs or vessels
20. Use towel clamps to clamp the outside area of incision (skin) to the sterile drapes
21. Use rib spreaders to improve access to the heart
22. Pass suture needle with quantum dot loaded hMSC seeded biological microthreads through left ventricular wall and cut the biological microthread end attached to the needle as soon as it appears OR inject 35 µL of hMSC suspension (10,000 cells) into the left ventricular wall
23. Wait 1 hour, making sure to monitor vital signs (heart rate $Sp0_2$
24. Euthanize the animal with pentobarbital
25. Remove the heart for histological analysis
26. Rinse heart 3x with PBS
27. Place heart in 4% paraformaldehyde at 4^0C